AFRL-SA-WP-TR-2017-0013

Cellular Sentinels Toxicity Platform

Michael Jackson, PhD
Layton H. Smith, PhD
Anne Bang, PhD
Siobhan Malany, PhD
Sanford Burnham Medical Discovery Institute, La Jolla, CA

February 2017

Final Report
for August 2013 to August 2016

Air Force Research Laboratory
711th Human Performance Wing
U.S. Air Force School of Aerospace Medicine
Aeromedical Research Department
2510 Fifth St., Bldg. 840
Wright-Patterson AFB, OH 45433-7913

NOTICE AND SIGNATURE PAGE

AFRL-SA-WP-TR-2017-0013 HAS BEEN REVIEWED AND IS APPROVED FOR PUBLICATION IN ACCORDANCE WITH ASSIGNED DISTRIBUTION STATEMENT.

//SIGNATURE//	//SIGNATURE//
MS. LINDA ARMSTRONG	DR. RICHARD A. HERSACK
Chief, Aeromedical Research Support	Chair, Aeromedical Research Department

REPORT DOCUMENTATION PAGE

Form Approved
OMB No. 0704-0188

1. REPORT DATE *(DD-MM-YYYY)*	**2. REPORT TYPE**	**3. DATES COVERED *(From – To)***
1 Feb 2017	Final Technical Report	August 2013 – August 2016

4. TITLE AND SUBTITLE

Cellular Sentinels Toxicity Platform

5a. CONTRACT NUMBER

5b. GRANT NUMBER
FA8650-12-2-6453

5c. PROGRAM ELEMENT NUMBER

6. AUTHOR(S)
Michael Jackson, PhD; Layton H. Smith, PhD; Anne Bang, PhD; Siobhan Malany, PhD

5d. PROJECT NUMBER

5e. TASK NUMBER

5f. WORK UNIT NUMBER

7. PERFORMING ORGANIZATION NAME(S) AND ADDRESS(ES)
Sanford Burnham Medical Discovery Institute
10901 N Torrey Pines Road
La Jolla, CA 92037-1005

8. PERFORMING ORGANIZATION REPORT NUMBER

9. SPONSORING / MONITORING AGENCY NAME(S) AND ADDRESS(ES)
USAF School of Aerospace Medicine
Aeromedical Research Department/FHS
2510 5th St., Bldg. 840
Wright-Patterson AFB OH 45433-7913

10. SPONSORING/MONITOR'S ACRONYM(S)

11. SPONSOR/MONITOR'S REPORT NUMBER(S)
AFRL-SA-WP-TR-2017-0013

12. DISTRIBUTION / AVAILABILITY STATEMENT

DISTRIBUTION STATEMENT A. Approved for public release. Distribution is unlimited.

13. SUPPLEMENTARY NOTES
Cleared, 88PA, Case # 2017-3638, 27 Jul 2017.

14. ABSTRACT

The ultimate goal of toxicity testing is to assess the likely risks posed to human populations at ambient exposure levels. Unfortunately, current approaches to toxicology are expensive and are vastly outpaced by the rate of discovery of new compounds. To address this imbalance, research scientists at Sanford Burnham Prebys have developed the Cellular Sentinels Toxicity Platform. This approach combines induced pluripotent stem cells and their derivatives with rapid high-throughput screens of cellular morphology and physiology. Over the last three years, we have successfully advanced and validated the platform, demonstrating utility in its application to the rapid identification of potentially toxic compounds.

15. SUBJECT TERMS
Toxicity, pluripotent stem cells, neurons, cardiomyocytes, hepatocytes, screening

16. SECURITY CLASSIFICATION OF:			**17. LIMITATION OF ABSTRACT**	**18. NUMBER OF PAGES**	**19a. NAME OF RESPONSIBLE PERSON**
a. REPORT	**b. ABSTRACT**	**c. THIS PAGE**			Cole Hutchison
U	U	U	SAR	76	**19b. TELEPHONE NUMBER *(include area code)***

This page intentionally left blank.

TABLE OF CONTENTS

Section **Page**

LIST OF FIGURES

Page

LIST OF FIGURES (concluded)

Page

LIST OF TABLES

Page

1.0 SUMMARY

The ultimate goal of toxicity testing is to assess the likely risks posed to human populations at ambient exposure levels. For the past 50 years, this goal has been met by high dose testing in experimental animals with specific approaches for extrapolation from high to lower doses and from the experimental animals to the human population. These observational studies remain of great value, but yield little understanding of the molecular mechanisms underlying the toxic response, thereby limiting the ability to predict potential human risk. Adding to the scope of the problem is the exponential increase in the rate of discovery of new chemical matter. It is estimated that there are >100,000 new chemicals for which little to no risk assessment has been performed. While animal studies represent the foundation of toxicology, and as such are unlikely to be entirely replaced, current methodologies, capacities and budgets of the regulatory agencies tasked with toxicity testing are wholly unsuited and ill-equipped to meet this critical and growing need.

To address this need, research scientists at Sanford Burnham Prebys (SBP) have developed the Cellular Sentinels Toxicity Platform (CSTP). This approach combines induced pluripotent stem cells and their derivatives with rapid high-throughput screens of cellular morphology and physiology. CSTP is comprised of three cellular modules defined by cell type (neurons, cardiomyocytes and hepatocytes). Each consists of a tiered assay cascade with 1st line and 2nd line assay technologies including high content imaging analysis, cellular impedance and electro-potential arrays, mass spectrometry and routine plate-based assays. This approach is distinct from other such high-throughput toxicity screening efforts like ToxCast and Tox21, in two ways. First, it utilizes the most advanced models of human cellular function available to date, human induced pluripotent stem cells. These emerging cellular technologies are superior to traditional immortalized cell lines in that they more accurately reflect the genomic, transcriptomic and proteomic milieu of adult cells, thus they are a significantly more relevant model for interrogating the effects of potentially toxic agents on human tissues. Second, the platform combines functional analyses such as cellular impedance, and phenotypic read-outs that do not require the engineering of genetic constructs to report on cellular function. Together these technologies and approaches represent the most relevant *in vitro* models of neurotoxicity, cardiotoxicity and hepatotoxicity available for high-throughput screening and toxicological profiling available.

Over the last three years, we have successfully advanced and validated the platform, demonstrating utility in its application to the rapid and cost effective identification of potentially toxic compounds. We assembled a library of compounds with known toxicities and pharmacological properties as well as structurally related compounds lacking such effects. We deployed an array of phenotypic and physiologic assays against three cellular modules: neurons, cardiac myocytes and hepatocytes. The effects of the compounds with known toxicities were applied to these assays and cells, and their cellular response measured. These studies formed the basis of our pilot studies and facilitated the establishment of test compound concentration levels, exposure times, and overall assay workflows and Go/No-go decision points. Following the successful execution of this assay development and confirmation phase, the platform was then rigorously validated using a second, related collection of compounds with both known toxicities and unknown toxic potential. In all, the platform exhibited a robust capability to distinguish compounds with known neuro, cardiac or hepatotoxic effects from those without such toxic

effects. The methods used, results obtained and conclusions drawn from this work, are provided in detail in the following pages of this report.

As indicated above the overall effort was successful, with the primary objective of the project having been met. Despite these successes, there were some technical failures that required alternative approaches. For example, currently human induced pluripotent stem cells derived hepatocytes do not express the full range of xenobiotic metabolizing enzymes expressed by adult hepatocytes. As such, these cells were replaced with a more physiologically relevant immortalized human hepatocyte cells line. These cells perform more robustly and consistently in our assay. Likewise it was necessary to use a different neuronal cell line that was originally proposed. Perhaps the most significant issue encountered was that the phenotypic screens were not as informative as we originally hypothesized. Indeed, in its final form the CSTP is not a linear testing funnel that starts with high-content image analysis and ends with robust physiological assays. Our results showed that these various assay platforms had variable sensitivity and specificity, requiring that we rethink our global approach to the application of each assay technology. Ultimately, instead of a step-wise approach progressing from a series of image-based assays toward increasingly complex physiological assays, the CSTP work-flows employ combinations of higher-throughput, lower information assays such as general cytotoxicity, with high-relevance, lower throughput physiological and medium throughput image-based assays, to assess the compound. The various stages and decision points for each assay are provided in the following pages of this report. In brief, the CSTP as a more mature technology is not a linear process, but an iterative one that is informed at each stage by empirical testing, with next steps determined by validated criteria and an established decision tree. Compounds submitted for analysis progress through the various assays and cellular modules until they are determined to have a toxic effect in a particular cell type. This allows for a more flexible approach to the compound testing funnel placing the assay with the most decisional value at the earliest stages of the process. This increases efficiency and is expected to keep overall costs low as each compound will not be progressed through a fixed series of assays regardless of data obtained in prior experiments. Ultimately, these impediments and our alternative approaches yielded a more robust and relevant platform than originally conceived.

Like any developing technology, there will continue to be room for improvement of the CSTP. Testing of compound metabolites after biotransformation would further extend the predictive power of the platform. Development of new cellular modules for assessing exposure (for example a lung epithelial cell module) or elimination (i.e. a renal tubule epithelial cellular module) would expand the applicability of the platform beyond the brain, heart and liver. Likewise, developing additional neuronal cell types will allow for the identification of compounds that are uniquely toxic to distinct neuronal populations. Importantly, this system is limited to testing compounds that are soluble in an aqueous environment. Additional engineering technologies, whose development and integration with CSTP are beyond the scope of this effort, are required for testing volatile compounds or those not soluble in dimethyl sulfoxide.

In summary, we have met the primary objective of the project. We have developed a highly-relevant toxicity screening platform based on high-throughput human biology and physiology. Compounds can be screened at a scale that can be rapid, informative and cost-effective. Although work to improve the technology remains, the core platform is ready for application.

2.0 INTRODUCTION

The objective of this project was the development and validation of the Cellular Sentinels of Toxicity Platform (CSTP), a suite of high-throughput, multiplexed assays of cellular phenotype and physiology for the purpose of assessing the potential toxicity of large collections of chemicals. The long-term goal of this three-year project was to demonstrate that these technologies could be combined in an integrated platform, and that platform would allow for the early assessment and identification of potentially toxic compounds in a rapid, cost effective manner. Results from this effort will simultaneously improve the relevance of the data produced while having the potential to reduce the downstream use of animal studies.

The current approach to quantitatively assessing the health risks of chemical exposure relies extensively on high dose studies in animals. This expensive, low-throughput approach depends on conservative extrapolations to relate animal studies to much lower-dose human exposures. While animal studies represent the foundation of toxicology and as such are unlikely to be entirely replaced, the low-throughput and high cost makes them entirely unsuitable for assessing the potential toxicities of the 10,000's of chemicals present in commercial processes, chemicals to which the population is exposed. A new generation of technologies is now poised for development into a high-throughput platform for toxicological screening, that can be used to assess in a first line of *in vitro* evaluation on normal human cells, the potential toxicity of large collections of chemicals.

In vitro cell systems are clearly a part of the solution, and are being explored by government initiatives like ToxCAST, Tox21, and IMI. These efforts are limited by their reliance on cells from human cadavers and animals, and engineered cell lines. Although such models can be adapted to high throughput screens, they each have issues that restrict their utility in predicting toxicity. Primary human cells are limited by sporadic supply and inherent variability in phenotype and quality, resulting in significantly compromised *in vitro* function. Transformed cell lines are similarly limited by their transformed nature, rapid proliferation; aneuploidy and lack of physiological relevance are all well recognized limitations that contribute to their poor capacity to recapitulate *in vivo* human biology. Other initiatives in this arena that aim to develop an *in vitro* platform utilizing human organ model systems connected through microfluidics commonly referred to as "body on a chip" are complementary to the approach we describe (e.g. X.C.E.L Program BAA N66001-12-X-2002, NIH RFA-RM-11-022).

However, unlike these ambitious programs that are likely to take many years to engineer and validate before they find broad utility, the CSTP can be implemented immediately. Many of the components of this platform already exist and technical feasibility had been well established by our efforts prior to the start of this project. The CSTP consists of three cellular modules defined by cell type (neurons, cardiomyocytes and hepatocytes). Each consists of a tiered assay cascade that seeks to determine first, the optimal exposure concentration and time for each test article, and then the effects of compounds on specific aspects of cellular physiology. These assays provide the combined power of high throughput, imaged-based screens of cellular and moderate throughput functional assays that report the effect of the toxin on essential physiological processes of each cellular module. The execution of the assays and interpretation of the results are supported by sophisticated informatics and analytics tools to visualize the data, set threshold criteria and flag compounds that exhibit potential toxic effects in the assays (Figure 1).

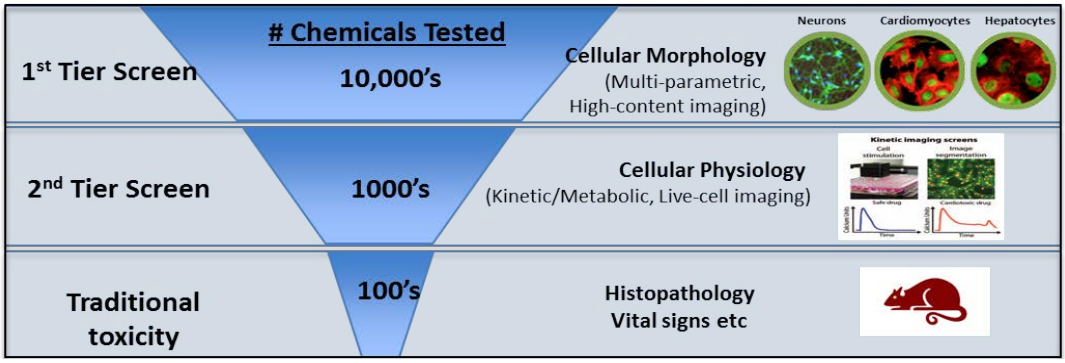

Figure 1. The CSTP toxicity screening funnel. *Initial assessments are made by applying rapid, image-based analyses of cellular morphology (1st Tier), followed by functional assays of Cellular Physiology Module (2nd Tier) to iPSC-derived neurons, cardiomyocytes and hepatocytes. Finally, those compounds that exhibit morphological and functional toxicities will be advanced into established in vivo models to assess toxicity.*

Our approach is differentiated from other efforts in this area of research in at least two ways. First, the application of human induced pluripotent stem cell (hiPSC) derived cell types provides a highly relevant *in vitro* model of human cellular function that is not only more representative of natural human biology, but as a commercial product produced at scale, affords a significant level of consistency and reproducibility across assays and over time. Prior to the advent of hiPSC technologies a comparable source of normal human cells in the quantities with the consistency and quality required for high-throughput screening did not exist. Commercially available hiPSC-derived neurons, cardiomyocytes, and hepatocytes (Cellular Dynamics International-CDI) have the distinct advantages that they are normal, non-transformed human cells and they are available in large consistent batches produced under quality controls. Although these iPSC derived human cell types all express some immature characteristics, they exhibit many of the morphological and functional hallmarks of normal adult human primary cells, from which, in many respects, they are indistinguishable. Second, the development of sophisticated bioassays based on cellular morphology/imaging and measurements of physical function provides us with the opportunity to avoid engineering a biologically active reporter system within these highly relevant cells. Although reporter genes such as firefly luciferase can be readily introduced into hiPSCs, that would be a step in the wrong direction. The insertion of synthetic constructs or exogenous genes would undermine the biological relevance inherent in the hiPSC models. Thus the application of assay technologies such as vital dyes, and cellular impedance analysis facilitates interrogation of the effects of toxic compounds without compromising the integrity of the human biology represented in the hiPSC-model. Moreover, these newer technologies offer an integrated cellular response to toxic compounds providing a global assessment of the effects of the compound rather than narrowly focusing on only a single gene target or product. Indeed, the non-invasive assays afforded by cellular impedance and microelectrode array technologies offer unique insight into cellular function that correlates with physiology. Taken together, the application of hiPSC-derived cellular models and newly developed assay technologies affords the development of a platform technology and strategic approach to the early assessment of potentially toxic compounds.

3.0 METHODS, ASSUMPTIONS, PROCEDURES AND RESULTS

3.1 Cardiomyocyte Module

3.1.1 Rationale. *Statement of Work (SOW) Task 4.2.2 Cardiomyocyte Assays*. Cardiac responses to environmental insults lead to myocardial death, remodeling and heart failure and a detailed examination of cardiac toxic effects is lacking. Human-induced pluripotent stem cells provide a cost-effective, higher throughput alternative to *in vivo* animal toxicology studies with increased relevance to human subjects that can be used to screen for cellular toxicity and flag compounds for further analysis. We have validated a human cardiomyocyte module screening approach outlined in Figure 2 that includes assays multiplexing phenotypic and functional readouts in human iPSC-derived cardiomyocytes (hiPSC-CM), as well as bioactivity dose-response determinations and bioinformatic analysis of the data set and of arrhythmic risk to assess potential toxicity of a large collection of test compounds.

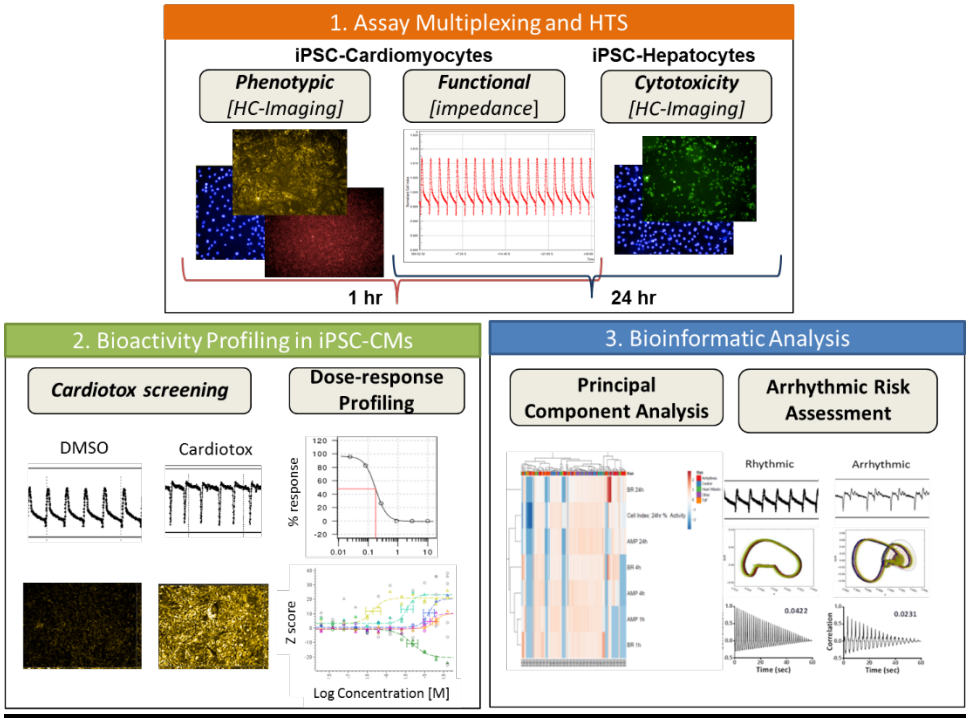

Figure 2. Cardiomyocyte module screening approach.

Compounds were also tested in human iPSC-derived hepatocytes (hiPSC-HEP) to determine non-specific cellular toxicity. In addition, we developed a bioenergetics assay measuring oxygen consumption rate and metabolic potential to evaluate select compounds downstream of the multiplexed assay platform depicted in Figure 2. Our approach provides a novel suite of medium-throughput quantitative tools for assessing compound effects on cardiac phenotype and contractility utilizing physiologically relevant human stem cell derived cardiomyocytes and predicting compounds with potential proarrhythmia and may be applied to

in vitro paradigms for environmental cardiac safety evaluation with the aim of reducing the overall number of compounds requiring extensive toxicity testing *in vivo.*

3.1.1.1 Cardiomyocyte Module Methods. Cardiomyocyte *Physiology (Intracellular Contractility)* – The physiology platform is a 96w multiparametric, real-time assay to monitor functional beating activity as impedance transients recorded from hiPSC-CM that provides readouts including the following: cellular index, beat amplitude, beat rate and beat irregularity at 1h, 4h and 24h post drug treatment (Figure 1, box 1). Cryopreserved hiPSC-CMs (Cellular Dynamics International, Madison, WI, CDI #CMC-100-010-001) were thawed in plating media supplied by the vendor and approximately $3x10^4$ cells/well plated directly onto E-Plate Cardio (ACEA Biosciences, San Diego, CA) precoated with 0.01mg/mL fibronectin in PBS for 3h at 37ºC. Cells were cultured for 14 days at 37ºC, 5% CO_2 to ensure synchronous batches of cells. The maintenance media (CDI) was changed every 2 days after plating and 24h prior to dosing using a Viaflo 96 channel pipettor (INTEGRA Biosciences Hudson, NH) placed in the tissue culture hood.

Viability and contractility of cardiomyocytes were monitored by impedance using the xCELLingence RTCA (real-time cell analyzer) Cardio system (ACEA Biosciences, San Diego, CA). Impedance was measured for 5 consecutive 60-s sweeps (recorded at a sampling rate of 12.9ms) at selected time points and reported as cell index (CI). Prior to drug treatment, a baseline was recorded to ensure the cells established a beat rate of 40-60 beats/min. Drug stocks were prepared at 10mM stock concentration and serial diluted in 100% DMSO and further diluted in maintenance media in a separate 96-well plate at 7x target concentration. The drug plate was equilibrated to 37ºC prior to diluting 1:7 into the E-plate using the Viaflo 96 channel pipet to give a final medium volume of 175µl/well in 0.1% DMSO. All compounds were tested in duplicate on two separate E-plates seeded with cells from separate thaws. Impedance was measured at 1h, 4h, and 24h following treatment. Normalized cell index values for each sweep were exported for all wells from the ACEA software. Amplitude, beat rate, and gross cell index were double normalized to intra-well measurements prior to compound addition and to DMSO controls using software integrated in the ACEA xCELLingence RTCA Cardio monitor system.

3.1.1.2 Quantification of arrhythmia. Cell index values were normalized both to the time point just prior to compound treatment and to the mean cell index of DMSO control wells. Normalized cell index values for all 96 wells were exported in list format as tab-delimited text files for each of five consecutive 60s sweeps prior to compound addition and at 1h, 4h, and 24h following treatment. The 5 exported RAW files associated with each time point are suffixed with "_(1-5) min" to identify the 5 sweeps, and placed in a directory for each time point. Normalized impedance cell index values are smoothed using moving windows of size 10 time interval of output series (default time interval of instrument is 12.9ms). (*Limit Cycle Analysis)* - 2-dimensional phase portrait of the inter beat intervals were plotted as the amplitude vs. the first derivate for each recorder. *Autocorrelation Analysis* **–** Autocorrelation is calculated as the cross-correlation of the cell index signal with itself with different time lag, which was implemented using the auto-correlation function for one-dimensional arrays (time series) from the StatsModels library. For every 1-min sweep and every well, characteristic correlation time, tau is calculated in two steps as follows: first, the sum of the squared values of auto-correlation for that well is calculated, then result is normalized by the length of the data series for the given well (4633 data points).

3.1.1.3 Cardiomyocyte Phenotype (Cellular Mitochondrial Toxicity). The phenotypic hiPSC-CM platform is a 384w multiparametric, imaged-based assay to quantify the acute and chronic effect of compounds on the following parameters: (1) nuclear area, roundness and brightness; (2) mitochondrial intensity and (3) oxidative stress (Figure 2, box 1). HiPSC-CM obtained from Cellular Dynamics, Inc., were thawed in plating media supplied along with the cells and ~ 3500 cells/well were plated into 384-well cell bind black plate (Corning cat # 3683) with clear bottom and cultured for 7d in the incubator at 37°C, 5% CO2. Plaiting media was changed with maintenance media 48 hours after plaiting, and every 48 hours after that. Compounds were obtained from ENZO Life Sciences as 10mM stocks. Compound concentration for the single point screen and highest/starting concentration for the dose response assays was 20µM with the purpose of not exceeding max tolerable DMSO concentration for cardiomyocytes of 0.2%. The intermediate plate containing 7X compound concentration was prepared by dispensing the compounds using Echo 555 Liquid Handler into a 384-well Polypropylene plate containing media. The intermediate plate was centrifuged at 500xg for 1 min and 10µl of the 7X compound were transferred manually into the assay plate containing 60 µl of media for 1X final concentration. Cells were incubated with the compounds for 1h, and then stained with 50nM TMRE (mitochondria membrane potential - MMP), 1µg/ml Hoechst (nucleus), and 5µM CellRox Deep Red (oxidative stress, referred to as reactive oxygen species or ROS) for 30min. High content confocal images were obtained using Operetta microscope and analyzed using Harmony analysis software. The data was further imported into Genedata software. Genedata offers easy compound mapping, statistical data analysis as well as dose-response curve analysis and visualization. The analyzed data was exported as an excel file and sent to the bioinformatics group for further data processing such as cluster analysis and principal component analysis (PCA).

3.1.1.4 Hepatocyte Phenotype (See 3.2 hepatocyte module).

3.1.1.5 Bioenergetic Platform. hiPSC-CM were seeded in fibronectin coated 96 well-plate and incubated for 6 days at 37°C/ 5% CO2 with medium changes every 48h. On day 7, maintenance medium was replaced by Seahorse's bicarbonate-free medium containing 2.5mM Glucose, 1mM Sodium Pyruvate and 2mM Glutamine for Mitochondrial stress assay and 2mM Glutamine for Glycolysis stress assay. 10X concentration of compounds were added to the cells and the plate was incubated for 1h in a 37°C chamber (without CO_2). The cartridge was loaded with specific compounds dependent on the assay being performed. For Mitochondrial stress the each chamber of the cartridge was loaded with 10µM Oligomycin, 5µM FCCP and 5µM Rotenone/Antimycin A, respectively. For Glycolysis stress assay, each chamber was loaded with 80mM Glucose, 9µM Oligomycin and 100mM 2-Deoxy Glucose (2-DG), respectively. The cartridge and the assay plate were then loaded on the Seahorse XF96 analyzer where compounds pre-loaded in the cartridge are serially injected for measuring either mitochondrial or glycolytic function. Data is analyzed using the Seahorse's wave software.

3.1.1.6 High Throughput Screening and Dose-response Profiling. We screened the Enzo SCREEN-WELL cardiotoxicity library (Enzo Life Sciences, Farmingdale, NY). Screening data is recorded as standard deviation **(**SD) from control solvent and as percent change compared to multiple DMSO treated wells on each screening plate. Results are presented in a heat map using a common software package facilitating a global view of the dataset and comparison of

each parameter alone or in combination with others. From the heatmap values, we determined the minimal threshold criteria required to classify compounds as "hits" and advance compounds to further interrogation as % response ≥25% for the physiology platform and > 3SD for the phenotypic platform. Statistical analysis and graph generation was performed with GraphPad Prism version 7.0 for Windows (GraphPad, La Jolla, CA, USA). Dose-response curves (DRC) were analyzed by non-linear, four parameters regression. Experimental data were statistically analyzed as indicated for each experiment. The data reported are individual values or rounded means and corresponding SD.

3.1.1.7 Bioinformatic Analysis - Principal Component Analysis (PCA) Plots. We used ClustVis to construct Principal Component Analysis (PCA)[1]. In general, compounds for each of the libraries were annotated into several risk categories and saved as a csv file for simplified data import. For each row we ensured that there were equal number of columns, and no duplicates. After this data was imported into Clustvis, row values (readout values e.g. TMRE) were scaled using the unit variance scaling option, and the PCA method was set to SD with imputation. We did not use any other options for both, row scaling and PCA Method. While representing each of the heat maps in this report, the following options were used; clustering distance for rows (and columns): correlation; clustering methods for rows: average; tree ordering for rows: tightest cluster first and the color scheme was set to Diverging RdBu. All plots were exported as pdf files.

3.1.1.8 Software development and automation. A stand-alone Windows based tool to perform high-throughput limit-cycle and tau analysis was developed using Python v2.7. Other open-source libraries, e.g., PySide (www.pyside.org), Numerical Python v1.9.2 (www.numpy.org), and matplotlib v1.4.3 (www.matplotlib.org), were used to develop a simple graphical user interface, perform mathematical calculations and generate plots, respectively. The tool was designed to process RAW data of up to four time points, each time point consisting of fixed 5-min sweeps for a 96-well plate format from the ACEA xCELLigence RTCA Cardio system. The 5 RAW files associated with 1 time point are suffixed with "(1-5)min," to identify the 5 sweeps, and placed in a directory. The GUI allows the end-user to choose the directory, along with simple dropdown options for output image resolution, image type, an option to scale limit-cycles based on a threshold cutoff value obtained from the adjacent slider and 4 options for smoothing the initial RAW data. The output will consist of images of limit cycles per individual well and a complete 96 well-plate view, tau values per plate as flat text (.csv) files, and heat map plots of the average tau values for the entire plate and a composite image consisting of the image of limit-cycles and heat map of tau values in a plate-view format. All the output files will be saved in the directory of the chosen time point. An executable of the program along with sample data and results is available upon request and it has no additional dependencies. The software was developed and tested on a machine with Windows 7 Pro (SP1), 16 G.B. RAM. The software program is available for download as an executable file complete with protocol and demonstration.

3.1.2 Cardiomyocyte Results

3.1.2.1 High Throughput Screening. We applied the approach outlined in Figure 2, box 1 to screening of the cardiotoxicity library which contains 130 structurally diverse and

mechanistically distinct compounds as well as nontoxic controls divided into five categories. The full library was tested in single point in the physiology and phenotypic cardiomyocyte platforms. The distribution of control values and percent coefficient of variance (% CV) for each parameter in the physiology platform and the phenotypic platform is shown in Figure 3. In addition, we tested the library for general cytotoxicity in hiPSC-HEP after 24h exposure by measuring activation of apoptotic activity in a phenotypic imaging assay (described in hepatocyte section).

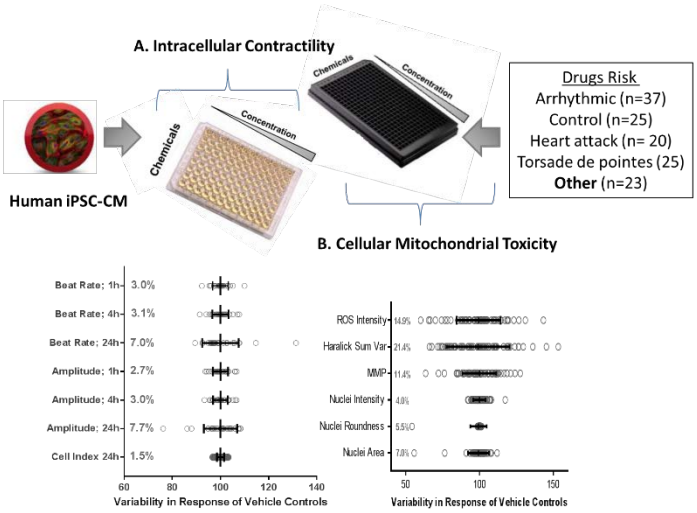

Figure 3. HTS process: Coefficients of variance and standard deviations for DMSO control wells on each screening plate for the physiology and phenotypic platform readouts.

Categorized drugs identified as hits using the minimal threshold criteria defined in the methods are shown in red in Figure 4. Of the 25 compounds classified as controls, 17 had no effect in cardiomyocytes and 16 had no effect across all 15 parameters (leucine caused cytotoxicity in hepatocytes after 24h exposure but is a false positive because the compound did not show toxicity when tested in the hepatotoxicity library). Seven control compounds exhibited some effect in the phenotypic platform. Amoxicillin and Tiabendazole affected only one of three nuclear parameters and we do not consider a compound toxic unless it hits more than one nuclear parameter. We define a compound as a cytotoxic when 2 or more nuclear parameters are significantly affected. Aspartame and Benzoic Acid caused an increase in ROS at single point and confirmed in DRC (Aspartame is a weak hit with EC_{50} >20µM and Benzoic acid is a strong hit with EC_{50} =0.18µM) and are considered true hits. Ranitidine caused a decrease in mitochondrial potential and is reported to have cardiotoxicity (ZANTAC drug insert). Atenolol and Lisinopril also caused a decrease in mitochondrial potential at single point but. These two compounds are false positives in our screening assay as the compounds did not confirm in DRC (These compounds were tested in the Tox21 screen and did not show mitotoxicity up to 100µM - USAF communication). Hexylresorcinol, an anesthetic, was the only control compound to affect amplitude and beat rate at 1h in the physiology platform. The compound did not have an effect at 4h or 24h and did not have a dose-dependent effect. Thus, of the control compounds, three were false positives in single point testing and none of these confirmed in DRC.

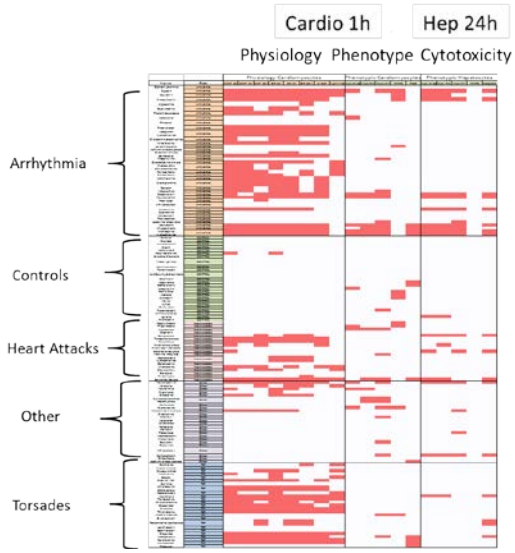

Figure 4. Screening hits in red for ENZO cardiotoxicity library tested in the phenotypic and physiology platforms at the indicated incubation times.

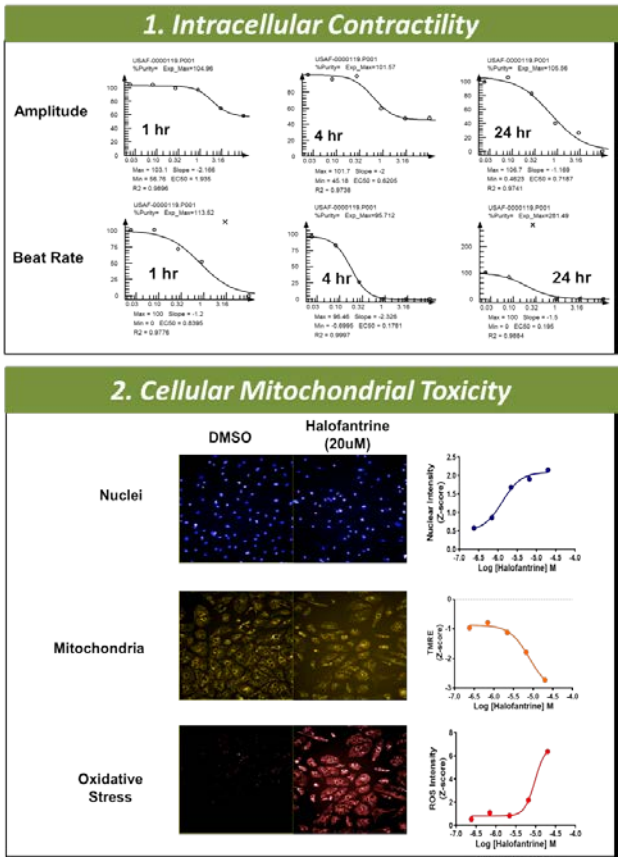

Figure 5. Dose-response profiling of halofantrine in physiology and phenotypic platforms.

Fifty-eight of 130 compounds tested at 10 µM were determined to have acute or chronic effects on cardiomyocyte viability or contractility. A majority of the cardiotox compounds (non-control compounds) that exhibited significant toxicity in the physiology platform are categorized as arrhythmic or causing Torsade de Pointes (TdP). Drugs grouped as arrhythmic but also chemotherapeutics such as daunorubicin, idarubicin and doxorubicin were toxic across all parameters including hepatotoxicity. Nine cardiotox compounds were classified as hits from the ROS parameter and included the following: 4 showed nuclear cytotoxicity in addition to ROS increase, Amiodarone increased nuclear intensity along with ROS increase and the remaining 4 compounds are the TdP classified drugs Haloperidol, Halofantrine and Probucol plus the highly oxygenated compound, sodium stibogluconate which all caused significant ROS increase in the absence of any other phenotypic effects. Of the nine ROS hits in the phenotypic assay, seven had an effect in the physiology assay. Only 8 known cardiotox drugs significantly inhibited mitochondrial membrane potential (MMP) at 1h; 4 of these also showed cytotoxicity in the phenotypic platforms. Among the 4 drugs that affected MMP without overt cytotoxicity are two antidiabetic thiazolidinedione-based drugs, rosiglitazone and pioglitazone. Rosiglitazone has been previously reported in studies profiling of the Tox21 Chemical Collection to decrease the MMP [2]. Three of the four compounds also affected contractility. A total of 12 compounds showed general cytotoxicity in the nuclear parameters at 1 h and eight additional cytotoxic compounds showed toxicity at 24h hepatotoxic phenotypic platform.

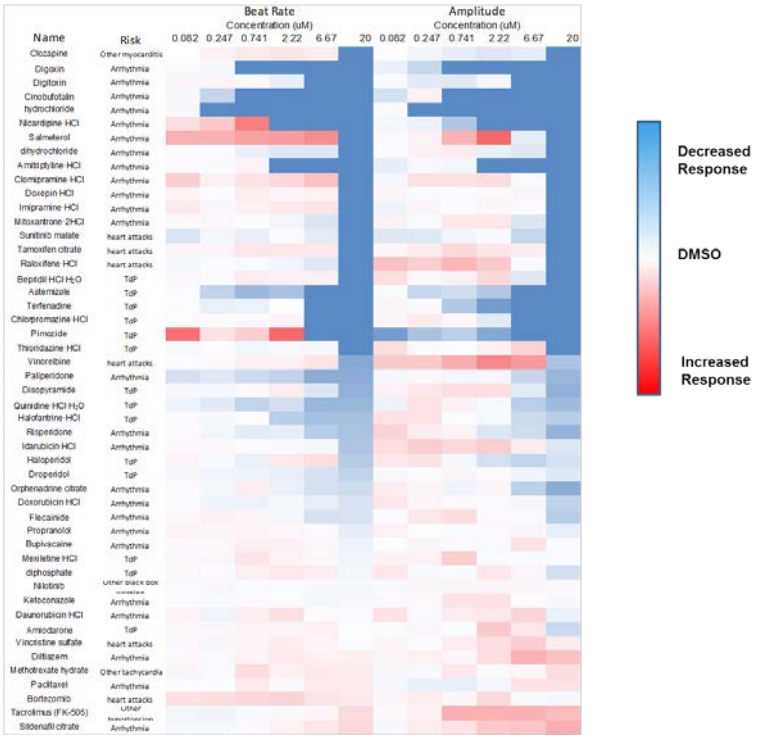

Figure 6. Bioactive profiling of hits in the cardiomyocyte physiology platform.

3.1.2.2. Bioactive Profiling in Dose-response. Dose-dependent and time-dependent changes in cell viability and beat patterns induced by the 58 hits in the physiology platform were further characterized using both the impedance platform and high content live cell imaging to assess the effect of the compounds on nuclear cytotoxicity, mitochondrial integrity and cellular oxidative stress. Example DRCs across all assays for halofantrine is shown in Figure 5. Halofantrine is an anti-malaria drug that exhibits serious cardiotoxicity including cardiac arrhythmia and prolongation of the QT interval. Bioactive profiling showed the drug inhibited amplitude and beat rate with greater potency over time (Figure 4, Box 1) and an increase in nuclear intensity (blue), decrease in mitochondrial potential (yellow) and increase in oxidative stress (red) (Figure 5, Box 2).

Figure 6 shows a heatmap based on percent response values for beat rate and amplitude after 1h incubation for the 58 compounds tested at each indicated concentration. 53 compounds tested in DRC confirmed activity in one or more of the seven physiological parameters, providing a 91.3% confirmation rate.

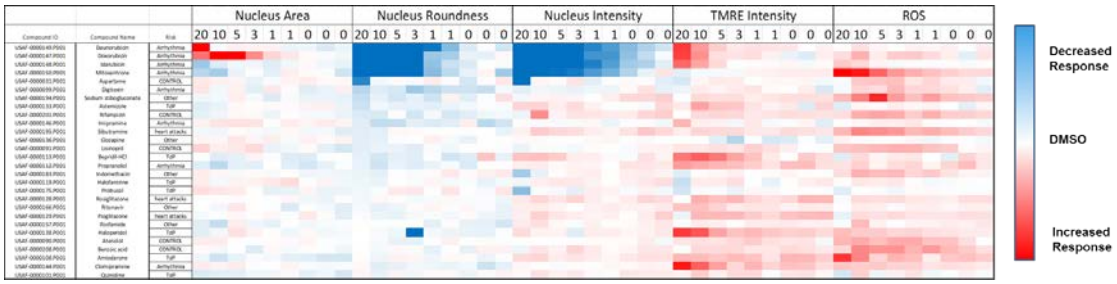

Figure 7. Bioactive profiling of hits in the cardiomyocyte phenotypic platform.

Twenty-eight compounds were tested in dose-response in the phenotypic platform and uploaded and analyzed in GeneData and exported as SD. Figure 7 shows a heatmap based on SD for nuclear cytotoxicity, mitochondrial membrane potential and oxidative stress after 1h incubation for the 28 compounds tested at each indicated concentration. Eighteen of these compounds hit one or more parameters with the average SD >3 in the single point screen and 8 confirmed in a DRC assay (44% parameter-specific confirmation rate). The remaining 10 compounds were non-hits from the single point screen and none showed significant toxicity across phenotypic parameters in DRC.

3.1.2.3 Bioinformatic Analysis. (1) We further clustered the cardiomyocyte screening data using principal component analysis (PCA) to evaluate the distribution of reference compounds relative to unknowns (Figure 8A and B). In brief, PCA transforms multivariate dataset to a set of uncorrelated variables called Principal Components. These multiple principal components together explain the variance in a given dataset and are often ranked in descending order, i.e. Principal Component 1 (PC1) explains 40% of variance, Principal Component 2 (PC2) explains 23% and so on. Heatmaps are one way of visualizing data and give an overview of which annotated groups lie in close proximity or otherwise in the data under consideration. Pairwise distances between each record of the dataset is calculated and pairs of objects (compounds in our case) are with smallest distances are merged together. Figure 8A shows the PCA plot for the cardiotoxicity library tested in the physiology platforms at the indicated incubation times. The plot highlights the compound classes that affect all parameters versus

those that affect early time points. The control compounds are clustered in the middle of the graph and do not show significant deviations from DMSO. Figure 8B shows the PCA plot for the cardiotoxicity library tested in the phenotypic cardiomyocyte platform at 1h and in the caspase activation assay in hepatocytes at 24h. The plot highlights the compound classes that affect nuclear parameters (necrosis) versus caspase activation (apoptosis) versus acute ROS and MMP effectors.

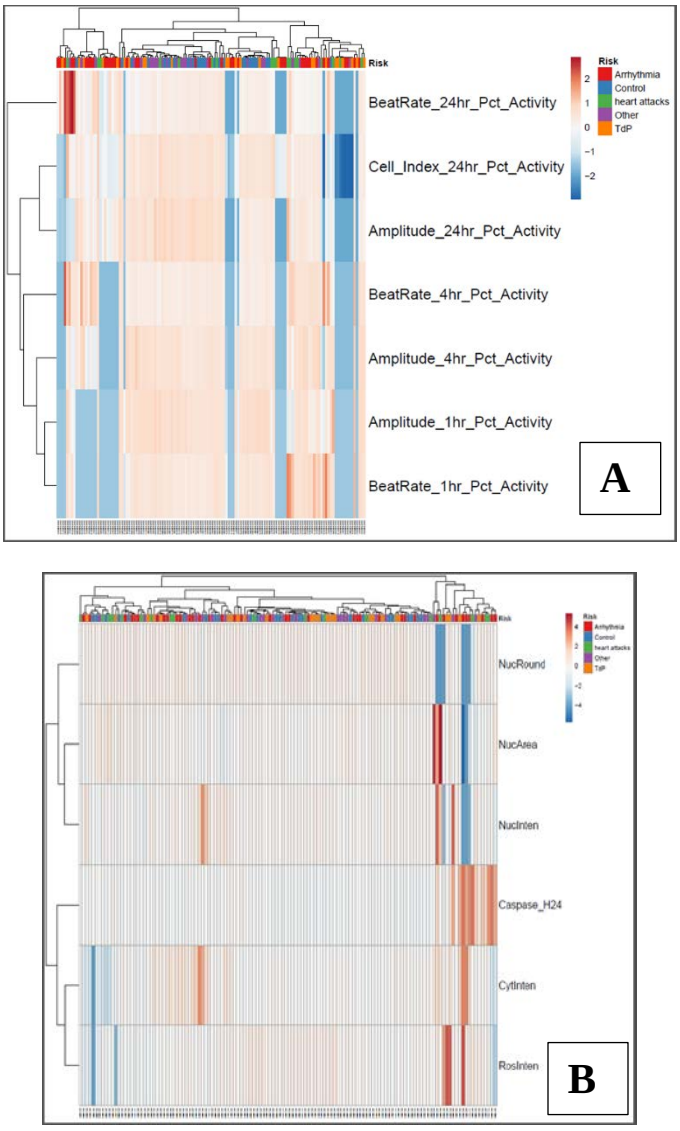

Figure 8. Principal component analysis for ENZO cardiotoxicity library. *(A) Tested in the Physiology Platforms at the indicated incubation times. (B) Tested in the Phenotypic Platforms at the indicated incubation times. (_H24 denotes hepatocytes testing at 24h).*

(2) Compounds that cause beat irregularity may lead to life-threatening arrhythmia. We assessed beat irregularity by applying a nonlinear dynamical system analysis to the impedance recordings to generate limit cycle and autocorrelation graphs to visualize and quantitate oscillatory irregularities of impedance-based contractility patterns generated by hiPSC-CMs as we recently described [3]. The mathematical models provide distinct information as to pattern type and persistence over the time series. Application of these computational approaches to

cardiomyocyte contraction provides a novel and powerful tool for assessing proarrhythmic risk. Our results identified pro-arrhythmic compounds in the library that induce clinical cardiac liabilities.

To evaluate the influence of known proarrhythmic drugs on the contractile activity of hiPSC-CMs, we characterized dose-dependent and time-dependent effects of dofetilide, astemizole, and cisapride on cardiomyocyte beat pattern and regularity. These drugs belong to distinct drug classes based on their primary activity but are hERG channel blockers with known cardiac liabilities. Human iPSC-CMs incubated with 0.12µM of each of the compounds for one hour exhibit drug-induced irregular impedance traces reminiscent of arrhythmias associated with TdP compared to control cells (Figure 9a). Limit cycle phase plots were generated from impedance data reflecting cardiomyocyte contractile state every 12.8ms and recorded over 300s to identify variation in the number of periodic oscillations following drug treatment of hiPSC-CMs. Control treatment yields a stable oscillation that traces the closed phase trajectory and approaches the limit cycle as *t* approaches infinity (Figure 9b). Treatment with the proarrhythmic compounds caused a deviation from the phase trajectory, creating new dynamic patterns which are illustrated by additional limit cycles with varying amplitude and duration. In order to quantify the decay of beat rate regularity, we implemented the autocorrelation function, derived from nonlinear dynamics, to model the contraction time series. Control treatment yields a strong autocorrelation that decays slowly with time and results in a highly ordered periodic correlation; whereas, treatment with the proarrhythmic drugs yields a weak autocorrelation that decays rapidly with significant noise (Figure 9c). The average of the autocorrelation function applied to five sequential 60s impedance recordings results in a calculated order parameter (tau). By applying autocorrelation to the concentration-response data, dofetilide, astemizole, and cisapride exhibited tau EC_{50} (pEC_{50} ± SD) values of 1.5nM (8.81 ± 0.10), 7.2nM (8.14 ± 0.12) and 14.1nM (7.70 ± 0.14), respectively (Figure 9d). The data is averaged from three separate cell thaws showing the robustness and reproducibility of the tau determination.

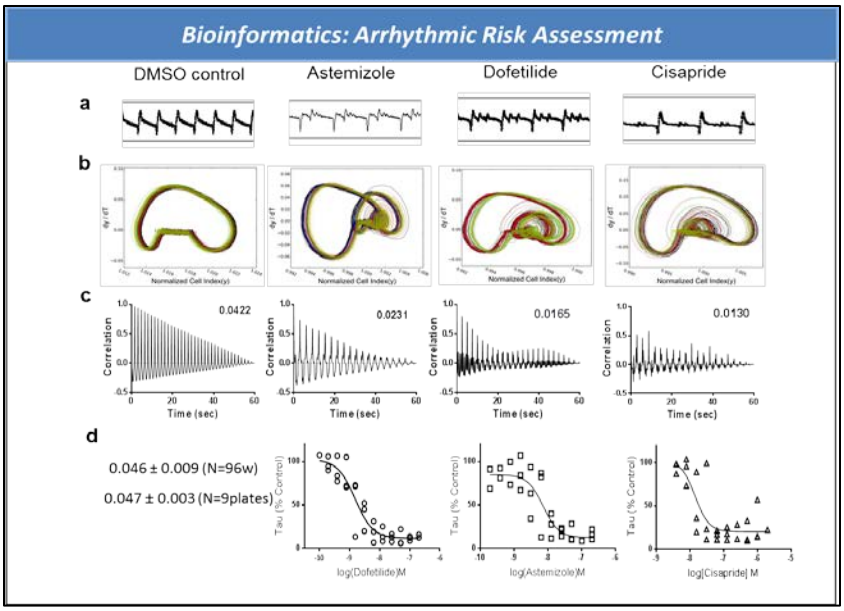

Figure 9. Limit cycle and autocorrelation analyses of impedance data monitoring cardiomyocyte contraction patterns following 1h treatment with 0.1% DMSO or 0.12µM or varying concentrations of astemizole, dofetilide, or cisapride.

The hiPSC-CM impedance traces, limit phase plots, and tau heat maps for pre- and 4h post-treatment with compounds tested at 10µM are shown in Figure 10. The limit cycle phase plots provide a visual representation for well-to-well consistency in beating rhythm in the pre-treated iPSC-CMs (Figure 10c) and flags wells that exhibit distinct oscillations after compound exposure (Figure 10d). Proarrhythmic compounds exhibit limit cycle plots with additional oscillation patterns; whereas, the limit cycle flattens in cases where beating ceases. The tau values provide a quantitative value for beat rhythm persistence. Tau values determined prior to compound treatment (Figure 10e) were uniform across a single plate with a mean tau value of 0.046 ± 0.009 (N=96 wells). These values are consistent plate-to-plate providing an average tau of 0.047 ± 0.003 (N=9 plates) and serve as quality control prior to treatment. Wells that exhibit a decrease in tau value, post-treatment, identify compounds that induce arrhythmia as shown in blue in Figure 10f. Tau values are sensitive to minor fluctuations in beat consistency, therefore, comparison of pre- and post-treatment for both the phase plots and tau values and replicate analysis will help in discriminating false positives from persistent cardiac arrhythmias.

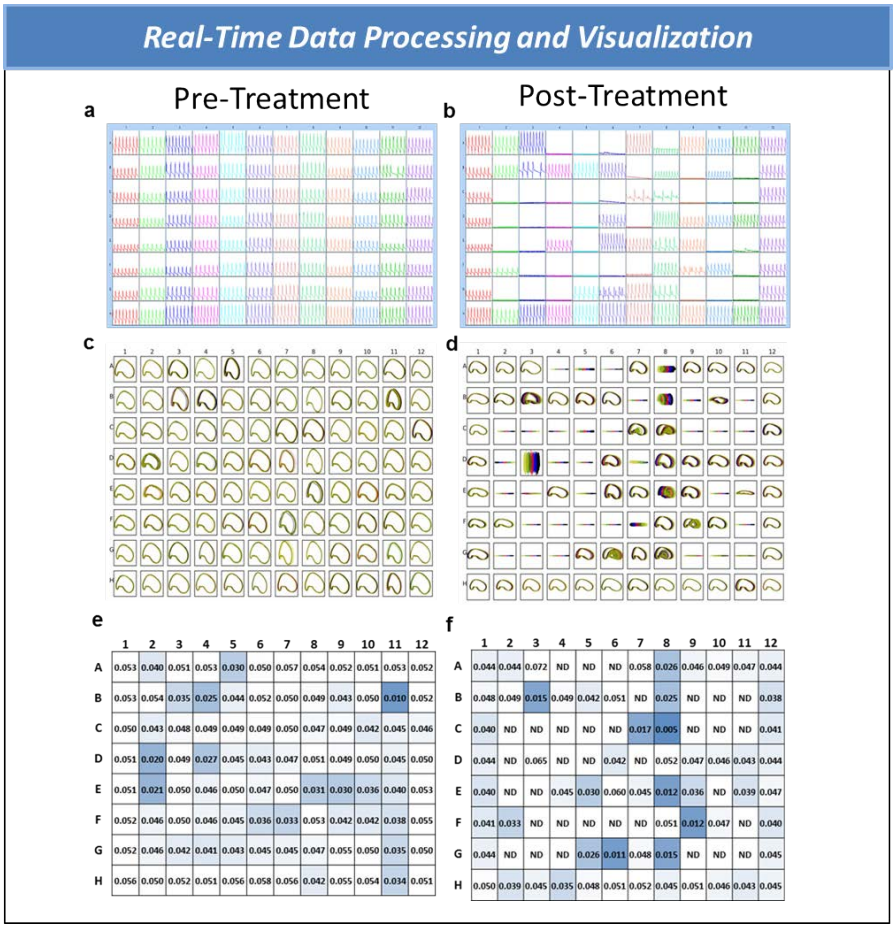

Figure 10. Automated limit cycle and autocorrelation analysis of 96-well impedance data from the xCELLigence RTCA Cardio system for hiPSC-derived cardiomyocytes prior to drug treatment (a,c,e) and 1h post treatment with 10µM compounds form the Enzo cardiotoxicity library (b,d,f).

From the results of our screen, 10 compounds were flagged as proarrhythmic based on their effect on the limit cycle and tau values. An additional 11 compounds that stopped cardiomyocyte beating at 10µM were found to induce arrhythmia when tested in concentration-response. These compounds are listed in Figure 11A along with their classification, tau IC_{50} values determined from autocorrelation function, IC_{50} values reported in the literature from manual and automated patch clamp studies, and whether the drugs are reported to have (+) or not have (-) occurrence of QT prolongation or TdP in the clinic. We also tested known proarrhythmics E4031, ibutilide and alfuzosin and include results in

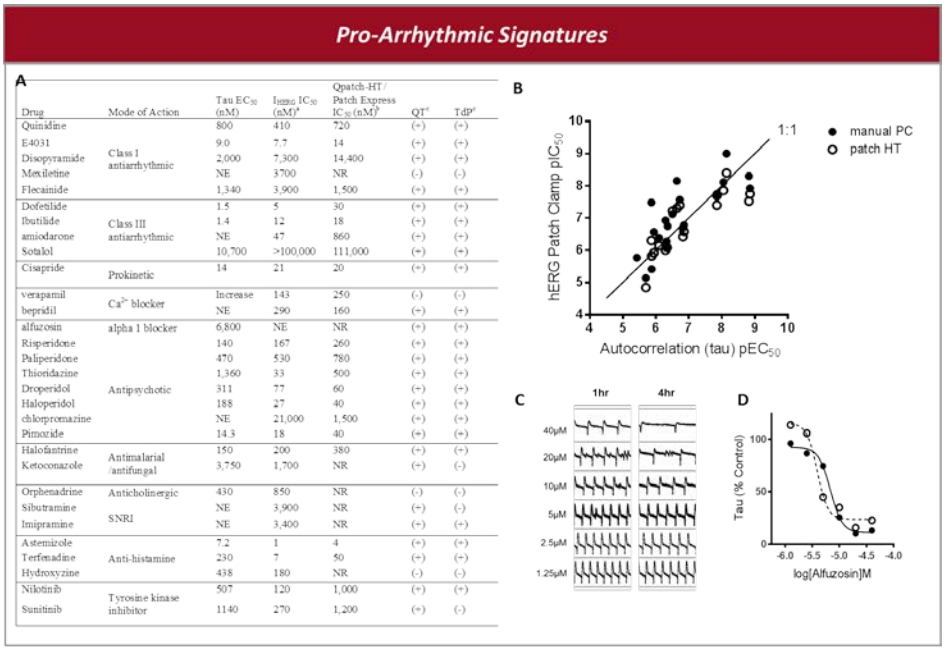

Figure 11. Pro-arrhythmic signatures. *(A) List of drugs and corresponding IC50 values for tau and hERG patch clamp. (B) Correlation of Tau pIC50 values versus pIC50 values for manual (open circles) and automated (closed circles) patch clamp. (C) Alfuzosin dose-dependent effect on impedance trances and D. Calculated tau.*

Figure 11A. A correlation graph of the pEC_{50} values determined by autocorrelation versus those determined by patch clamp for hERG inhibition is shown in Figure 11B. A Pearson correlation analysis resulted in statistically significant correlation ($r = 0.7882$ and 0.8345, $p < 0.0001$ for manual and automated patch clamp reported values, respectively); the comparison indicates our assay platform is selective and sensitive to hERG inhibitors. Drugs absent from the correlation but listed in Figure 11A include: (1) verapamil which showed a dose-dependent increase in tau corresponding to increased beat rate; the drug does not exhibit clinical liabilities; (2) mexiletine and sibutramine, which had no effect on tau; these drugs exhibit weak hERG inhibition and no reported TdP liabilities; (3) chlorpromazine, which stops beating below the reported IC_{50} value for hERG inhibition; (4) amiodarone, bepridil, and imipramine, which also had no effect on tau; these drugs inhibit hERG and have reported cardiac liabilities and are false negatives in our assay; and (5) sotalol and alfuzosin which induce irregular beating in the impedance assay and dose-dependently decrease tau. These drugs increase the risk of QT elongation and clinical arrhythmia but are not identified by hERG patch clamp assays.

Impedance traces illustrating beat irregularity induced by alfuzosin are shown in Figure 11C and concentration-response curves show alfuzosin decreased tau with EC_{50} = 3.9 and 6.8µM at 1h and 4h, respectively (Figure 11D). Taken together, our assay system is sensitive to both hERG and non-hERG arrhythmogenic compounds with an 86% accuracy rate.

3.1.2.4. Bioenergetic Platform. The bioenergetics assay was developed in hiPSC cardiomyocytes to assess cell's ability to meet an energy demand under stress via mitochondrial respiration (OCR) and identify mitochondrial dysfunction. The mitochondrial profile provides four parameters of mitochondrial function that can be measured in one experiment: basal respiration rate, ATP-linked respiration, proton leak, and reserve capacity (Figure 12A). As an example, the mitochondrial profile of bipredil at various concentrations is shown in Figure 12B. The results described here suggest that the development of cardiomyocyte injury, in this case caused by disruption of intracellular calcium, decreases ATP-linked oxygen consumption, diminishes respiratory efficiency, and depletes the bioenergetic reserve capacity (Figure 12C). The assay also measures the metabolic potential determined by comparing the baseline values from both the mitochondrial and glycolytic activity of the cells with metabolic activity under stressed conditions. The dose-dependent decrease in metabolic potential for the most potent compounds in the cardiotox library is shown in Figure 12D. During development, we found the assay platform to require testing compounds in quadruplicate for statistical significance. The assay is laborious and not cost effective to screen large collections of compounds. Thus, we decided to use the bioenergetic assay as a downstream characterization assay for the most toxic/potent hits. We first screened the selected hits at single dose of 20µM in quadruplicate and then in 5-point dose response in duplicate. The top twenty most toxic compounds identified from the functional physiology platform were compared with results in the phenotypic platform and the bioenergetics platform (Figure 13). Results indicate that the channel blockers showed the strongest decrease in bioenergetics reserve capacity and metabolic potential; whereas the antidepressants and anti-arrhythmic drugs increased the metabolic potential of the cells to respond to energy demand.

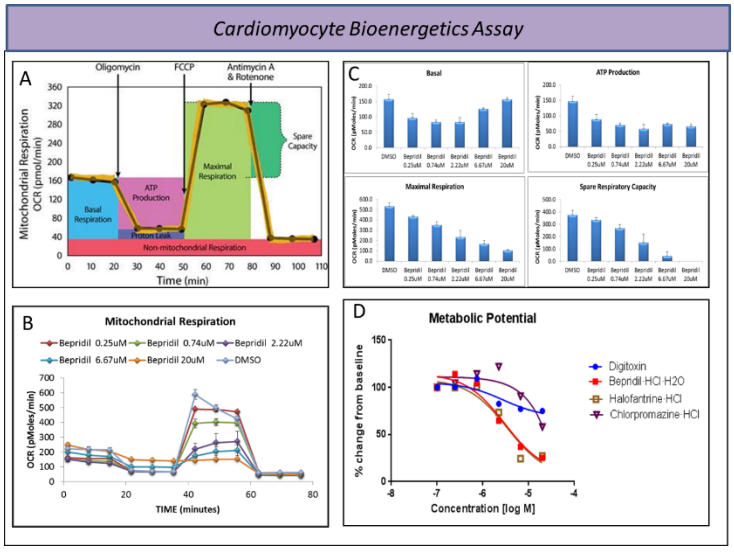

Figure 12. Cardiomyocyte bioenergetic assay platform.

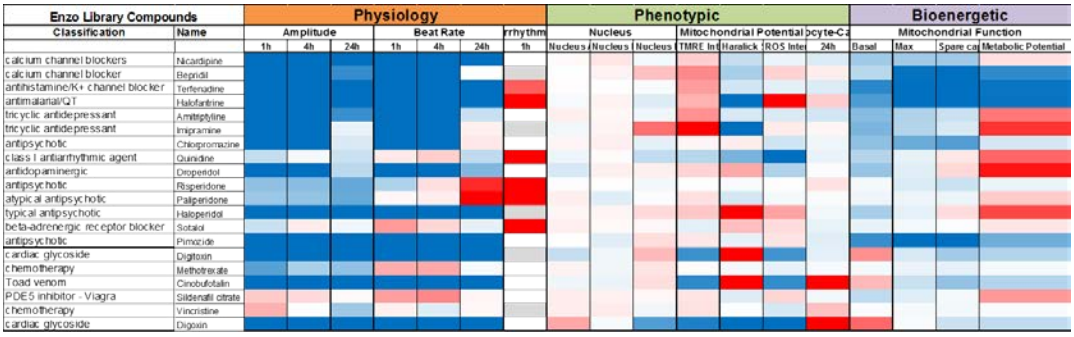

Figure 13. Top 20 cardiotoxic compounds from the library screen compared across the functional physiology, phenotypic and bioenergetics platforms.

3.1.3 Cardiomyocyte Conclusion. We have developed a robust 96w assay platform to monitor functional beating activity as impedance transients recorded from hiPSC-derived cardiomyocytes. In addition, we developed a 384w multiparametric, imaged-based assay platform. Both platforms were used to screen and identify toxic compounds from a library consisting of known cardiotoxicities and non-toxic controls. Readouts from our screen in the physiology assay include cellular index, beat amplitude, rate and irregularity at 1h, 4h and 24h. In the phenotypic screen, we quantified the acute effect of compounds on the following parameters: (1) nuclear area, size and brightness; (2) mitochondrial intensity; and (3) oxidative stress. Results from all readouts are recorded as standard deviation (SD) compared to DMSO treated wells. Each test plate performed with ≥ 3 SD in the mean of control wells. Results are presented in a heat map using a common software package facilitating a global view of the dataset, comparison of each parameter alone or in combination with any others, and determination of minimal threshold criteria required to advance compounds to further interrogation. PCA is employed to evaluate the distribution of reference compounds relative to unknowns. Concentration-response data is reported in CBIS database as separate test sets per readout per time. Changes in beat irregularity are quantified using a bioinformatic program we developed that processes raw data from the Cardio system. Genedata is used for the phenotypic DRC data analysis and visualization. Datasets are exported into excel files using a visualization/data-sharing program to feed into the QSAR analysis system.

We found the physiology platform to be the most sensitive in identifying acute cardiotoxicity. 55% of the cardiotoxic compound collection exhibited an effect on cardiomyocyte contractility at 10µM concentration and 91% of these are classified as drugs causing arrhythmia, heart attacks or TdP. Of the single point hits, 91.3% confirmed in DRC. None of the non-toxic control compounds in the ENZO library exhibited significant cardiotoxicity indicating a 0% false positive rate for the control compounds. On the other hand, only 6.9% of the cardiotox collection showed either a decrease in mitochondrial potential or increase in ROS without affecting nuclear parameters. It's important to point out that the concentration for the single point screen and for the DRC is 20µM due to limitation on maximum DMSO concentration that is tolerated by the cardiomyocytes, which is 0.2%. Considering the tox21 library tested at 100µm in HepG2 cells

only showed 11% mitotoxicity, our results are in line with this hit rate considering the library composition and the test concentration [1]. In future experiments we plan to obtain higher stocks of environmental toxins and perform screening at a starting concentration of 100uM and test compounds at three 10-fold dilutions in both the physiology and phenotypic platforms to determine the appropriate dose-range subsequent to 6-point DRC for all compounds.

As an additional readout for the physiology platform, we assessed compound beat irregularity by applying a nonlinear dynamical system analysis to the impedance recordings to generate limit cycle and autocorrelation graphs which provides a quantitative measure of irregularity. Our results identified pro-arrhythmic compounds in the library that induce clinical cardiac liabilities with an 86% accuracy rate. The novelty of this study is the application of limit cycle and autocorrelation analyses to RTCA data providing novel, semi-automated method to observe deviation in contraction rhythmicity is correlative to traditional patch clamp data and predictive of hERG and non hERG inhibiting drugs that potentially cause QT prolongation. This method combined with data sharing and visualization programs provides a powerful platform that can be integrated into a broader pre-clinical and toxicological paradigms. The program is available as an executable file and can be used as a standalone program to analyze beat patterns and potentially be modified to analyze real-time calcium flux responses or action potentials.

Our automated high-throughput approach is a powerful qualitative and quantitative method to provide higher throughput methods for assessing cardiac liabilities of potential toxins and to rank order compounds according to their predictive cardiac risk utilizing physiologically relevant human stem cell derived cardiomyocytes to bridge the gap between assay throughput and clinical relevance and reducing the overall number of compounds requiring extensive toxicity testing *in vivo.*

3.2 Hepatocyte Module

3.2.1 Hepatocyte Module Rationale. Current approaches to environmental toxicity screening rely on low-throughput, expensive animal models. There is a need for high-throughput technologies using human cell-based assays as a front line to assess toxicity of large numbers of unknown environmental toxins for risk assessment. This section highlights the hepatotoxic module of the toxicity platform. We have developed a multi-parametric testing platform utilizing acute and chronic phenotypic-based imaging assays and liquid chromatography and mass spectrometry technology as shown in Figure 14 to evaluate mechanisms of compound toxicity in human-derived iPSC hepatocytes (hiPSC-Hep) and primary conditioned hepatocytes (Hepatocells). This approach was applied to screening of the Enzo SCREEN-WELL hepatotoxicity library, which contains 238 structurally diverse and mechanistically distinct compounds as well as nontoxic controls. Compounds were tested at 20μM in the live cell imaging platform at 1h, 4h, 24h and 48h to assess both acute and chronic effects on cell viability, mitochondria potential, apoptosis and oxidative stress in a 384-well, multiplex plate format using fluorescent dyes specific to each readout. Dose-dependent and time-dependent changes in cell health were further characterized using our liquid chromatography and mass spectrometry screening platform to monitor specific inhibition of cytochrome P450 enzymes responsible for metabolism of most toxins in the liver that can lead to hepatotoxicity. We further characterized compounds by measuring fatty acid oxidation, oxidative phosphorylation, and glycolysis. The combination of using human-derived hepatocytes and multi-parametric analysis measuring phenotypic and functional responses has resulted in a robust high-throughput method to assess

human hepatotoxicity while reducing the overall number of compounds requiring extensive toxicity testing *in vivo*.

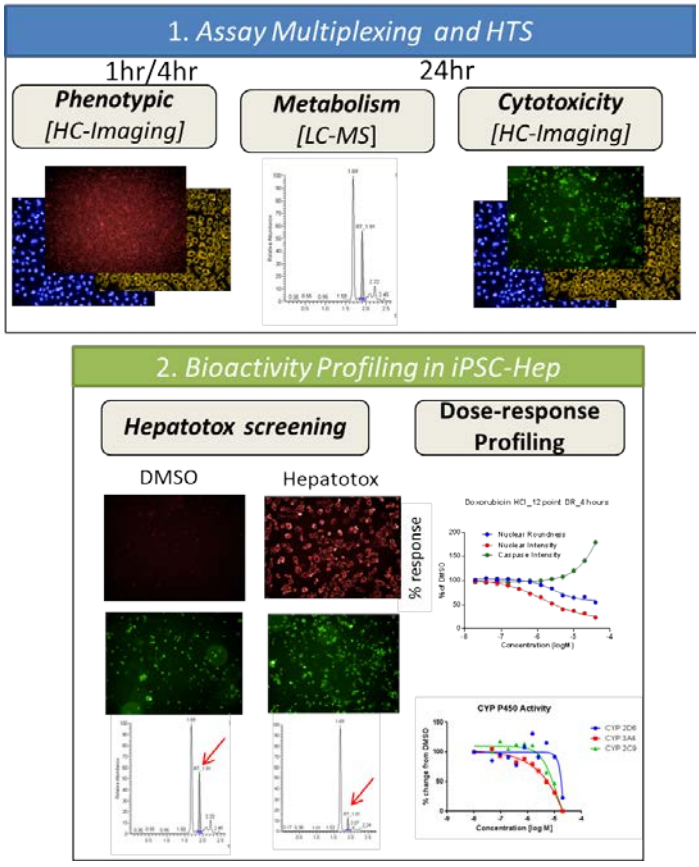

Figure 14. Hepatocyte module screening approach.

3.2.1.1 Hepatocyte Module Methods. *Phenotypic Assay* - Cellular Dynamics Inc. hiPSC-Hep were seeded at 18,000 cells/well on Corning Biocoat 384-well plates. The cells were incubated for 6 days with medium changes every 24h, after which they were treated with compounds for 24h. Following treatment cells were stained for 30 min with a dye solution containing 50nM TMRE for Mitochondrial Potential, 1ug/ml Hoechst for measuring effect on cell nuclei, 5µM Cell Event Caspase 3/7 for apoptosis, or 5µM CellRox Deep Red for measuring oxidative stress on cells. The images were obtained using Operetta High-Content Imaging System (Perkin Elmer) and analyzed using Harmony High-Content Imaging and Analysis software.

3.2.1.2 Cytochrome (CYP) P450 Metabolism. Corning Hepatocells were seeded at 20,000 cells/well. Two days post-seeding, cells underwent compound treatment for 24h. CYP Substrate cocktail containing Midazolam, Diclofenac & Dextromethorphan was added and incubated for 1h at 37°C/ 5%CO_2. Following incubation, 20µl of supernatant was transferred to a LCMS compatible plate. Stop solution containing Indomethacin as internal standard was added and plates were centrifuged at 3500 RPM for 10 mins. 60µL from the sample was aspirated and transferred to another plate and loaded on to the LCMS. Thermo Xcaliber software was utilized

for injecting the samples into the auto sampler and chromatograms are analyzed using the Xcaliber Quan Browser software. The area under the curve from the chromatograms was calculated by peak integration and exported in Microsoft Excel format. Cell viability was measured using CellTiter-Glo (Promega).

3.2.1.3 Cellular Bioenergetics. Cellular Dynamics Inc. hiPSC-Hep were seeded at 36,000 cells/well in collagen coated Seahorse plate and incubated for 6 days at 37°C/ 5%CO_2 with medium changes every 24h. On day 7, maintenance medium was replaced by Seahorse's bicarbonate-free medium containing 2.5mM Glucose, 1mM Sodium Pyruvate and 2mM Glutamine for Mitochondrial stress assay and 2mM Glutamine for Glycolysis stress assay. 10X concentration of compounds were added to the cells and the plate was incubated for 1h in a 37°C chamber (without CO_2). The Seahorse Cartridge containing compounds was loaded on the Seahorse XF96 analyzer for measuring either mitochondrial or glycolytic function. Data was analyzed using the Seahorse's WAVE software.

3.2.1.4 High Throughput Screening and Dose-Response Profiling. We screened the Enzo SCREEN-WELL hepatotoxicity library (Enzo Life Sciences, Farmingdale, NY). Screening data is recorded as standard deviation (SD) from control solvent and as percent change compared to multiple DMSO treated wells on each screening plate. Results are presented in a heat map using a common software package facilitating a global view of the dataset, comparison of each parameter alone or in combination with any others. From the heat map values, we determined the minimal threshold criteria required to classify compounds as "hits" and advance compounds to further interrogation as % response $\leq$ 40% for the LC-MS platform and > 3SD for the phenotypic platform. Statistical analysis and dose-response graph generation was performed with Genedata software for the phenotypic assays and GraphPad Prism version 7.0 for Windows (GraphPad, La Jolla, CA, USA) for the LCMS. Dose-response experiments were analyzed by non-linear regression (four parameters). Experimental data were statistically analyzed as indicated for each experiment.

3.2.2 Hepatocyte Module Results

3.2.2.1 Phenotypic Assay Development. We have developed and optimized a 3-color, multiplexed high content platform in the hiPSC-Hep (Figure 15). Compounds incubated for 1h and are analyzed for their effect on mitochondrial potential, oxidative stress (ROS), and nuclei morphology. Compounds incubated for 4h, 24h or 48h are analyzed for their effect on mitochondrial potential, apoptosis and nuclei morphology. Figure 15A highlights changes in TMRE intensity (yellow), caspase intensity (green), and nuclei channel intensity (blue) for DMSO or 1µM staurosporine after 24h treatment and changes in ROS (red) for DMSO or 50µM menadione after 1h treatment. The corresponding changes in phenotype across the dose-range in shown in Figure 15B.

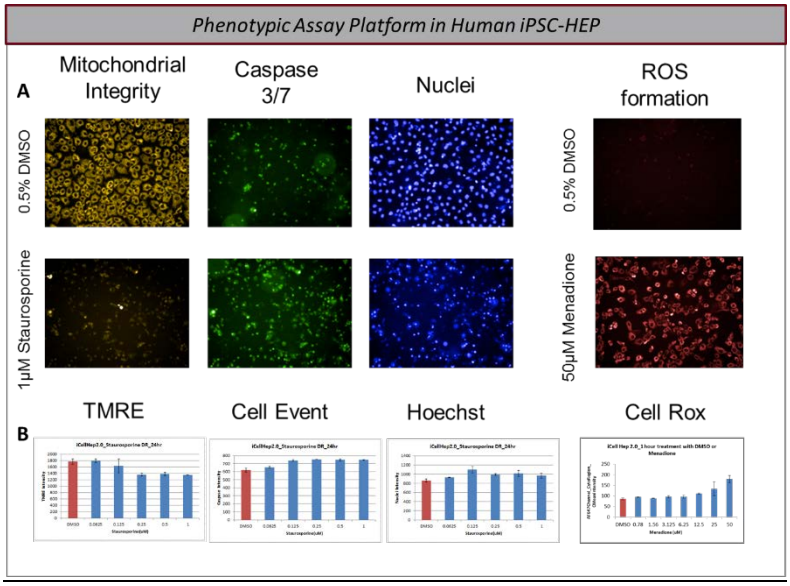

Figure 15. Hepatocyte phenotypic platform.

3.2.2.2 Metabolism LC-MS Assay Development. Transcriptome analysis performed on the hiPSC-Hep cells indicated that the most abundant CYP expression is 3A7 (2022) followed by 3A5 (48) and 3A4 (43). CYP 2C9 showed low expression (4.8) and CYP 2D6 was not detected. For this reason, we employed human primary conditionally immortalized hepatocytes to develop the metabolism assay. These cells exhibited significantly higher CYP P450 expression, are grown to scale, commercially available, and less expensive than iPSC-Hep. The iPSC-Hep cells were still superior over the primary cells for high content imaging; thus, we employed the iPSC-HEP cells for the phenotypic platform and primary-like Hepatocells for CYP P450 inhibition.

We chose to develop a 384-well LC-MS multiplexed assay to quantify CYP enzyme inhibition over commercially available luminescence protocols because the LC-MS approach allows for analytical peak quantification and is label-free and not subjected to dye interference. Figure 16 outlines the metabolite peak detection set-up and data analysis for CYP3A4, CYP2D6 and CYP2C9 metabolites per well of a 384-well plate. After 24h drug treatment, the supernatant is extracted and injected onto the liquid chromatography column to separate analytes based on polarity prior to injection into the mass spectrometer to determine analyte mass and abundance (Figure 16.1). The substrates for the three enzymes (i.e. CYP2C9, CYP3A4 and CYP2D6) are pooled together and incubated with cells for 1h prior to injection. The three CYP enzymes may be analyzed in a single well because the metabolites formed from the substrates specific to each CYP enzyme have distinct retention times (Figure 16.2). Three parameters are necessary to assess the quality of the metabolite peak. (1) The peak height is measured as peak intensity indicating the strength of the peak. (2) Retention time is the time at which the peak is detected (for example, the CYP 3A4 metabolite max peak intensity is detected at 1.81±2 min). (3) The total area under the curve (AUC) normalized to an internal standard is used to quantify the amount of metabolite detected (Figure 16.3). The resulting AUC for each CYP metabolite is quantified and shown in Figure 16.4.

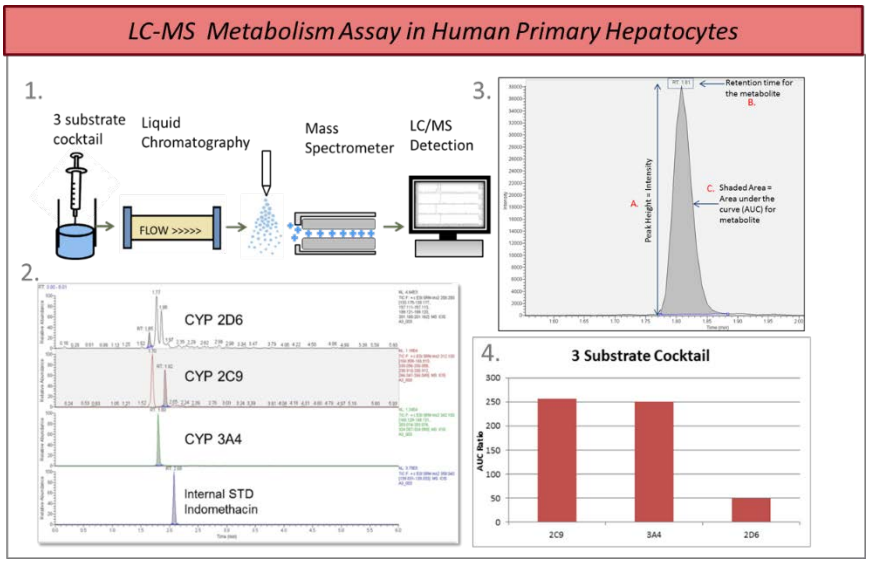

Figure 16. Hepatocyte module LC-MS metabolism assay development and validation.

We validated the LC-MS multiplexed assay in 384-well by testing 32 known compounds in duplicate and determining the AUC for each CYP metabolite. Sulfaphenazole, quinidine and ketoconazole are included as controls drugs that show selective CYP inhibition for 2C9, 2D6, and 3A4, respectively. To assess assay reproducibility, a set of 16 compounds were tested and analyzed on different days. The replicate data showed strong correlation for each CYP as shown in Figure 17. The assay is also multiplexed with viability to indicate cell health.

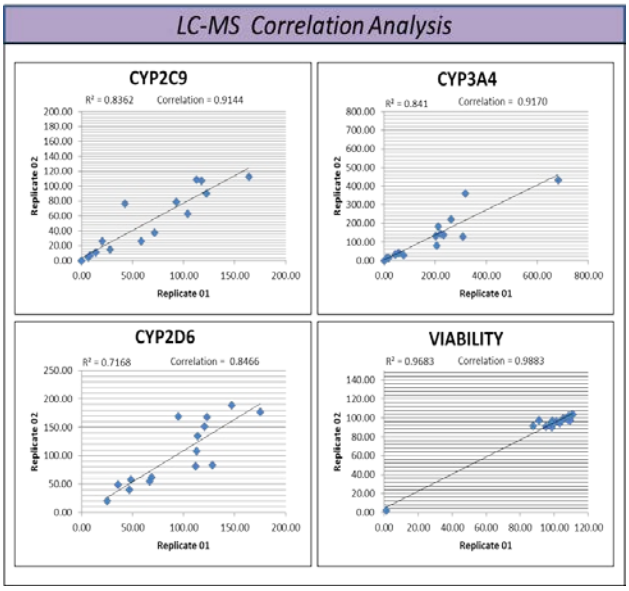

Figure 17. Correlation analysis per CYP tested in duplicate in the LC-MS metabolism platform.

3.2.2.3 High Throughput Screening. We applied the approach outlined in Figure 14, box 1 to screening of the hepatotoxicity library which contains 238 structurally diverse and mechanistically distinct compounds as well as nontoxic controls divided into 12 categories. The full library was tested in single point in duplicate in the phenotypic and metabolism platforms. The percent coefficient of variance (% CV) and SD of the control wells for each parameter in the phenotypic platform and the cellular metabolism platform is shown in Figure 18.

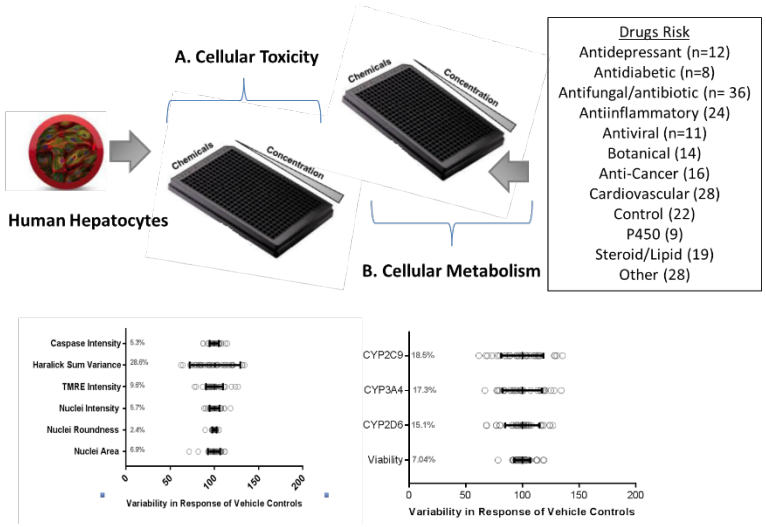

Figure 18. HTS hepatocyte module process: Coefficients of variance and standard deviations for DMSO control wells on each screening plate for the phenotypic and cellular metabolism platform readouts.

We employed PCA to plot and analyze the statistical distribution in the data set. PCA is used to convert the set of correlated observations into a set of uncorrelated variables called principal components. Figure 19 is a PCA plot of the set of 12 observations for the toxic and nontoxic compounds. The compounds are distributed according to the effects on each parameter. The overtly toxic compounds are shown on the left side of the PCA plot and highlight compounds that affect nuclear morphology versus caspase activation. In addition the cluster of compounds that decrease (blue shaded) MMP are shown on the right side of the plot. From the 30 control compounds, 3 controls affected two phenotypic parameters and were considered false positives (10%). Sorbitol was re-tested later and showed no effect in a dose-response assay at 24h. Three different compounds weakly effected CYP inhibition in the LC-MS metabolism platform also indicating a 10% false positive rate.

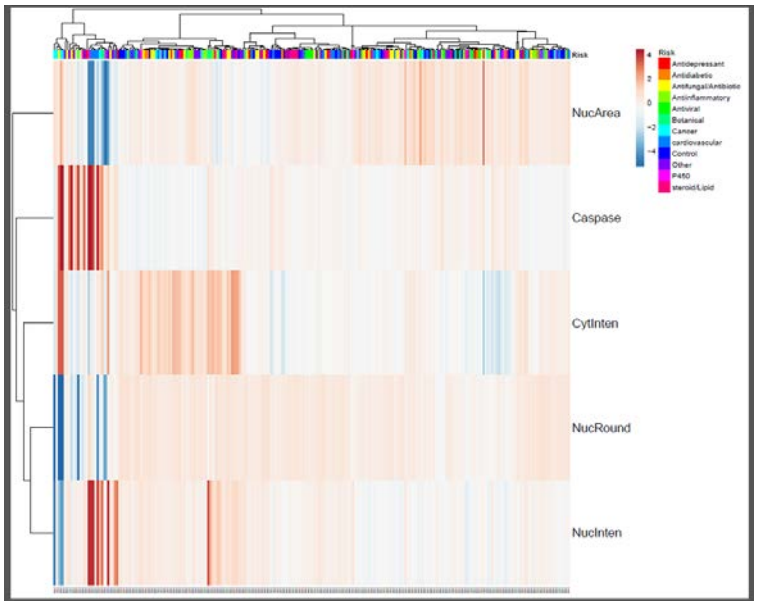

Figure 19. Principal component analysis for ENZO hepatotoxicity library tested in the phenotypic platform at 24h.

From the single point screen, 37 compounds were classified as toxic as they hit at least two nuclei parameters with the SD >3. Five additional compounds induced caspase activity. Eight compounds decreased MMP without affecting nuclear morphology. We binned compounds for acute and chronic effects on mitochondrial membrane potential, caspase and ROS and 7, 48, and 20 compounds were tested in 12-point concentration-response at 1h, 4h and 24h, respectively. These compounds represented the most toxic compounds as well as some not-toxic compounds. We obtained an 87% conformation rate for toxic compounds in DRC. In addition, 178 compounds were further tested at 48h in single point. Of these 178, 14 affected two or more nuclear parameters with the SD >3, 2 compounds decreased TMRE intensity and 18 showed Caspase 3/7 activation.

Compounds classified as antivirals, antidepressants, anti-inflammatory, antidiabetic and steroid/lipids exhibited little toxic effect in hiPSC-Hep; whereas compounds classified as P450 modulators, antifungal/antibiotic, botanical, anti-cancer, cardiovascular and other exhibited significant toxic effect in hiPSC-Hep.

For the LC-MS metabolism platform, we found annotations of CYP activity for 59 of the 208 hepatotoxic compounds (minus 30 non-toxic controls) which included all of the compounds that exhibited at least 60% or greater inhibition (≤ 40% enzyme activity) of any of the three CYP enzymes evaluated. Figure 20 shows the 59 annotated compound set and the corresponding CYP3A4 percent enzyme activity ranked from strongest inhibitors to strongest inducers and the corresponding results from the literature. A “Y” or “N” is noted indicating whether the compounds data is in agreement with literature results for CYP3A4 inhibitors. Therefore, in case of CYP3A4, 22 out of 30 are known/published inhibitors specifically of CYP3A4 (73.3% accuracy rate). We performed the same annotations for CYP2C9 and CYP2D6. For CYP2C9, 12 out of 16 are known/published inhibitors specifically of CYP2C9 (76% accuracy rate). For CYP2D6, 21 out of 25 (84% accuracy rate) are known/published inhibitors specifically of

CYP2D6. Additionally, 11 compounds showed significant inhibition of all three CYP enzymes and these compounds were shown to significantly decrease cell viability.

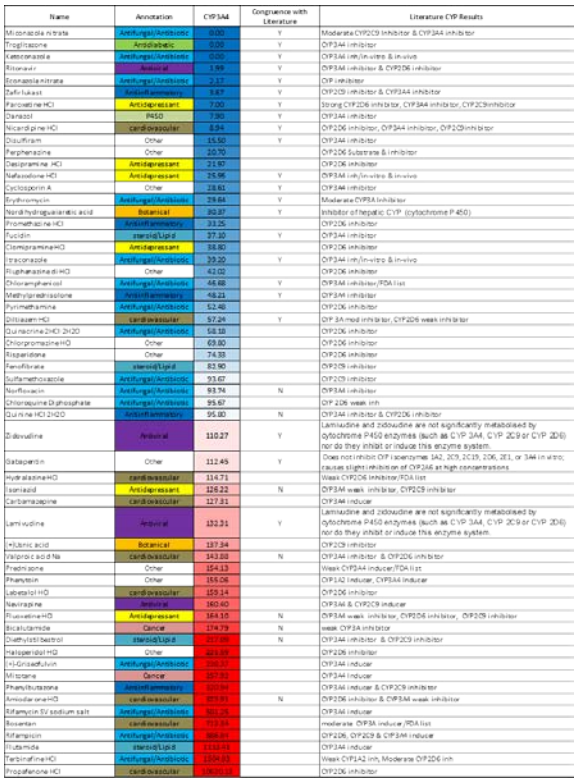

Name	Annotation	CYP3A4	Congruence with Literature	Literature CYP Results
Miconazole nitrate	Antifungal/Antibiotic	0.00	Y	Moderate CYP2C9 Inhibitor & CYP3A4 inhibitor
Troglitazone	Antidiabetic	0.00	Y	CYP3A4 inhibitor
Ketoconazole	Antifungal/Antibiotic	0.00	Y	CYP3A4 inh/in-vitro & in-vivo
Ritonavir	Antiviral	1.99	Y	CYP3A4 inhibitor & CYP2D6 inhibitor
Econazole nitrate	Antifungal/Antibiotic	2.17	Y	CYP inhibitor
Zafirlukast	Antiinflammatory	3.67	Y	CYP2D6 inhibitor & CYP3A4 inhibitor
Paroxetine HCl	Antidepressant	7.00	Y	Strong CYP2D6 inhibitor, CYP3A4 inhibitor, CYP2C9inhibitor
Danazol	P450	7.30	Y	CYP3A4 inhibitor
Nicardipine HCl	cardiovascular	8.94	Y	CYP2D6 inhibitor, CYP3A4 inhibitor, CYP2C9inhibitor
Disulfiram	Other	15.50	Y	CYP3A4 inhibitor
Perphenazine	Other	20.70		CYP2D6 Substrate & inhibitor
Desipramine HCl	Antidepressant	21.97		CYP2D6 inhibitor
Nefazodone HCl	Antidepressant	25.96	Y	CYP3A4 inh/in-vitro & in-vivo
Cyclosporin A	Other	28.61	Y	CYP3A4 inhibitor
Erythromycin	Antifungal/Antibiotic	29.84	Y	Moderate CYP3A inhibitor
Nordihydroguaiaretic acid	Botanical	30.37	Y	Inhibitor of hepatic CYP (cytochrome P-450)
Promethazine HCl	Antiinflammatory	33.25		CYP2D6 inhibitor
Fucidin	steroid/Lipid	37.30	Y	CYP3A4 inhibitor
Clomipramine HCl	Antidepressant	38.80		CYP2D6 inhibitor
Itraconazole	Antifungal/Antibiotic	39.20	Y	CYP3A4 inh/in-vitro & in-vivo
Fluphenazine di HCl	Other	42.02		CYP2D6 inhibitor
Chloramphenicol	Antifungal/Antibiotic	46.68	Y	CYP3A4 inhibitor/FDA list
Methylprednisolone	Antiinflammatory	48.21	Y	CYP3A4 inhibitor
Pyrimethamine	Antifungal/Antibiotic	52.48		CYP2D6 inhibitor
Diltiazem HCl	cardiovascular	57.24	Y	CYP 3A mod inhibitor, CYP2D6 weak inhibitor
Quinacrine 2HCl 2H2O	Antifungal/Antibiotic	58.38		CYP2D6 inhibitor
Chlorpromazine HCl	Other	69.80		CYP2D6 inhibitor
Risperidone	Other	74.38		CYP2D6 inhibitor
Fenofibrate	steroid/Lipid	82.90		CYP2C9 inhibitor
Sulfamethoxazole	Antifungal/Antibiotic	93.67		CYP2C9 inhibitor
Norfloxacin	Antifungal/Antibiotic	93.74	N	CYP3A4 inhibitor
Chloroquine Diphosphate	Antifungal/Antibiotic	95.67		CYP 2D6 weak inh
Quinine HCl 2H2O	Antiinflammatory	95.80	N	CYP3A4 inhibitor & CYP2D6 inhibitor
Zidovudine	Antiviral	110.27	Y	Lamivudine and zidovudine are not significantly metabolised by cytochrome P450 enzymes (such as CYP 3A4, CYP 2C9 or CYP 2D6) nor do they inhibit or induce this enzyme system.
Gabapentin	Other	112.45	Y	Does not inhibit CYP isoenzyme 1A2, 2C9, 2C19, 2D6, 2E1, or 3A4 in vitro; causes slight inhibition of CYP3A6 at high concentrations
Hydralazine HCl	cardiovascular	114.71		Weak CYP2D6 inhibitor/FDA list
Isoniazid	Antidepressant	126.22	N	CYP3A4 weak inhibitor, CYP2C9 inhibitor
Carbamazepine	cardiovascular	127.31		CYP3A4 inducer
Lamivudine	Antiviral	132.31	Y	Lamivudine and zidovudine are not significantly metabolised by cytochrome P450 enzymes (such as CYP 3A4, CYP 2C9 or CYP 2D6) nor do they inhibit or induce this enzyme system.
Kjubic acid	Botanical	137.34		CYP2C9 inhibitor
Valproic acid Na	cardiovascular	143.83	N	CYP3A4 inhibitor & CYP2D6 inhibitor
Prednisone	Other	154.13		Weak CYP3A4 inducer/FDA list
Phenytoin	Other	155.06		CYP1A2 inducer, CYP3A4 inducer
Labetalol HCl	cardiovascular	159.14		CYP2D6 inhibitor
Nevirapine	Antiviral	160.40		CYP3A4 & CYP2C9 inducer
Fluoxetine HCl	Antidepressant	164.15	N	CYP3A4 weak inhibitor, CYP2D6 inhibitor, CYP2C9 inhibitor
Bicalutamide	Cancer	174.79	N	weak CYP3A inhibitor
Diethylstilbestrol	steroid/Lipid	177.09	N	CYP3A4 inhibitor & CYP2C9 inhibitor
Haloperidol HCl	Other	183.99		CYP2D6 inhibitor
(+)-Griseofulvin	Antifungal/Antibiotic	186.37		CYP3A4 inducer
Mitotane	Cancer	187.80		CYP3A4 inducer
Phenylbutazone	Antiinflammatory	190.84		CYP3A4 inducer & CYP2C9 inhibitor
Amiodarone HCl	cardiovascular	193.91	N	CYP2D6 inhibitor & CYP3A4 weak inhibitor
Rifamycin SV sodium salt	Antifungal/Antibiotic	861.25		CYP3A4 inducer
Bosentan	cardiovascular	910.34		moderate CYP3A inducer/FDA list
Rifampicin	Antifungal/Antibiotic	966.84		CYP2D6, CYP2C9 & CYP3A4 inducer
Flutamide	steroid/Lipid	1132.43		CYP3A4 inducer
Terbinafine HCl	Antifungal/Antibiotic	1304.03		Weak CYP1A2 inh, Moderate CYP2D6 inh
Propafenone HCl	cardiovascular	1670.14		CYP2D6 inhibitor

Figure 20. Heat map of compounds in the Enzo hepatoxic library tested in single point at 24h in the LC-MS metabolism platform and analyzed as selective CYP3A4 inhibitors.

3.2.2.4 Bioactive Profiling in Dose-Response. The most toxic compounds that confirmed in DRC at 48h included: fluoxetine, ketoconazole, atorvastatin, aflatoxin B2, deoxynivalenol and paclitaxel. Figure 21 shows a heat map of compounds in the Enzo hepatoxic library tested in 12-pt concentration-response at 4h and analyzed against four parameters. Colors blue, white, and red denote decreased, equivalent and increased deviation from DMSO, respectively. We only consider decreases in TMRE intensity as toxic. An increase in TMRE intensity is most likely due to an effect not related to mitochondrial potential. Compounds did not significantly decrease TMRE intensity (not shown). Of the 48 compounds tested at 4h, 40% showed dose-dependent activity. Anti-fungal, anti-inflammatory and anti-cancer classified drugs showed dose-dependent effect on nuclear morphology and apoptosis activation. Seven of these compounds were retested at 1h (Figure 22A). The dose-dependent effect of daunorubicin on nuclear intensity and roundness and ROS is shown in Figure 22B.

Figure 21. Heat map of compounds in the Enzo hepatoxic library tested in 12-pt concentration-response at 4h and analyzed against four parameters.

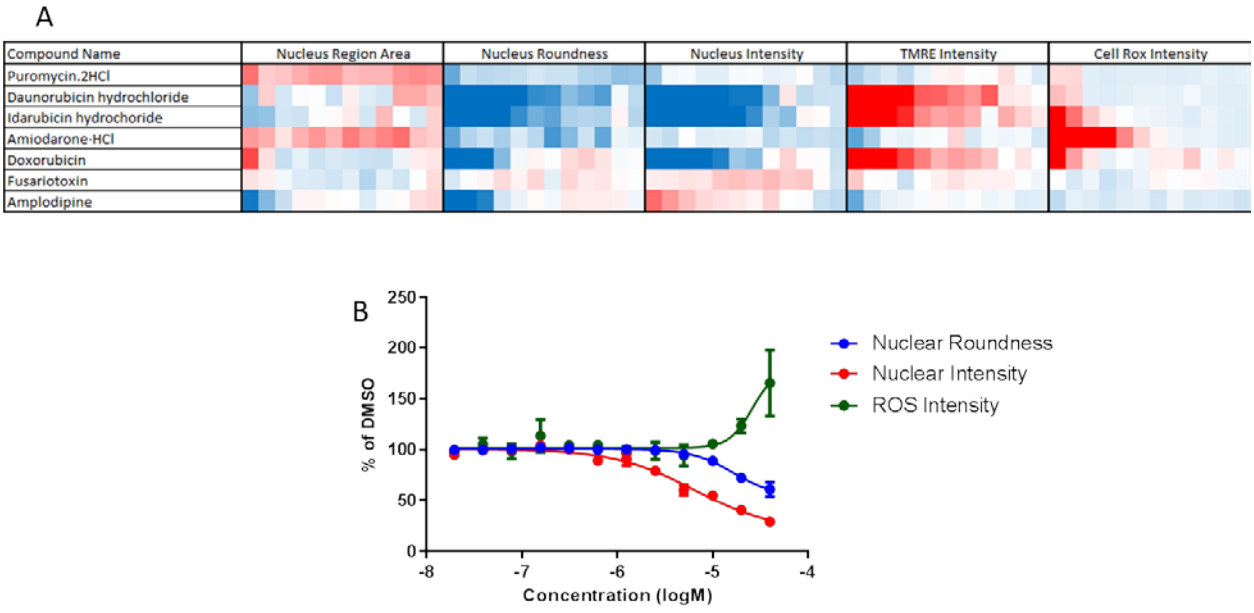

Figure 22. Heat map of compounds in the Enzo hepatoxic library tested in 12-pt concentration-response at 1h and analyzed against five parameters.

3.2.2.5 Bioenergetics Platform. The bioenergetics assay was developed in hiPSC hepatocytes to assess cell's ability to meet an energy demand under stress via mitochondrial respiration (OCR) and identify mitochondrial dysfunction. As described in the cardiomyocyte platform, the mitochondrial profile provides four parameters of mitochondrial function that can be measured in one experiment: basal respiration rate, ATP-linked respiration, proton leak, and reserve capacity. As an example, the mitochondrial profile of nefadazone at various concentrations is shown in Figure 23A. The results described here suggest that the development of hepatocyte injury, in this case caused by potent inhibition of CYP 3A4, decreases ATP-linked oxygen consumption, diminishes respiratory efficiency, and depletes the bioenergetic reserve capacity (Figure 23B). The assay also measures the metabolic potential determined by comparing the baseline values from both the mitochondrial and glycolytic activity of the cells with metabolic activity under stressed conditions (Figure 23C). During development, we found the assay platform to require testing compounds in quadruplicate for statistical significance. The assay is laborious and not cost effective to screen large collections of compounds. Thus, we decided to use the bioenergetic assay as a downstream characterization assay for the most toxic/potent hits. We validated the assay by testing 32 known hepatotoxic compounds. Ketoconazone, troglitazone, nefazadone and tamoxifen showed the most significant decrease in stressed OCR and metabolic potential.

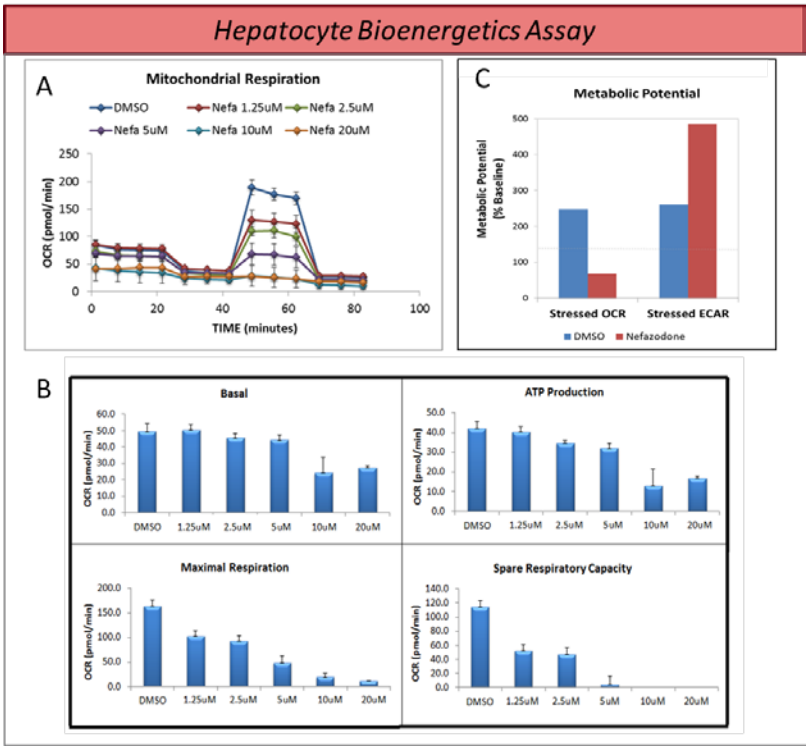

Figure 23. Hepatocyte bioenergetic assay platform.

3.2.3 Hepatocyte Module Conclusion. The liver is the main organ responsible for the metabolism of xenobiotics and the variety of toxic agents potentially resulting in acute live injury is extensive. We developed dual 384-well multiplexed assay platforms to detect acute and

chronic phenotypic changes in hiPSC-Hep cells and to measure hepatic function via CYP enzyme activity in human Hepatocells.

We find that the phenotypic parameter to detect toxin induction of apoptosis at 24h and 48h in hiPSC-Hep cells is informative. As hepatocytes exhibit more resistance to toxicity as compared to cardiomyocytes, identifying a toxic compound as inducing apoptosis or general necrosis is important. We also find that we detected significant enzyme activity of CYP2C9, CYP3A4 and CYP2D6 by LC-MS in conditionally immortalized, adult human primary hepatocytes. These CYPs metabolize nearly 90% of xenobiotics. We validated specificity and selectivity for known CYP inhibitors with robust assay performance and identified CYP inhibitors in the hepatotoxic library with between 83-87% accuracy indicating that the human conditionally immortalized hepatocytes represent mature human hepatocytes. Our robust approach allows us to classify compounds as nontoxic or as mito-toxic, apoptotic, or nuclear toxic and will provide a statistical cut-off for testing compounds according to dose and exposure time.

We are interested in the bioactivation of environmental toxins by the liver and the subsequent toxicity to other tissues and plan to apply our LC-MS platform to the development and validation of a biotransformation assay. Compound biotransformation is an important factor that can lead to the generation of toxic metabolites by the liver that may lend to toxicity in other organ systems such as the heart. As described, we have developed a sensitive cardiomyocyte contractility platform. We will optimize media conditions and apply hepatocyte supernatant, from treated and untreated cells with controls, to human hepatocytes, establish a baseline response and monitor changes in physiology due in part by phase 1 liver biotransformation which we track by LC-MS.

Environmental Toxin Library and USAF Compounds Tested on the Cardiomyocyte and Hepatocyte Modules: We applied our established screening approach to testing the environmental toxin (neurotox) library in the cardiomyocyte physiology assay at 20μM at 1h, 4h and 24h, cardiomyocyte phenotypic assay at 1h and hepatocyte phenotypic assays at 1h and 24h. The PCA plots are shown in Figure 24A and 24B. In both graphs, the group of compounds classified as pesticides (purple) cluster together as exhibiting the strongest deviations from DMSO in contractility and phenotype; whereas, the pharmaceutical classified compounds (orange) are clustered together and exhibit the weakest deviations from DMSO.

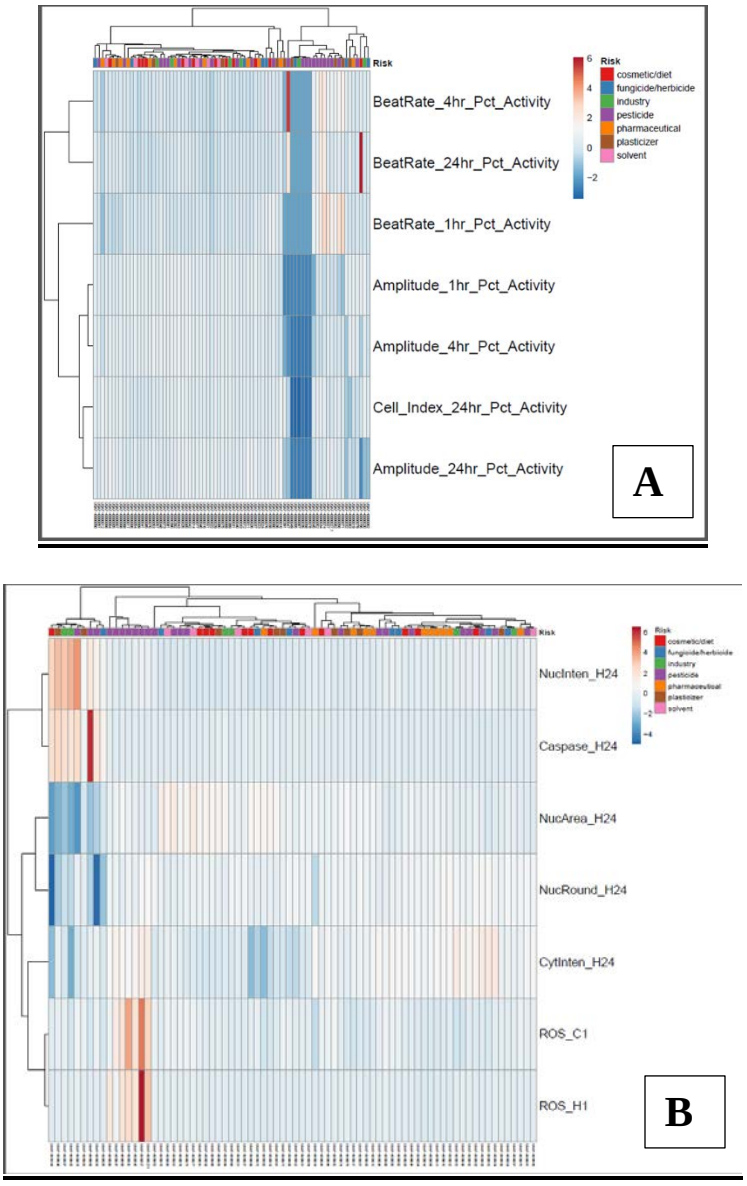

Figure 24. Principal component analysis for neurotoxin library. *(A) Tested in the Physiology Platforms at the indicated incubation times. (B) Tested in the Phenotypic Platforms at the indicated incubation times. (_H24 and _H1 denotes hepatocytes testing at 24h and 1h respectively. _C1 denotes cardiomyocytes testing at 1h).*

In addition, we tested 7 USAF compounds in single point at 100µM in physiology and LCMS assays and at 50 µM in phenotypic assay and in DRC. The compounds are listed in Figure 25A along with their toxin class and denoted in red whether the compound hit in the various parameters. The skin irritant, scotchguard and corrosive compounds did not show significant toxicity across the parameters with the exception of perfluorooctanoic acid which showed CYP2C9 inhibition. The two tricresyl phosphate isomers (AChE inhibitors) and the insecticide transfluthrin (sodium channel blocker) exhibited significant toxicity across the parameters predominately in the contractility platform. The tricresyl phosphate isomers showed

significant dose-dependent activity in the CYP P450 platform (Figure 25B). Transfluthrin exhibited dose-dependent decrease in cardiomyocyte beat rate and amplitude (Figure 25C), dose-dependent increase in cardiomyocyte ROS and decrease in nuclear roundness at 1h (Figure 25D), and dose-dependent increase in hepatocyte ROS and decrease in nuclear roundness at 1h Figure 25E).

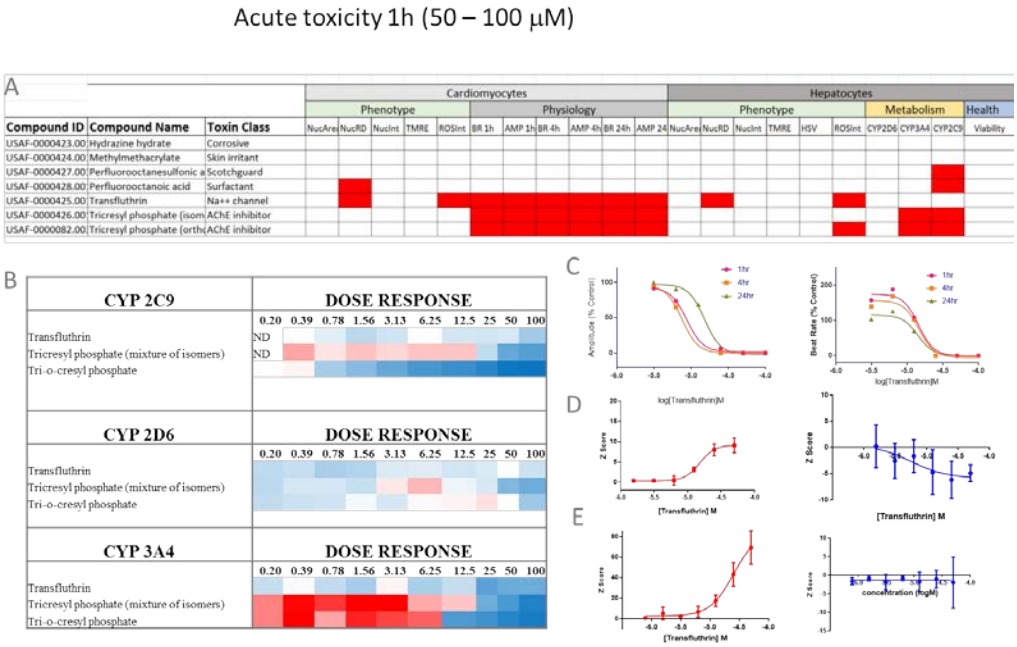

Figure 25. (A) USAF compounds tested in single point in the cardiomyocyte and hepatocyte modules and denoted as a hit in red. (B) Heatmap of SD at various concentrations for three USAF compounds tested in the LC-MS platform. (C-E) Dose-dependent response of transfluthrin tested in cardiomyocyte physiology platform, cardiomyocyte phenotypic ROS (red) and nuclear roundness (blue), and hepatocyte phenotypic ROS (red) and nuclear roundness (blue), respectively.

3.3 Neuronal Module

3.3.1 Neurotoxin Chemical Library. The neurotoxin library and associated control compounds were assembled based on published reports for developmental neurotoxicity by the United States Environmental Protection Agency (EPA) and relevant literature [4,5]. Compounds were entered into our Chemical and Biological Information System (CBIS). They were then solvated in water (18) or DMSO (63) to 33mM and plated on master plates. The master plates were then distributed to multiple individual 384 low dead-volume daughter plates containing the entire library in 10µl aliquots.

Compounds were selected for a variety of proposed toxic mechanisms including effects on morphology, mitochondria and neural activity. 9 main categories of toxin exposure are represented as well as multiple subgroups, such as 7 types of pesticides (Table 1).

Table 1. Neurotoxin Library Classification by Toxin Exposure and Chemical Subgroup

Compound	Exposure	Toxin Subgroup
Butylated hydroxytoluene	cosmetic and diet	
Lead acetate	cosmetic	
Aluminum (lactate)	cosmetic and diet	
Butylated Hydroxy Anisole	diet	
Monosodium Glutamate	diet	
Arsenic(III) oxide	diet and industry	
Saccharin sodium salt	diet	
D-Sorbitol	diet	
Aspartame	diet	
Acrylamide	diet and industry	
Chlorine dioxide	diet	
Methylmercury	industry	
Cadmium chloride	industry , production	
Manganese (II) chloride	industry , production	
Benzene	industry	
Lead Nitrate	industry	
Hexachlorobenzene	industry , production	
Carbaryl	pesticide	carbamate
Aldicarb	pesticide	carbamate
Hexachlorophene	pesticide	organochlorine
Dieldrin	pesticide	organochlorine
Heptachlor	pesticide	organochlorine
Lindane	pesticide	organochlorine
Chlorpyrifos	pesticide	organophosphorus,
Chlorpyrifos oxon	pesticide	organophosphorus,
Diazinon	pesticide	organophosphorus,
Dichlorvos	pesticide	organophosphorus,
Paraoxon	pesticide	organophosphorus,
Parathion (ethyl)	pesticide	organophosphorus,
Methylparathion	pesticide	organophosphorus,
Trichlorfon	pesticide	organophosphorus,
Trichloropyridinol	pesticide	organophosphorus,
Bis(tri-n-butyltin)oxide	pesticide	organotin
Tributyltin chloride	pesticide	organotin
Allethrin	pesticide	pyrethroid
Bifenthrin	pesticide	pyrethroid
Cypermethrin	pesticide	pyrethroid
Deltamethrin	pesticide	pyrethroid
Permethrin	pesticide	pyrethroid
2,4-Dinitrophenol	pesticide	
DEET (N,N-Diethyl-3-Methyl benzamide)	pesticide	

Compound	Exposure	Toxin Subgroup
Maneb	fungicide	
Fluazinam	fungicide	
Tebuconazole	fungicide	
Benomyl	fungicide	benzimidazole
Acibenzolar-S methyl	fungicide	
Glyphosate	herbicide	organophosphorus
Paraquat	herbicide	viologen
Dichlorophenoxyacetic acid	herbicide	
Acetaminophen	pharmaceutical	
Diphenhydramine HCl	pharmaceutical	
Omeprazole	pharmaceutical	
Menadione	pharmaceutical	
t-retinoic acid	pharmaceutical	
Dexamethasone	pharmaceutical	
Vincristine	pharmaceutical	
Cocaine	pharmaceutical	
U0126	pharmaceutical	
Amoxicillin	pharmaceutical	
Bis-indolylmaleimide 1 (Bis-1)	pharmaceutical	
Valproic acid	pharmaceutical	
Amphetamine	pharmaceutical	
5,5-Diphenylhydantoin	pharmaceutical	
Nicotine	pharmaceutical	
Ketamine	pharmaceutical	
Lithium Chloride	pharmaceutical	
Dimethyltin dichloride	plastics	organotin
Triethyltin chloride	plastics	organotin
Trimethyltin chloride	plastics	organotin
Dibutyltin	plastics, consumer goods	
Bis (2-ethylhexyl) phthalate	plastics, consumer goods	
Mercury (II) Chloride	plastics	
Bisphenol A	plastics, consumer goods	
Dimethyl Phthalate	plastics, consumer goods	
PBDEs-Polybrominated diphenyl ethers	consumer good	
Tricresyl phosphate	plastics, solvents	
2-ethoxyethyl Acetate	solvent	glycol ether
Ethanol	solvent	
Methanol	solvent	
Methoxyethanol	solvent	
Trichloroethylene	solvent	
Toluene	solvent	

Compounds group into 9 major categories by exposure type. Several chemical subgroups can be further classified, such as 7 chemical classes represented within the pesticide category.

3.3.2 Cellular Phenotypes

3.3.2.1 Objective. Neurotoxins can directly impact cellular function, lead to morphological changes and ultimately dysregulate systems level function. In order to determine whether an essential neuronal process has been disrupted by chemical exposure, we have developed two primary assays to assess autonomous neuronal phenotypes, one for neuron morphology and one for mitochondrial function. Neuron morphology was determined by multiparametric examination of neurite growth or retraction. Neuronal mitochondrial function was evaluated by measuring mitochondrial membrane potential changes and induction of reaction oxygen species. Both assays were developed as high content, high throughput, image based screening platforms with automated analysis. Overall, we have established and validated assays to assess neurotoxic phenotypes of chemical exposure.

3.3.2.1.1 Neurite Growth Assay. Axonal and dendritic (neurite) growth is a fundamental process of neuron development and function. Dysregulation of neurite growth can be detrimental. Excessive neurite growth has been linked to the onset of pain or excess synapses to neurological disease such as autism spectrum disorders [6,7]. Conversely, neurite retraction can be detrimental to the nervous system as there is a limited capacity for regeneration following injury. Neurite growth has been used to monitor the effects of small molecules on rodent primary neurons and neuron-like transformed cell lines, to monitor development and differentiation, model axonal regeneration, and assess neurotoxicity. We have used neurite growth and retraction as phenotypic read-outs to identify toxins that could negatively impact neuronal development and function.

We have established and validated an assay to assess neuronal morphology in response to toxin exposure. Our assay was developed to monitor phenotypic changes to multiparametric morphological measurements following chronic (3 day) toxin treatment. As neurite degeneration is a precursor to cell death, as evidenced in neurodegenerative disease or toxin exposure (ref), we have included nuclear measures of cell health to distinguish between frank cytotoxicity and neurite specific effects.

3.3.2.1.1.1 Methods

3.3.2.1.1.1.1 Cell culture. HiPSC-derived neurons (iCell neurons; Cellular Dynamics Inc.) were cultured according to manufacturer's protocols. Neurons were thawed and plated directly onto poly-D-lysine coated 384-well clear-bottom plates (Corning Life Sciences) at a density of 4000 cells/well using a 384-well electronic pipette (Integra Biosciences Corp.). Neurons were plated in manufacturer's provided medium supplemented with 3.33 µg/ml laminin (Sigma-Aldrich). Adult human dermal fibroblasts were cultured in DMEM high glucose (Corning) supplemented with 10% fetal bovine serum (Corning) and 1% L-Glutamine (Gibco). For screening assays, fibroblasts were plated at a density of 4000 cells/well in tissue-culture treated 384-well plates (Greiner).

3.3.2.1.1.1.2 High content screening assay. Prior to compound addition 25 µl/well of medium was removed from screening plates (25 µl/well remaining). Compounds were transferred to screening plates from in a 16-point half-log dose series from 33 µM to 0.8 pM using an Echo liquid handler (Labcyte Inc.). Assay plates were backfilled with DMSO to maintain a constant DMSO level of 0.1% across all concentrations screened. After compound addition 75 µl/well fresh medium was added to the screening plate for a final assay volume of 100 µl/well. Assay plates were then incubated for three days prior to fixation and immunostaining (Figure 26). Control compounds were added to each assay plate to produce neurite outgrowth (Staurosporine, 0.2 µM) or neurite retraction (BIO, 2.5 µM).

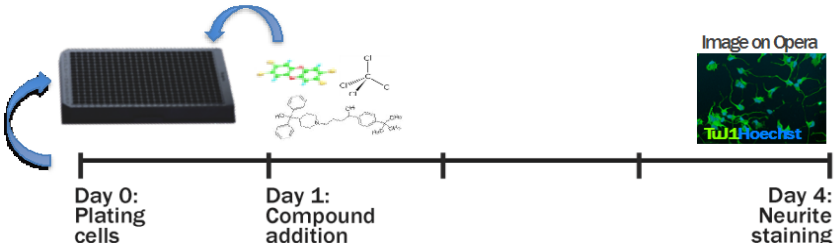

Figure 26. Neurite growth assay timeline. *hiPSC-derived cortical neurons (iCell) were plated on 384-well high throughput imaging plates. One day post-plating, compounds were added by acoustic dispenser to the neurons. Three days later, neurons were fixed and stained for neuron structural protein marker, TUJ1 and nuclear marker Hoechst.*

3.3.2.1.1.1.3 Immunofluorescence. At the endpoint of the screening assay culture medium was removed and cells were fixed with 4% formaldehyde for 20 minutes at room temperature. For neural staining, cells were then washed three times with DPBS and incubated overnight with anti-TUJ1 antibody (1:500 dilution, from Covance Inc.) in DPBS supplemented with 5% normal donkey serum (Jackson ImmunoResearch Laboratories, Inc.) and 0.1% Triton X-100 (Sigma-Aldrich). Following primary antibody incubation plates were washed three times with DPBS and incubated with an Alexa Fluor 488 conjugated donkey anti-mouse secondary antibody (1:500 dilution, from Thermo Fisher Scientific) in DPBS supplemented with 1% normal donkey serum and 0.1% Triton X-100 for two hours at room temperature. Assay plates were then washed three times with DPBS and nuclei were stained with Hoechst 33342 (5 µg/ml; Thermo Fisher Scientific) for imaging. Fibroblast plates were washed after fixation and proceeded directly to nuclear staining with Hoechst 33342.

3.3.2.1.1.1.4 High content imaging and analysis. Assay data was acquired using an Opera confocal microplate imaging system (PerkinElmer, Inc.) using a 20x air objective. For each well screened six fields were imaged. Acquired images were analyzed using Columbus software (PerkinElmer) to identify nuclei and neurite segments (Figure 27). The parameters used with the find nuclei block to identify healthy nuclei in hiPSC derived neurons are: method: B, common threshold: 0.40, area > 60 µm^2, split factor: 7.0, individual threshold: 0.40, contrast > 0.10. The parameters used for the find neurites block are: method: CSIRO Neurite Analysis 2, smoothing width: 3 px, linear window: 9 px, contrast > 2, diameter ≥ 7 px, gap closure distance ≤ 9 px, gap closure quality: 0, debarb length ≤ 10 px, body thickening: 5 px, tree length ≤ 0 px. Fibroblast images were analyzing with a modified find nuclei block as follows: method: B, common threshold: 0.60, area > 50 µm^2, split factor: 7.0, individual threshold: 0.40, contrast > 0.10.

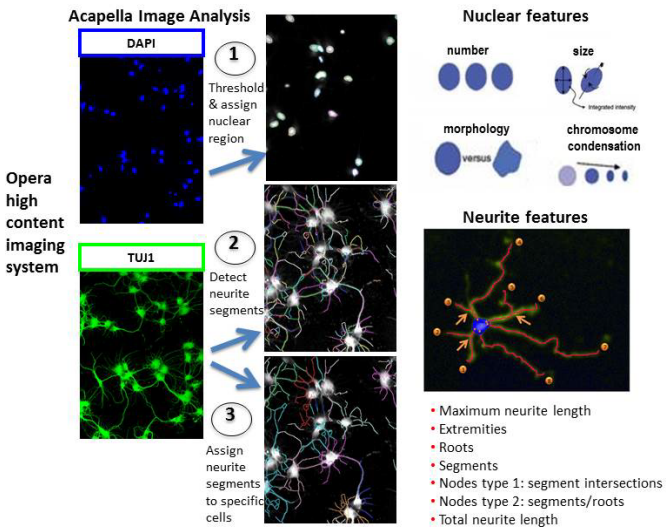

Figure 27. Automated algorithm detection of neurite parameters. *High throughput 384-well plates were imaged on the automated Opera high content microscopy system. Images were quantified for neurite growth by Acapella based image analysis. 1. Detection of nuclei by Hoechst staining. 2. Detection of neurite segments visualized by TUJ1 staining. 3. Algorithm assigns neurites to each nuclei, resulting in a quantification of 7 neurite growth parameters per neuron. Additionally, 4 measures of nuclei were analyzed as correlates of overall cell health.*

3.3.2.1.1.2 Results

3.3.2.1.1.2.1 Assay development. hiPSC-derived iCell neurons (CDI) were used to develop a high content assay for neurite growth. iCell neurons are a population of highly enriched (>90%) human cortical-like neurons derived from iPSC, comprised primarily of GABAergic and glutamatergic subtypes, with a small percentage of dopaminergic neurons [8]. By one day post-thaw, they exhibit typical neuronal morphology with branching neurites [8] and by day 10 will respond to Glutamate, NMDA, AMPA, and GABA, and display expected physiological characteristics in patch clamping experiments that indicate multiple receptor subtypes present at synapses (CDI literature). These cells were selected to use for screening because they are human, express appropriate neuronal characteristics and they are available in commercial quantities that are cryopreserved.

In previous studies we developed a high content assay to monitor neurite growth and retraction, as described below. In developing this assay, multiple parameters were optimized to enable screening on a 384-well format. A density of 4000 cells per well was selected to allow for identification of individual neurites. Image analysis was performed in a sequential process. Briefly, detection of healthy nuclei was followed by neurite segment detection and then neurite tree assignment to specific cells. Values for 11 different parameters were determined: four nuclear and seven for neurites.

Using the broad-spectrum kinase inhibitor staurosporine, which promotes neurite growth [9,10], as a control compound, we explored various timing schemes to maximize assay sensitivity, and determined that compound addition one day after plating, and analysis three days later was optimal. We also considered whether it would be beneficial to include in our plating conditions laminin, an extracellular matrix protein known to support growth of neurites[11]. To simplify the high-throughput process, rather than coating wells, laminin was included in the

plating media. Comparison of staurosporine-induced neurite growth in the presence and absence of laminin indicated that the magnitude of response between the two conditions was similar, but that laminin supported the development of more neurites in basal conditions, and as well resulted in increased numbers of neurons that plated down. Thus, we chose to perform the screen in the presence of added laminin in the plating media reasoning that it effectively increased the numbers of neurites for analysis without affecting the detection window, increased plating efficiency, and as well represents a more physiological substratum for neurite growth.

Comparison of staurosporine treated to DMSO vehicle controls resulted in Z-factors for neurite parameters that ranged from 0.2 to 0.5, indicating the assay was sufficiently robust, but that screening should be run in duplicate to improve hit identification [12]. Finally we also determined that iCell neurons are tolerant of DMSO concentrations up to 0.5%.

A select, validation set of compounds from our Neurotoxin library was tested including both those expected to impact neurite growth, and those not expected to have an effect, based on previous studies [4] (Figure 28). In general, our results were in agreement with those of Radio and Mundy [4] and we suggest that the few observed differences can be explained by the length of compound exposure in our study, three days, versus six days in the Radio and Mundy [4] study (Figure 28).

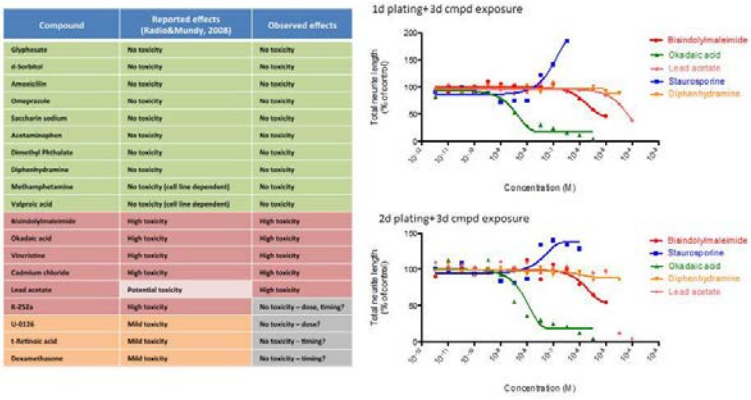

Compound	Reported effects (Radio&Mundy, 2008)	Observed effects
Glyphosate	No toxicity	No toxicity
d-Sorbitol	No toxicity	No toxicity
Amoxicillin	No toxicity	No toxicity
Omeprazole	No toxicity	No toxicity
Saccharin sodium	No toxicity	No toxicity
Acetaminophen	No toxicity	No toxicity
Dimethyl Phthalate	No toxicity	No toxicity
Diphenhydramine	No toxicity	No toxicity
Methamphetamine	No toxicity (cell line dependent)	No toxicity
Valproic acid	No toxicity (cell line dependent)	No toxicity
Bisindolylmaleimide	High toxicity	High toxicity
Okadaic acid	High toxicity	High toxicity
Vincristine	High toxicity	High toxicity
Cadmium chloride	High toxicity	High toxicity
Lead acetate	Potential toxicity	High toxicity
K-252a	High toxicity	No toxicity – dose, timing?
U-0126	Mild toxicity	No toxicity – dose?
t-Retinoic acid	Mild toxicity	No toxicity – timing?
Dexamethasone	Mild toxicity	No toxicity – timing?

Figure 28. Comparison of exposure timeline for neurite growth assay. *Left, Table comparing results of test set against results published on rodent neurons [4]. The majority of strong effects were reproducible with human neurons. Right, Neurons were cultured for either 1 or 2 day prior to compound exposure. Maximal outgrowth response of positive control Staurosporine in 1 day culture.*

Additionally, we tested whether plating the neurons for 1 or 2 days prior to exposure changed the test results. We found the effect of days post-plating similar across the test set. However, the degree of outgrowth with our positive control compound, Staurosporine, reached its maximum response at 1 day post-plating exposure; thus, we continued with this paradigm for the validation set screen.

Having validated the assay using a subset of compounds, we went on to assess all 81 compounds comprising our Neurotoxin library. Additionally, each screening plate included the outgrowth control Staurosporine and the retraction control BIO, a GSK3β inhibitor (Figure 29). Neurons were exposed to compound for 3 days followed by fixation and immunocytochemistry for neuronal morphology.

Validation Screen

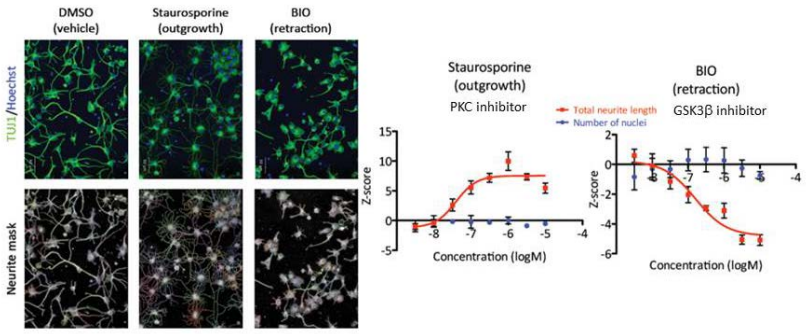

A. B.

Figure 29. Controls for neurite growth validation screen. *(A) Representative images of vehicle, outgrowth control Staurosporine and retraction control, BIO. Top, TUJ1 shows excessive growth of fine processes in Staurosporine. Bottom, skeleton view of how algorithm detected each neuron and its processes. (B) Staurosporine increases and BIO decreases neurite growth after 3 day exposure without effects on cytotoxicity.*

The majority of compounds had no effect on any of the 7 neurite growth or 4 nuclear parameters (Table 2). 29/81 compounds exhibited cytotoxicity, which included neurite degeneration (Figure 30). Four compounds out of 81 caused specific effects on neurite growth, Bis-1, Vincristine, Triethyltin chloride and PBDEs, which resulted in neurite retraction at a lower dose than cytotoxicity. Vincristine is a chemotherapy agent known for its clinical neuropathy side effects, and causes microtubule depolymerization. Microtubule dynamics are precisely regulated for neurite growth and maintenance, with depolymerization acting to destabilize the cytoskeleton leading to degeneration. Furthermore, Bis-1 and PBDE are known to cause decreased neurite growth in the developing nervous system.

Table 2. Neurite Growth Validation Set Results

No observed effects			Neurite retraction prior to toxicity	Toxic only at 33 µM	Toxic
2-ethoxyethyl acetate	Cocaine	Mercury (II) chloride	Bis-1	Acetaminophen	Bifenthrin
2,4-dinitrophenol	Cypermethrin	Methanol	Vincristine	Omeprazole	Bis(tri-n-butyltin) oxide
Acibenzolar-S methyl	D-sorbitol	Methoxyethanol	Triethyltin chloride	5,5-diphenythydantoin	Dibutyltin
Acrylamide	DEET	Methylparathion	PBDEs	Benomyl	Dichlorophenoxyacetic acid
Aldicarb	Deltamethrin	Monosodium glutamate		Butylated hydroxy anisole	Dieldrin
Allethrin	Dexamethasone	Nicotine		Butylated hydroxytoluene	Fluazinam
Aluminum lactate	Diazinon	Paraoxon		Dichlorvos	Heptachlor
Amoxicillin	Dimethyl phthalate	Parathion ethyl		Hexachlorophene	Methylmercury
Amphetamine	Diphenhydramine	Permethrin		Paraquat	Tebuconazole
Aspartame	Ethanol	Saccharin		Bis (2-ethylhexyl) phthalate	Toluene
Benzene	Glyphosate	T-retinoic acid		Lead acetate	Tributyltin chloride
Chlorpyrifos oxon	Hexachlorobenzene	Trichloropyridinol		Cadmium chloride	Trichlorfon
Bisphenol A	Ketamine	Tricresyl phosphate		Arsenic trioxide	Trichloroethylene
Carbaryl	Lead nitrate	Trimethyltin			Dimethyltin
Chlorine dioxide	Lindane	U-0126			Lithium dichloride
Chlorphrifos	Maneb	Valproic acid			Manganese chloride

The majority (59/81) of compounds had no effect on cell health or neuron morphology. 29/81 compounds caused cytotoxicity. We found varying degrees of sensitivity, such as compounds that only caused cell death at the highest dose point versus compounds toxic in dose response. 4 compounds caused neurite retraction at lower doses and cytoxicity at higher doses, showing the assay is sensitive to detect primary degeneration effects to axons.

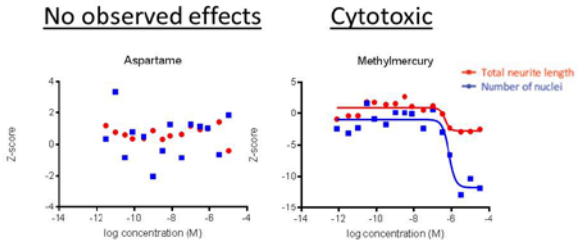

Figure 30. Examples of neurite growth dose response curves. *59/81 neurotoxin library compounds, such as Aspartame, had no effect on neurite growth. 29/81 caused cytotoxicity, including methylmercury. Cytotoxicity quantified by decreased number of nuclei also resulted in decreases to total neurite length.*

3.3.2.1.1.2.2 Cell type specific cytotoxicity of neurotoxin library. We also screened the validation set on human dermal fibroblasts to determine whether any of the compounds exhibited neuron-specific toxicities. We exposed neurons or fibroblasts to the validation set library for 3 days, followed by fixation and immunocytochemical analysis for neuronal morphology and nuclear measures of cell death. We found that 16 of 29 (55%) of compounds that were toxic to neurons were also toxic when tested on fibroblasts. 13 compounds exhibited selective toxicity on hiPSC-derived neurons relative to fibroblasts, including the organotin tributyltin (Figure 31).

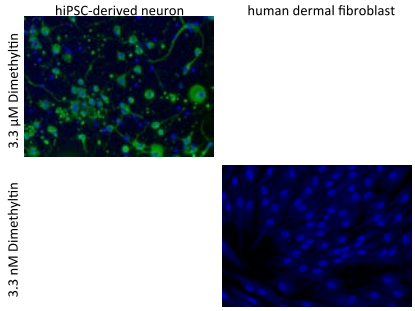

Figure 31. Tributyltin exhibits neuron specific toxicity. *TUJ1 (green) and Hoechst (blue) staining shows neurons (left) exhibit dose response for cell death and neurite.*

3.3.2.1.2 Mitochondrial Function Assay

3.3.2.1.2.1 Introduction. Neurons are known to be particularly sensitive to mitochondrial toxicity due to their high bioenergetic demands. One of mitochondria's essential functions is to provide energy substrate for cellular metabolism in the form of ATP. Dysfunctions in this process are associated with cell death. In mitochondria, the biochemical processing of ATP in the respiration chain establishes an electrochemical gradient. This gradient can be measured as the mitochondrial transmembrane potential (MMP) by dyes that accumulate in negatively charged mitochondria relative to the cytosol. Chemicals affecting the polarization across the mitochondria, either causing depolarization or hyperpolarization, impact the function of energy generation and can lead to reactive oxygen species (ROS) production.

Environmental insult, disease and genetic vulnerabilities can all lead to mitochondrial dysfunction in the brain, which in turn can cause or exacerbate neurodegenerative and other neurological conditions. Neuronal mitochondrial dysfunction is often associated with exposure to environmental toxins, leading to cell death due to reduced MMP, ROS generation, and an inability to provide high levels of energy required. For example, many pesticides are classified as neurotoxins that affect mitochondrial function. A well-known case is the fungicide Maneb which selectively inhibits complex III of the electron transport chain leading to loss of MMP and ROS production.

We have established a multiplexed assay to screen for MMP and ROS. This assay specifically detects acute compound effects at exposures of exposures of 45 minutes, 2 hour 15 minutes, 6 hours or 24 hours at high dose ranges (maximum 250uM). Time points <24hrs will investigate the direct effect on mitochondrial functions, as mitochondrial dysfunction is a downstream effector of many cellular processes such as the activation of cell death pathways.

To minimize false negatives we implemented a decision tree format workflow. We initially captured the strongest toxins at the earliest time point (45 min) and established that ROS levels reached maximum >2h after effect onset. All positive results were then examined >2 hrs post initial effect to increase the sensitivity of the assay. All compounds with negative results at the acute time point were confirmed by a longer exposure of 24 hours. In the discussion, we provide retrospective points for increasing efficiency for future compound screening. In the discussion, we provide retrospective points for increasing efficiency for future compound screening.

A compound was designated as a hit for mitochondrial toxicity if it generated a change in MMP or ROS more than 2 standard deviations from the mean of the vehicle (Z-score>2, or <-2). Additionally, the effect on MMP or ROS must be at a dose without a significant effect on cytotoxicity (see methods: statistics for details).

3.3.2.1.2.2 Methods

3.3.2.1.2.2.1 Cell culture. HiPSC-derived neurons (iCell neurons; Cellular Dynamics Inc.) were cultured according to manufacturer's protocols. Neurons were thawed and plated directly onto poly-D-lysine coated 384-well clear-bottom plates (Corning Life Sciences) at a density of 7500 cells/well using a 16-channel multipipette. Neurons were plated in manufacturer's provided medium supplemented with 3.33 µg/ml laminin (Sigma-Aldrich). Experiments were performed 2-4 days post-plating.

3.3.2.1.2.2.2 Dye loading. JC-10 (0.75uM; Enzo Life Sciences) or TMRE (50nM; Life Technologies) were used for potentiometric measurement of mitochondrial membrane potential. Mitotracker green (MTG, 50nM; Thermo Fisher Scientific) was used in the test set experiments to permanently stain mitochondria. CellROX deep red (1 uM; Thermo Fisher Scientific) was used to measure cellular reactive oxygen species. Optimal dye concentrations were determined in assay development. All dyes were loaded for 30 minutes prior to compound exposure, except for the 24h timepoint when dye was loaded terminally for 45 minutes. Dyes were prepared as a 2x stock and added to cells as a 50% exchange. JC-10 required addition of 0.2% pluronic (Thermo Fisher Scientific) for loading.

3.3.2.1.2.2.3 High content screening assay. Neurotoxin library compiled of 81 compounds in addition to the positive control Menadione (Sigma-Aldrich) were assayed for in the screen. The primary screen was conducted as a 3-point ½ log dose response, the 2 hour 15 minute and 6 hour positive hit confirmation screen as an 8-point ¼ log dose response, and the 24-hour negative hit confirmation as a 4-point dose response. Menadione control was included on every plate in the screen at a 3-point ½ log dose response. All compounds and positive control were assayed in replicate wells.

Neurotoxin compounds and 0.3% DMSO or water vehicle were prepared to 2x concentration via echo acoustic dispense from library source plate to a 384 well plate. Menadione was prepared to 2x concentration in ethanol fresh for each experiment. After iCell neurons were loaded with dye, 2x concentration compounds were added by a 50% exchange of media. Neurons were exposed for either 45 minutes, 2 hour 15 minutes, 6 hours or 24 hours (see decision tree, Figure 32).

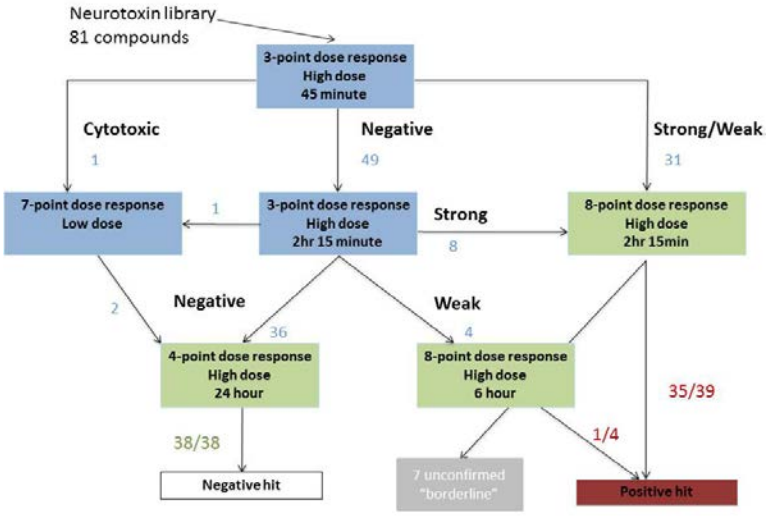

Figure 32. Decision tree for assay workflow. *All compounds were initially screened at high dose at the acute timepoint. Follow-up assays were performed to confirm initial results. Numbers indicate numbers of compounds in each pathway. Blue, primary screen; red, confirmation screen positive hits; grey, confirmation screen negative hits.*

After compound exposure, neurons were washed once by 98% exchange with light cell imaging buffer solution (LCIB + 25mM glucose + 10nM TMRE (for TMRE experiments); Thermo Fisher Scientific), incubated at room temperature in LCIB solution + Hoechst (1:2000; Thermo Fisher Scientific) by 98% exchange for 5 minutes, and washed once with 98% exchange with LCIB solution. The plates were sealed with foil and immediately imaged.

3.3.2.1.2.2.4 High content imaging analysis. Assay data was acquired using an Opera confocal microplate imaging system (PerkinElmer, Inc.) using a 20x air objective. For each well screened five fields were imaged. Acquired images were analyzed using Columbus Acapella based software (PerkinElmer) to identify nuclei and cytoplasmic compartments (Figure 33). Data generated in Columbus was exported to Excel (Microsoft) for statistics and Prism software (GraphPad) for graphing.

3.3.2.1.2.2.5 Statistics. Statistical significance was determined as Z-score greater than 2 compared with vehicle control mean across replicate treatment wells. For the screen, cytotoxicity was defined as a change of at least 2 standard deviations (Z-score) for both replicates in at least 2 of the 4 following measures: ratio healthy nuclei to total nuclei, nuclei intensity, nuclei roundness, nuclei area. MMP depolarization was defined as a decrease in TMRE dye intensity of at least 2 StdDev for both replicates without a corresponding decrease in ratio of healthy cells (cytotoxicity). Oxidative stress (ROS) was defined as an increase in CellROX deep red dye intensity of at least 2 StdDev for both replicates without a corresponding decrease in ratio of healthy cells (cytotoxicity).

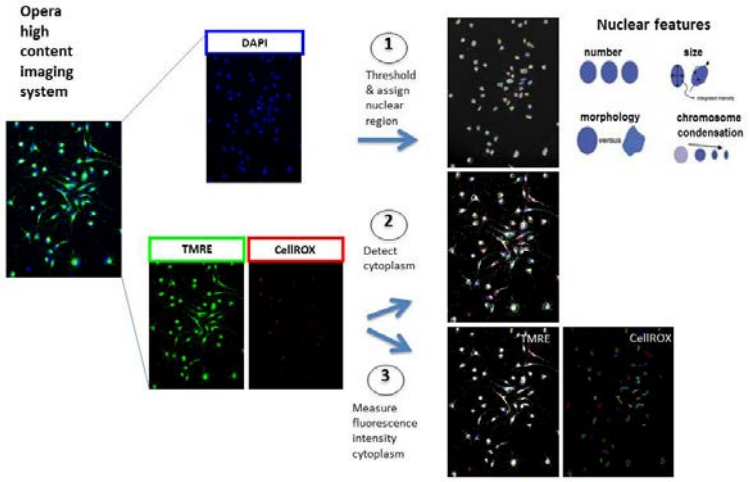

Figure 33. Automated algorithm detection of multiplexed dyes for mitochondrial function. *Images are acquired on the automated Opera high content microscopy system. 1. Nuclei are detected by Hoechst dye thresholding. 2. Algorithm detects cytoplasm for each associated nuclei with TMRE dye. 3. TMRE and CellROX intensities are measured per neuron in the cytoplasmic compartment. Four nuclear measures are quantified for correlates of cell health.*

3.3.2.1.2.3 Results

3.3.2.1.2.3.1 Assay development. Based on two control compounds, Menadione and Antimycin A, basic parameters for the assay were established including order of dye and compound addition, and length of compound exposure (Figure 34). After examination of 10-90 minutes Menadione exposure following dye loading, we found 30 and 60 minutes produce optimal dose response curves. For the primary validation screen we will bracket the timepoint at 45 minutes. The bracketed multiplexed assay was then performed with 8 replicates of each condition to generation statistical measure of robustness (Z"). Z' for ROS >0.5. and Z' for JC-10 >0, acceptable given that the assay is always run at multiple doses in at least duplicate (Table 3).

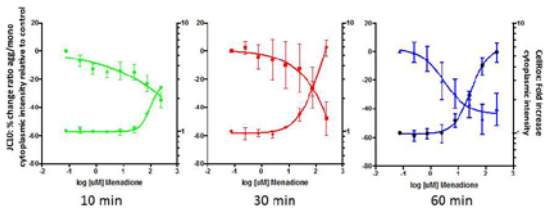

Figure 34. Testing exposure timepoints for multiplexed measurement of MMP decrease and ROS increase by control compound Menadione. *JC-10 and CellROX show dose curves for Menadione with optimal curves occurring after 30 minutes. Validation screen was performed at the bracketed timepoint of 45 minutes compound exposure.*

Table 3. Z Prime Factor for Positive Controls

	Antimycin		Menadione			
	JC-10		JC-10		CellRox	
Mean	0.7606	0.4629	0.8346	0.5456	78.050	310.067
StdDev	0.0567	0.0398	0.0330	0.0549	5.534	31.419
Z' Factor	0.0270		0.0873		0.522	

A test set of mitochondrial toxins was run in dose response against the MMP/ROS assay using JC-10 and CellROX dyes. 6/11 compounds were found to decrease MMP, and 1/11 to increase ROS at 45 minute exposure. These initial results suggested that the assay was not sensitive enough.

One approach to increase assay sensitivity was to test longer compound exposure times as the 45 minute timepoint was based on the control menadione. We generated assay conditions for longer-term drug exposures from 45 minutes to 2h 15 minutes. Using our control compound, Menadione, we found a left-shift in the JC-10 dose response curve for longer time points as expected. In addition, the highest 2 concentrations (75uM and 250uM) became frankly toxic at the longer time point. Therefore, we have included necessary cell health measures to designate doses that are specific to mitochondrial toxicity without overt cell death. The four measures of general cell health are nuclei area, percent large healthy nuclei/total nuclei, nuclear roundness and nuclear brightness (Hoechst intensity). These results indicated that increased exposure times can increase the sensitivity with which mitochondrial toxicity was detected.

Another approach to increase assay sensitivity was to test an alternative MMP dye, TMRE. TMRE, a rapidly equilibrating, potentiometric dye, was combined with the mitochondrial stain, Mitotracker Green (MTG), which localizes to mitochondria independent of MMP, to create a dual-dye ratiometric output. With our control compound Menadione, we found a greater dynamic range with TMRE/MTG compared to JC-10 (93% vs. 40% change at 45 minutes) and generated dose response curves for Menadione. TMRE successfully multiplexed with CellROX deep red for simultaneous measurement of reactive oxygen species (Figure 35). Given the increased sensitivity of TMRE relative to JC-10, we adopted TMRE as our primary method to determine MMP.

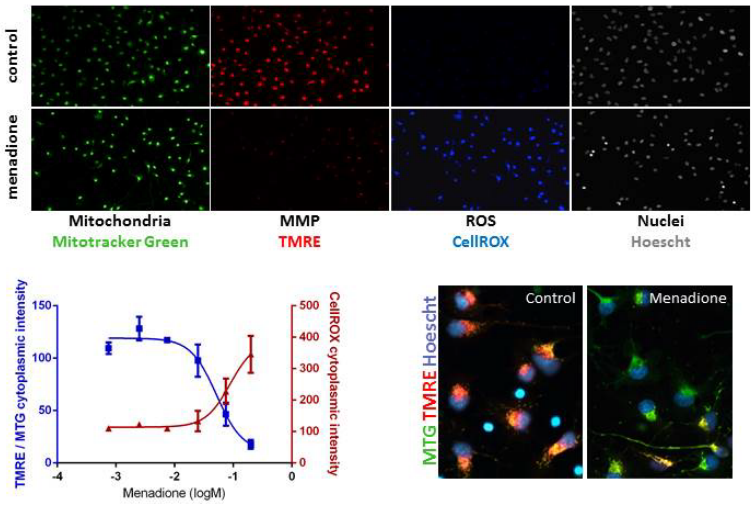

Figure 35. Mitotracker Green, TMRE, and CellROX deep red multiplexing. *Mitotracker green intensity is maintained after mitochondria are depolarized indicated by loss of TMRE. Ratio of TMRE/MTG is used to normalize mitochondrial potential to mitochondrial mass. CellROX measured ROS in multiplexed assay.*

3.3.2.1.2.3.2 Validation set screen. The 81 Neurotoxin library compounds were first screened in 3-point dose response at 2 time points, 45 minutes (1X) and 2 hours 15 minutes (3X). In addition, cytotoxicity was evaluated and defined as a change of at least 2 standard deviations (Z-score) in at least 2 of the 4 following measures: ratio healthy nuclei to total nuclei, nuclei intensity, nuclei roundness, nuclei area. Mitochondrial membrane potential (MMP) depolarization was defined as a decrease in TMRE dye intensity of at least 2 StdDev without a corresponding decrease in ratio of healthy cells (cytotoxicity). Oxidative stress (ROS) was defined as an increase in CellROX deep red dye intensity of at least 2 StdDev without a corresponding decrease in ratio of healthy cells (cytotoxicity). Compounds were considered negative, but borderline if they exhibited both mitochondrial toxicity and cytotoxicity at the same doses. Data were binned into positive, negative and borderline categories according to these criteria.

Out of the 81 compounds screened, 31 were positive at 45 minutes (Figure 36) and 12 became positive at 2 hours 15 minutes (Table 4). 38 compounds were negative at all timepoints. The majority of mitochondrial toxins caused MMP depolarization. 2 compounds, Omeprazole and Tricresyl phosphate, caused both MMP depolarization and ROS increase, while 3 compounds, Maneb, Dimethyltin, and Dichlorvos, increased ROS without affecting MMP. Mitochondrial could not be resolved from cytotoxicity in 8 compounds and these were considered negative-borderline. In addition, 2 compounds, Chlorine dioxide and D-sorbitol, were cytotoxic at all doses tested without mitochondrial toxicity.

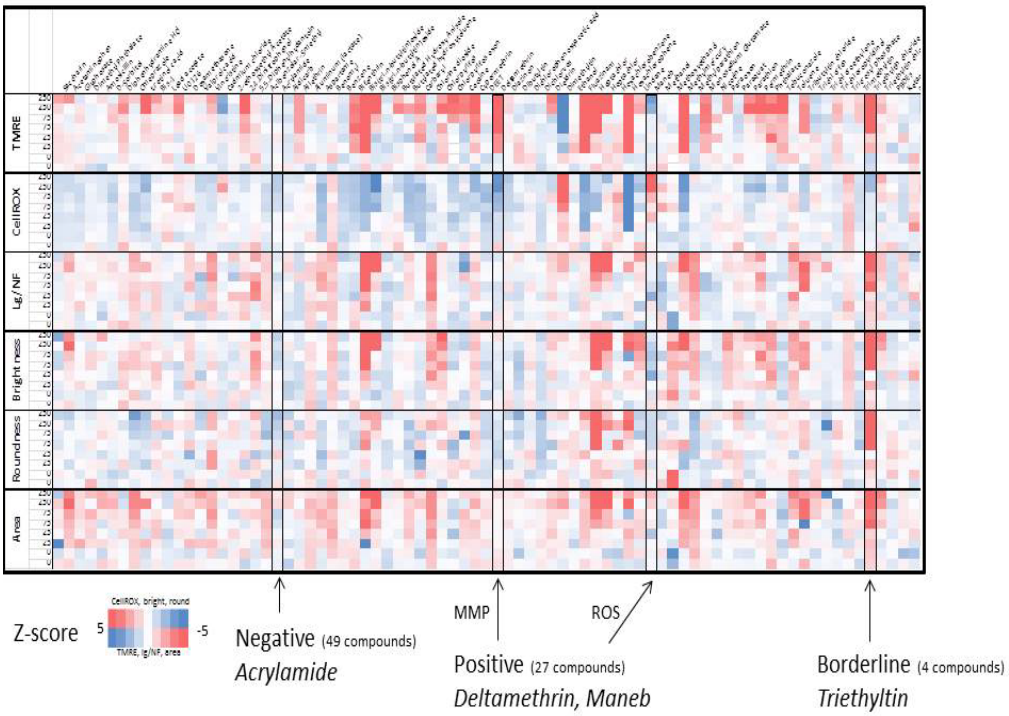

Figure 36. Heat map for 45min primary screen. *Validation set compounds were binned by z-score greater than 2 STD. Examples of each bin are outlined in black boxes. Borderline compounds with co-incident TMRE decrease and cytoxicity were re-tested at narrower dose points. All were determined to be positive.*

Table 4. MMP/ROS Data Binned into Strong Positive, Weak Positive, and Negative Categories

Strong Mitochondrial Toxins •Replicate hits in dose response		Weak/possible toxins •Unconfirmed hits •High dose only hits	Negative for mitochondrial toxicity •No effect at any timepoint or dose		
Allethrin	Fluazinam	Acetaminophen	2-ethoxyethylacetate	Dichlorophenoxyacetic acid	Saccharin
Bifentrhin	Hexachlorophene	Arsenic trioxide	5,5 diphenhydantoin	Dimethyl pthalate	Sorbitol
Bis-phthalate	Heptachlor	BHA	Acibenzolar-s methyl	Ethanol	Trichloroethylene
BisTBToxide	Maneb	BHT	Acrylamide	Glyphosate	Toluene
Cocaine	Manganese	Cadmium	Aldicarb	Hexachlorobenzene	Trichlorfon
Cypermethrin	Mercury chloride	Carbaryl	Aluminum	Ketamine	Trichloropyridinol
Deltamethrin	Methyl mercury	Chloripyrifos	Amoxicillin	Lead acetate	Trimethyltin
Diaznon	MSG	Chloripyrifos Oxon	Amphetamine	Lead nitrate	Valproic acid
Dibutyltin	Parathion	Dexamethasone	Aspartame	Lithium	
Dichlorvos	Permethrin	Lindane	Benomyl	Methanol	
Dieldrin	Retinoic acid	Omeprazole	Benzene	Methoxyethanol	TMREa
Dimethyltin	Tebuconazole	Paraoxon	Bis-1	Methyl parathion	TMRE and CellROX
Diphenhydramine	Triethyltin	Tributyltin	BPA	Nicotine	
ONP	U0126	Tricresyl Phosphate	Chlorine	Paraquat	
		Vinicristine	DEET	PDBEs	

Borderline compounds in the primary screen were all re-tested ¼ log dose response to determine if mitochondrial effect could be separated from cytoxicity. 8/8 borderline compounds became positive, indicating their primary target was mitochondrial toxicity. Heptachlor is an example compound that was binned to the borderline group at 45 minutes and became positive for TMRE decrease after re-testing (Figure 37A, B). All positive compounds were then confirmed at the 2h 15min time point in ¼ log 8-point dose response (Figure 37C). ROS increased at a lower dose than cytotoxicity, suggesting a specific effect of Heptachlor. In contrast, the longer time point caused the window between TMRE decrease and cytoxicity to narrow.

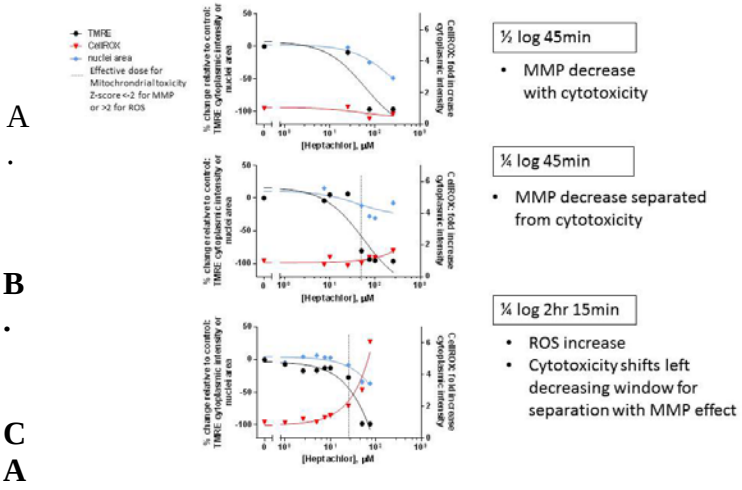

Figure 37. Borderline example. *Borderline compounds in the primary screen were all re-tested at closer dose points to determine if mitochondrial effect could be separated from cytoxicity. A, Heptachlor was binned to the borderline group at 45 minutes and B, became positive for TMRE decrease after re-testing. C, All positive compounds were then confirmed at the 2hr15min time point in ¼ log 8-point dose response. ROS increased at a lower dose than cytotoxicity, suggesting a specific effect of Heptachlor. In contrast, the longer time point caused the window between TMRE decrease and cytoxicity to narrow.*

3.3.2.2 Summary. We have established and validated assays to examine neurotoxicity of chemical exposure to human stem cell-derived neurons. The majority of compounds in our neurotoxin library (52/81) exhibited neurotoxicity across the cellular phenotype assays. Interestingly, 9/13 neuron selective toxins causing cell death were primary mitochondrial toxins, highlighting the sensitive nature of neurons to mitochondrial dysfunction.

Retrospective analysis of the mitochondrial assay decision tree has resulted in a revised version to increase future screening efficiency, by conducting the primary screen at the 2 hour 15 minute timepoint (Figure 38). By inverting the primary screen, the longer timepoint will catch a larger number of hits thereby decreasing the number of compounds requiring additional timepoint screening.

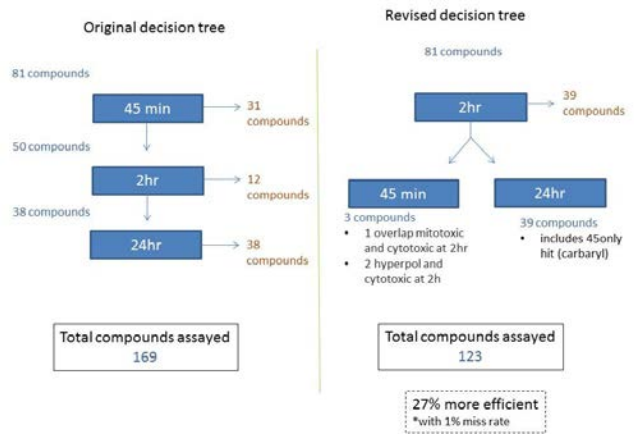

Figure 38. Optimized decision tree.

In comparison of the hit set between our mitochondrial assay on hiPSC neurons and the EPA results on HepG2 cells, the overwhelming majority of compounds were overlapping. However, 8/81 neurotoxin library compounds were found to be neuron specific pointing to the benefit of relevant cell typesin establishing toxicity signatures (Figure 39).

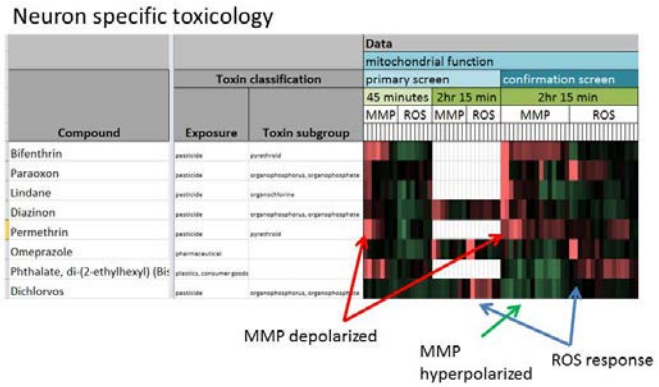

Figure 39. Neuron specific mitochondrial toxins compared to HepG2 cells. *Most are neuroactive pesticides. A diversity of responses was measured from the neuron-specific mitochondrial including MMP depolarization (red arrows), MMP hyperpolarization (green arrows, and ROS generation (blue arrows).*

3.3.3 Cellular Physiology

3.3.3.1 Objective. We have developed an approach that will offer a biologically relevant model system for higher predictability of chemical toxicity to neural circuitry function. This section utilized human induced pluripotent stem cell (hiPSC)-derived neuronal cells in co-culture with human astrocytes combined with multi-electrode array technology, a higher throughput *in vitro* cell-based platform, for evaluating neuronal networks.

3.3.3.1.1 Multielectrode Array Screen for Neurotoxicity

3.3.3.1.1.1 Introduction. Dopaminergic (DA) neurons play a significant role in neural circuits involving reward, movement and cognition, while their selective degeneration is the hallmark of Parkinson's disease. Dopaminergic neurons are uniquely sensitive to specific neurotoxic substances, and their firing activity is modulated by a variety of exogenous neuroactive chemicals such as ethanol. However, the links between neurotoxicity and neural activity remain unclear. Indeed, emerging models of neural degenerative diseases suggest that changes in neural activity can be an early biomarker for eventual cell death.

Interrogating the defining properties of neurons such as action potential firing and synaptic interactions, offers a powerful perspective on how exposure can lead to toxicity through changes in neural activity. Recent advances in hiPSC technology empowers strategies to understand the physiological impact of toxins on human neurons.

Broadly, neural activity can be divided into two interrelated categories, action potential firing and synaptic activity. Action potentials derive from a neurons intrinsic membrane properties, reflecting a specific complement of ion channels and ion homeostasis. Synaptic activity is the primary way neurons communicate, reflecting the precise regulation of the machinery for sending and receiving synaptic input, giving rise to networks of neurons. Extracellular recording of neural activity is a powerful tool to detect firing patterns. Furthermore, by analyzing effects of synaptic transmission blockers a picture of network interactions can be generated.

Dopaminergic neurons display range of firing patterns associated with behavioral state. Upon beginning an action sequence for example, DA neurons switch from a tonic low frequency firing mode to bursts of high frequency firing. Bursting activity is hypothesized to drive a supra-linear increase in dopamine release, increasing the effect of DA neurons on their postsynaptic targets [13,14].

Both cellular and synaptic mechanisms have been proposed for the regulation of DA firing regimes. Modeling studies suggest that the temporal structure of GABAergic inhibition can suppress or enhance DA neuron bursting in the ventral tegmental area (VTA) [15]. Likewise, expression of ATP sensitive potassium channels is required for substantia nigra dopaminergic neuron busting *in vivo* and *in vitro*. These results suggest that the DA neuron bursting is a sensitive, behaviorally relevant endpoint for compounds altering the intrinsic and synaptic properties of neurons.

To this end we have established a protocol for chronically recording firing patterns in human dopaminergic neurons derived from hiPSC cells. By culturing these neurons electrode arrays we have obtained high temporal resolution recordings of their firing patterns and network activity. This experimental paradigm allows for long-term recordings of neural activity, complex pharmacological manipulation, and controlled exposure to putative toxins.

3.3.3.1.1.2 Methods

3.3.3.1.1.2.1 Cell culture. HiPSC-derived neurons (iCell or iDopa neurons; Cellular Dynamics Inc.) were cultured according to manufacturer's protocols. 48-well Multielectrode Array plates (MEA, Axion Biosystems), with 16 electrodes per well, were pre-coated with 0.1% polyethylenimine (Sigma-Aldrich) for 1 hour, washed 4 times and dried overnight. On the day of neuron plating, electrodes were spotted with 20ug/ml laminin (Sigma-Aldrich) and incubated for

1 hour at 37°C. Neurons were thawed and plated directly onto MEA plates at a density of 80,000 cells/well, spotted over the center of the electrodes. Neurons were plated in manufacturer's provided medium supplemented with 10µg/ml laminin. Cells were maintained in media with 1ug/ml laminin during the course of the experiment in a humidified 37°C incubator with 5% CO_2. Media was 60% exchanged 3 times per week. On day 5 post-plating, neurons were changed to Neurobasal A with 10% Knockout Serum Replacement and 1% Pen-Strep (Life Technologies). At 4 weeks post-plating, media was changed to Brainphys media (STEMCELL Technologies) with 2% B27, 1%N2, 1% Pen-strep (Brainphys basal; Life Technologies), and supplemented with brain-derived neurotrophic factor (BDNF, 20 ng/ml; Peprotech), glial cell line-derived neurotrophic factor (GDNF, 20ng/ml; Peprotech), Dibutyryl cyclic AMP (cAMP, 1mM), ascorbic acid (AA, 200nM), and laminin (1ug/ml; Sigma-Aldrich) (Bardy et al). Also, at 4 weeks post-plating on the MEA, Human astrocytes were added to the hiPSC-derived dopaminergic neurons (ScienCell Research Laboratories) at a density of 80,000 cells/well. 7-20 days prior to screening, media was changed to Brainphys basal without supplements to minimize interactions.

3.3.3.1.1.2.2 Multielectrode array recording. MEA rrecordings were acquired with the Axion Maestro and Integrated Studio (Figure 40). A Butterworth band-pass (10-2500Hz) filter and adaptive threshold spike detector set to 5.5X standard deviations were applied to the raw data. 5 minutes spontaneous activity was measured as baseline, followed by compound exposure at 5 increasing doses with a 5 minute recording after each addition. Compounds were washed out 1 hour following the last dose. 5 minutes of activity was recorded at 2 hour, 24 hour, 48 hour and 96 hour post-washout (Figure 41A,B).

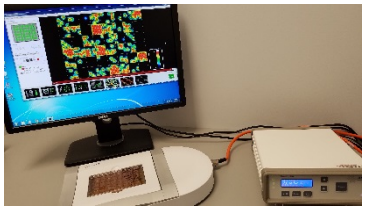

Figure 40. Axion Maestro and Integrated Studio System with MEA plate.

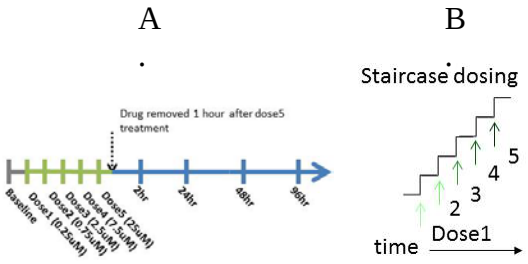

Figure 41. Assay timeline. *(A) A total of 10 recordings are taken across 96 hrs. (B) Staircase dosing paradigm where each dose is sequentially added to the same well allowing longitudinal studies of response.*

3.3.3.1.1.2.3 Compound exposure. Neurotoxin library compiled of 81 compounds were assayed for in the screen. Each compound was prepared EA plate was subjected to the positive controls, Picrotoxin (25 uM; Tocris Bioscience), 2R-amino-5-phosphonovaleric acid (APV, 75 uM), and 6-cyano-7-nitroquinoxaline-2,3-dione (CNQX, 10 uM; Sigma-Aldrich) and DMSO or

water vehicle. In order to determine specific effects on network function in the absence of cytotoxicity, maximum tolerated neurotoxin doses were extrapolated from the neurite growth and mitochondrial cellular phenotypes assays. Maximum DMSO solvated compound concentration was limited to 25uM which was equal to 0.1% DMSO to diminish the effects of DMSO vehicle on bursting activity (Figure 42). Water compounds were exposed up to 150uM. 5-point, ½ log dose screening was performed by sequential dosing of the same well with increasing compound or vehicle concentration, termed "staircase dosing" (Figure 41B). Only wells meeting the following minimum inclusion criteria were dosed: number of active electrodes>18%, wMFR>0.5Hz, Network burst frequency>0.017Hz.

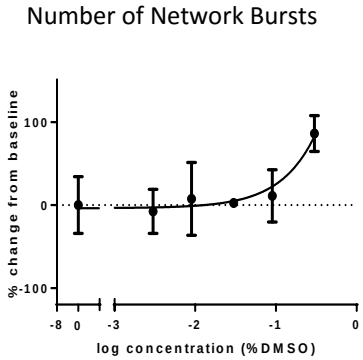

Figure 42. DMSO effect on network bursting. *Increasing concentration of DMSO increases network burst frequency 5 minutes after addition.*

3.3.3.1.1.2.4 Multielectrode array analysis. Raster plots and parameters of neuronal spiking activity were generated using Axion Neural Metrics Tool. Single electrode bursts were determined by Poisson with min surprise of 5. Network bursts were determined by envelope algorithm method with threshold factor between 1-3.5, min interburst interval (ms) 2000, min electrodes (%) 25-75, and burst inclusion (%) 25. Data was imported to the Axion MEA plotting tool for compilation of treatment groups and calculation of percent change from baseline for each well. Data was processed in R to subtract vehicle effect from each treatment and to compile results from all plates and treatments into a single file for display or import to Prism software (GraphPad) for graphing or statistics.

Final data was reported as percent change from baseline, vehicle corrected for 15 parameters: well wide mean for firing rate (MFR), number of active electrodes, weighted firing rate (wMFR), single channel burst properties for number of electrodes with bursts, frequency, duration, duration IQR, interburst interval (IBI) coefficient of variance (CV), and percentage of spikes organized in bursts, network burst properties for frequency, duration, percentage of spikes organized in network bursts, IBI CV, duration IQR, and overall degree of spike synchrony between electrodes for area under cross-correlation normalized for autocorrelations. Representative traces of burst and network burst spike activity is displayed in Figure 43.

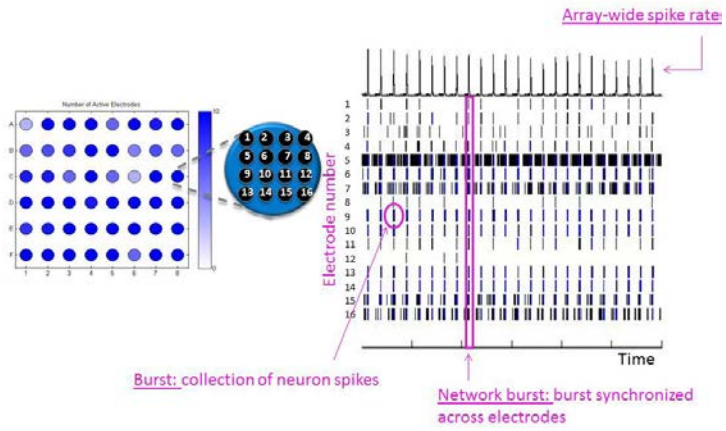

Figure 43. MEA neuronal network spike organization. *The 48-well MEA plate contains 16 electrode/well. The activity within a well is displayed as a raster plot, with one electrode per row and its spikes across the 5 minute recording. Spikes can be organized into bursts, a collection of spikes within a short time window. Network bursts are single channel bursts that are synchronized across the electrodes.*

3.3.3.1.1.2.5 Statistics. Each well was compared to itself at baseline and a percent change was calculated. Mean percent change and standard deviation for each treatment group (n=4-6) was determined in the Axion MEA plotting Tool. All treatments on a single 48-well plate were subjected to vehicle effect subtraction at each recording for normalization. To determine whether a treatment has a significant effect on neural activity at a given dose or timepoint, a one-way ANOVA with Dunnett's multiple comparisons test was performed in Prism software (GraphPad) comparing vehicle to all treatments on a single plate for each recording (Figure 44). Multiplicity adjusted p-values are reported for the main parameters of neural activity, weighted mean firing rate (wMFR), number of active electrodes, network burst frequency and network burst percentage (synchrony) with a significance level of *p<0.05.

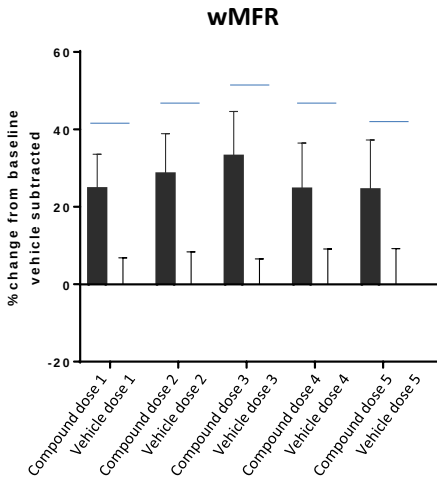

Figure 44. Representative example of statistical comparison for hit criteria. *At each recording, the treatment is compared to vehicle effect on the same plate.*

3.3.3.1.1.3 Results

3.3.3.1.1.3.1 Assay development. We found that appearance of synchronous network bursting was highly dependent on a balance of excitation and inhibition in the culture. We first cultured hiPSC-derived cortical iCell neurons on the MEA. While spontaneous activity developed, the activity lacked network coordination (Figure 45). As the composition of iCells is predominately inhibitory neuron subtype, we next tested the culture of hiPSC-derived dopaminergic (iDopa) neurons on the MEA, which represents a mixed population of excitatory and inhibitory neurons of the ventral midbrain. After 4 weeks of maturation, some wells developed network bursting phenotype. Because network burst phenotype was not consistent well to well, we developed and optimized two variables that could compensate for batch to batch variation and provide reliability in our assay. The two variables that promote network bursting work by regulating level of excitation, presence of astrocytes and removal of supplements from growth media (Figure 46). The effect of astrocytes on network behavior was similar whether they were present during network development or added to a mature culture (Figure 46A, B). Synchronous bursting could be revealed in mature networks by removal of supplements from growth media (Figure 46C).

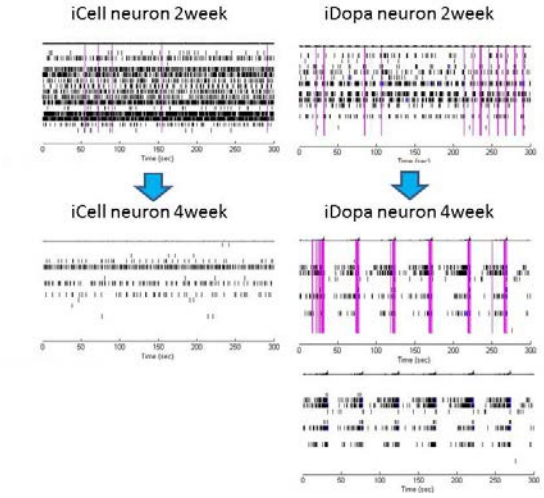

Figure 45. Comparison of network burst phenotype between cortical (iCell) and dopaminergic (iDopa) neuron products. *2 weeks post plating on the MEA both cell types exhibit spontaneous activity. At 4 weeks, iDopa neurons develop synchronized network activity, whereas iCell neurons decrease firing without becoming synchronized.*

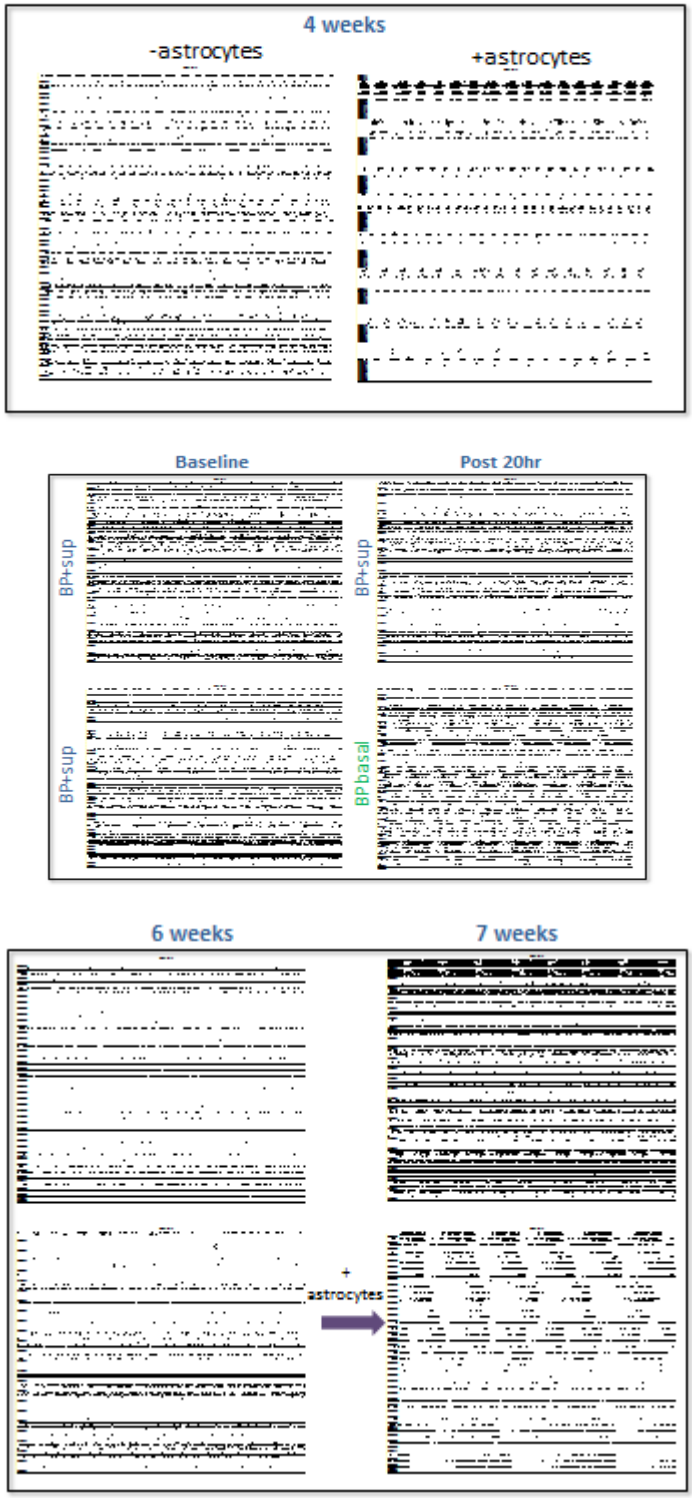

Figure 46. Optimizing network burst phenotype in iDopa neurons. *(A) iDopa neurons co-cultured with human astrocytes (n=13 wells) display greater synchronous network activity than neurons grown alone (n=10 wells). (B) Astrocytes added to mature iDopa cultures cause network bursting behavior within 1 week of co-culture (n=10 wells) compared to cultures maintained as mono-culture (n=12 wells). (C) Acute removal of growth media supplements increased network bursting (n=12 wells/treatment).*

To test the consistency of our culture paradigm, an entire 48 well plate was subject to identical culture conditions. Neurons were grown for 6 weeks on the MEA at which time human astrocytes were added and the media changed to Brainphys, a media conducive for electrical recording. The supplements were removed from the media the day before assay initiation. Figure 47 is a raster plot showing every iDopa neuronal spike across 16 electrodes per well, on the entire 48 well plate, during a 5 minute recording on the MEA. Rhythmic periods of intense activity oscillating with periods of low activity are indicative of synchronous bursting.

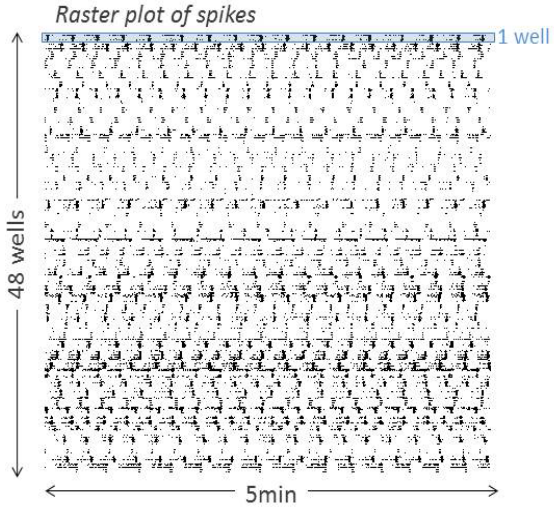

Figure 47. Raster plot of synchronously bursting iDopa neurons. *Represented here is the spiking activity across a 5 minute recording for an entire 48-well MEA plate. All 4wells show consistent network bursting phenotype. Blue bar highlighting data from 1 well.*

We performed a test set screen for acute toxicity using compounds with varied neurophysiological targets (Figure 48). The test was conducted after the culture reached consistent network bursting phenotype post-astrocyte addition. Two compounds with significant effects on increasing firing rate were identified, the acetylcholinesterase (AchE) inhibitor, Chlorpyrifos oxon (CO), and the potassium channel inhibitor, 4-aminopyridine (4-AP). CO increased firing rate but the number of network bursts was confounded by an effect specific to network bursting of the DMSO vehicle. 4-AP increased overall excitability at low dose, with increased firing rate and network bursts, but caused decreased firing rate concomitant with decreased number of active electrodes at high dose. 4-AP was in aqueous vehicle, so the results on network bursting are reliable as water had no effect in any measure. Thus, the staircase dosing paradigm can identify and flag compounds causing shifts in single cell and network activity.

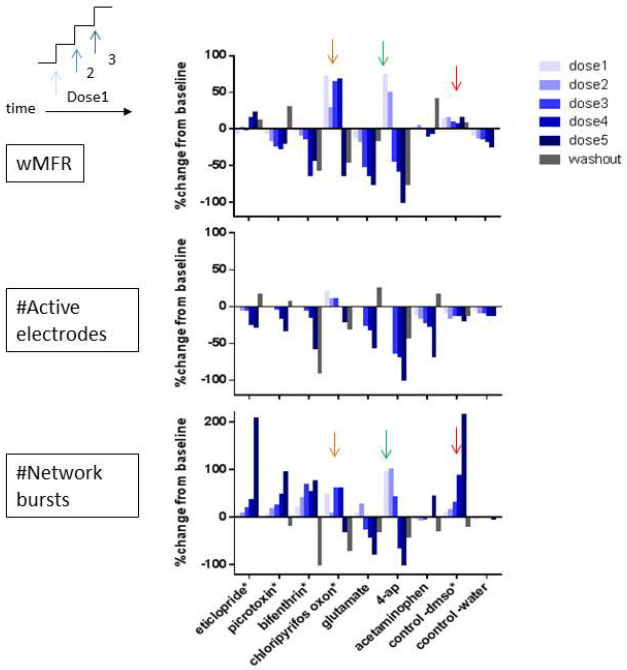

Figure 48. Results of test set screen for acute toxicity on neurophysiology. *Staircase dosing paradigm, with sequential doses given to the same well over time. Chlorpyrifos oxon (orange arrow) increased weighted mean firing rate (wMFR) but its effects on network bursting were confounded by DMSO vehicle (red arrow). 4-aminopyridine (green arrow) increased excitability at low dose and inhibited activity at high dose.*

We have established a process that supports consistent development of synchronous bursting behavior in co-cultures of iDopa neurons, indicated by rhythmic periods of intense activity oscillating with periods of low activity. Briefly, neurons are cultured for six weeks on the MEA at which time human astrocytes are added and the media changed to Brainphys, a media conducive to electrical recording. The supplements are removed from the media before assay initiation. We previously utilized a test set composed of neurotoxin library compounds and pharmacological tools to validate our stair case dosing paradigm for acute and persistent effects on network activity.

The sensitivity of our assay for statistically significant changes <100% in the test set with 3 replicate wells was low. To increase the assay sensitivity, we increased the number of well replicates from 3 to 6 and performed the acute staircase dosing paradigm for a neurotoxin library subset (amphetamine, Chlorpyrifos oxon, and lindane). First, our results confirmed our previous findings that all three compounds increase network excitation measured by network burst frequency (Figure 49). Second, by increasing the replicate number we were able to calculate statistically significant differences between the vehicle and compound treated groups at greater than 50% change from baseline (Table 5). Furthermore, we have determined a statistical workflow for the data, where each compound will be compared against its own baseline value or the vehicle control depending on vehicle effect.

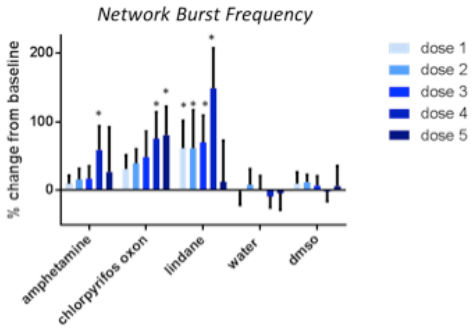

Figure 49. Neurotoxin library subset increases network excitation. *Network burst frequency increases in dose response for Chlorpyrifos oxon and lindane, while amphetamine has a peak dose effect. *p<0.05.*

Table 5. Increased Sensitivity with Increased Replicates

	Dose 1	Dose 2	Dose 3	Dose 4	Dose 5
Amphetamine	10%	16%	17%	59%	27%
Chlorpyrifos oxon	31%	39%	49%	75%	80%
lindane	61%	61%	70%	149%	13%

Network burst frequency calculated as percent change from baseline. Red indicates statistically significant results as compared to vehicle.

Next, we examined transferring our protocol on the 48-well MEA plates to the 96-well MEA plates for increased throughput. We compared 6 conditions of neuron plating techniques and monitored for development of activity (number of active electrodes and weighted mean firing rate, Figure 50). Overall, laminin coating the wells and flooding with cell suspension generated a level of activity at 3 weeks post-plating that meets our inclusion criteria for the neurophysiology studies.

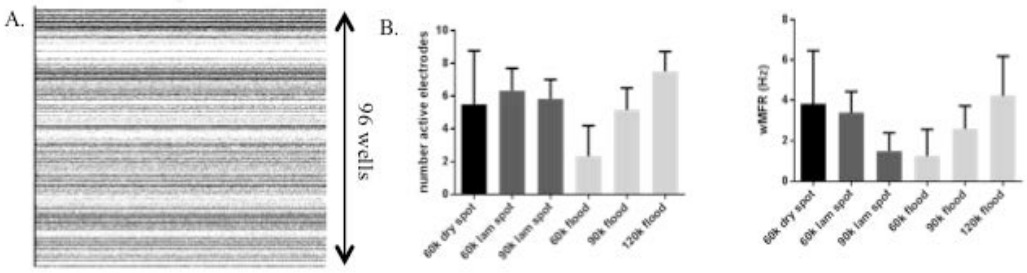

Figure 50. 96-well MEA plate assay development. *(A) 96 well raster plot showing high frequency of neuronal action potentials across a majority of wells. (B) Comparison between neuron plating conditions in activity endpoints, number of active electrodes and weight mean firing rate.*

3.3.3.1.1.3.2 Validation screen. Using the assay established in 4.3.1.1, we employed a compound exposure protocol with the following parameters. iDopa neurons are matured on the 48-well MEA plates in co-culture with human astrocytes for up to 8 weeks. Once network bursting behavior is established, supplements are removed from the Brainphys media to optimize recording conditions. The assay is performed 3-7 days later. Each plate is subject to positive control validation prior to compound exposure on the same day as the assay. Next, we record the neuronal activity at 10 timepoints for 5 minutes for both acute and persistent effects on network activity (Figure 50). First, we record activity at baseline followed by increasing doses in 5 minute increments, with 4-6 well replicates per compound/vehicle (acute effect). Finally, the last dose remains on the cells for 1 hour, then is washed out. We examine network response in the washout time period at 2h, 24h, 48h, and 96h (persistent effect).

Each plate was tested for excitatory inhibitory balance by pharmacological manipulation (Figure 51). First picrotoxin was added to decrease the inhibition, revealing the excitatory network. Next, APV was added to remove NMDA receptors and finally CNQX was added to block AMPA receptors. Remarkably after all fast neurotransmission was blocked, the number of active electrodes remained relatively constant, although at a much lower spike rate due to loss of high intensity bursting in the absence of excitation. The remaining activity could represent either contribution from neuromodulation and/or intrinsically active neurons, such as pacemaker neurons [16].

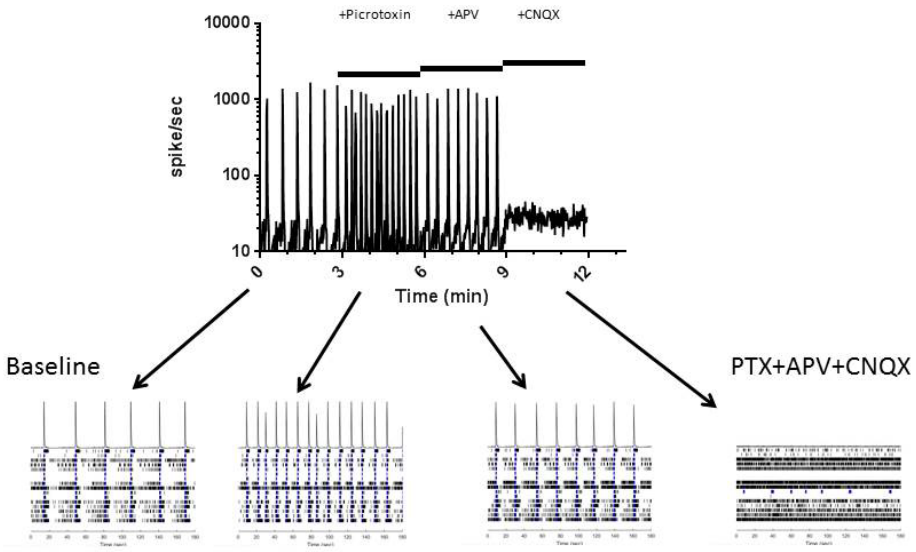

Figure 51. Inhibitory-excitatory balance at baseline. *Representative well for pharmacological positive control in validation screen. Trace of firing rate across time shows oscillation of array wide synchronized firing at baseline. Raster plots, bottom, show single channel spike firing. Addition of GABA-A receptor blocker, Picrotoxin, increased oscillation frequency. Sequential addition of glutamate receptor blockers shifts the activity toward baseline and then with all fast synaptic transmission blocked, desynchronized spiking.*

To determine the degree of toxicity during the acute compound exposure, we calculated the maximum response across the dose range for each compound. As one of the advantages of using the MEA system is to examine response over time, we were able to follow the same wells for up to 96hrs post-washout. We compared response during the acute phase of compound administration to the 96 hour point to determine which compounds returned to baseline and which caused persistent changes to the network activity (Figure 52).

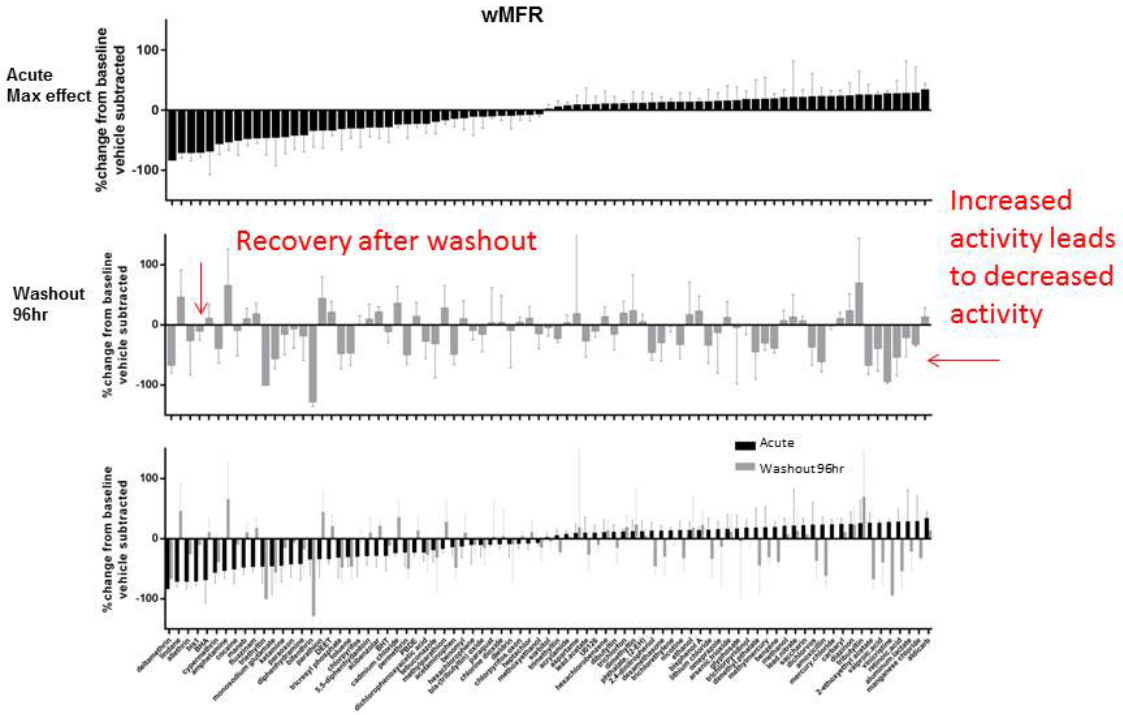

Figure 52. Relationship between acute effects on wMFR and 96 hours post-washout. *Top, maximum compound response across the dose range screened sorted from low to high. Middle, response compared to baseline at the 96 hour timepoint, post-washout. Bis-1, and others, return to baseline after washout. At 96hr, compounds such as Vincristine that had increased activity acutely, had lower firing rates after washout.*

wMFR was significantly decreased by 14 compounds and increased by 8 compounds during exposure. We found differential phenotypes in exposure with compounds such as Deltamethrin and Triethyltin, decreasing firing in the presence of drug and not recovering by 96 h. Other compounds, such as Bis-1 and BHA, decreased firing acutely but returned to baseline activity after washout. Another phenotype we measured was a trend in compounds that increased firing during exposure, such as Vincristine, to cause decreased activity after washout. This could represent a compensatory mechanism as hyperexcitablity can lead to glutamate receptor internalization. These results not only highlight the benefit of the MEA system in examining persistent effects to network activity, but also show the variety of phenotypes that are established with the multiplexed acute and washout exposure paradigm.

The overall results can be classified by effect on firing rate or network bursting, and then further classified in terms of effects on burst synchrony or frequency. For example, Cypermethrin, a pyrethroid insecticide and mitochondrial toxin, decreased firing rate while also desynchronizing the network activity. This effect occurred acutely, during compound exposure, but reversed by 96 hours post-treatment. As pyrethroids affect the intrinsic excitability of neurons through changing voltage gated sodium channel dynamics, we conclude that the MEA is a sensitive tool for sodium channel modifiers.

Two compounds, Aldicarb and vincristine displayed particularly interesting changes in neuronal activity in the validation screen. Aldicarb, a carbamate insecticide, is known to reversibly inhibit acetylcholinesterase, thereby increasing synaptic acetylcholine. This led to increased firing rate during the acute exposure, which returned to baseline upon washout (Figure

53). In contrast, vincristine, a chemotherapy medication, caused changes in neuronal activity which were not reversible, and progressively declined up to 96hr (Figure 54). Vincristine caused network de-synchronization in the washout time period, highlighting the value of including persistent effect time points for the neurophysiology assay. Overall, 72% (59/81) of compounds in our library had a significant effect on one of 4 primary metrics, wMFR, network burst frequency or network burst percentage at any time point during the experiment (Figure 55). The neurophysiology screen was validated in the detection of neuroactive compounds. The MEA assay results point to a variety of significant changes in neuronal activity across the multi-parameter data set.

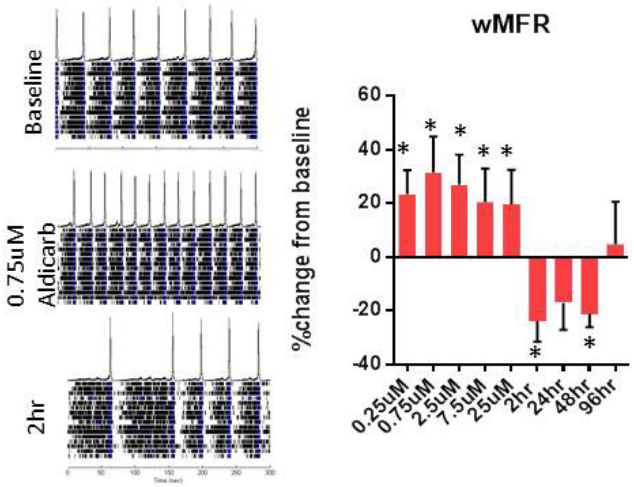

Figure 53. Aldicarb alters firing rate. *Aldicarb increased firing rate in drug, but decreased firing rate after washout. The effects returned to baseline by 96hr.*

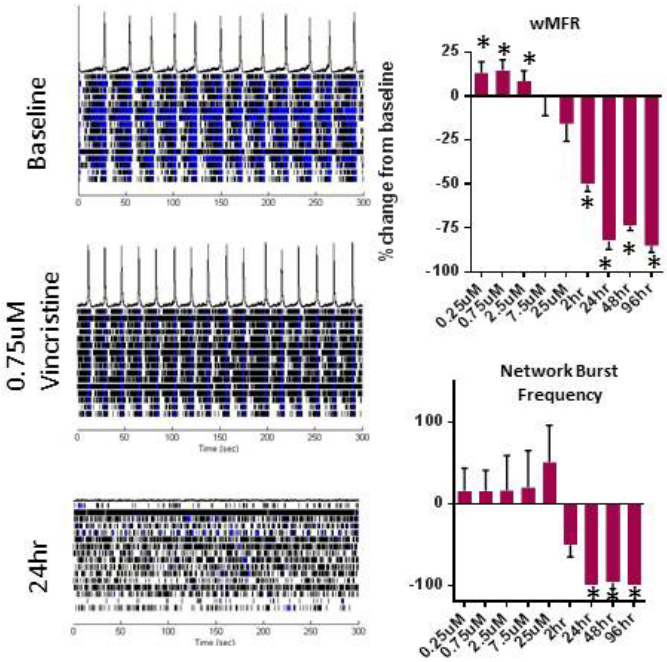

Figure 54. Vincristine de-synchronized network activity. *wMFR first increased and then decreased up to 96hr. The network behavior shifted from synchronized bursting to de-correlated, non-bursting spiking.*

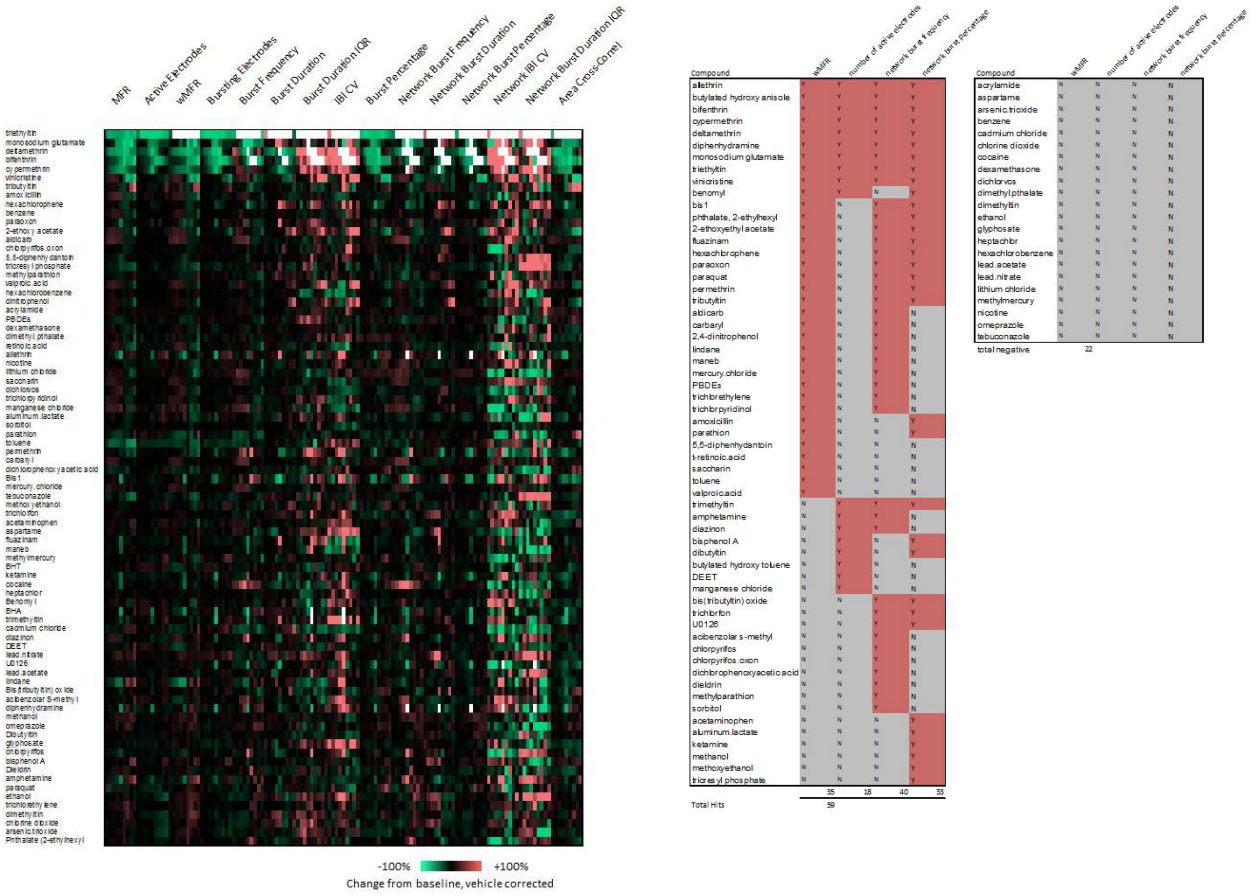

Figure 55. Heatmap results for Neurotoxin library MEA screen. *Results displayed as percent change from baseline across the 9 treatment points for 81 compounds (Left). Data analyzed according to 15 parameters of network activity. 4 metrics were analyzed for statistical significance compared to vehicle effect to designate hit status (Right, *p<0.05, one-way ANOVA Dunnett's multiple comparison test). 59/81 compounds had significant effects on neural activity including measures of network excitability (network burst frequency) and synchrony (network burst percentage).*

3.3.3.2 Summary

3.3.3.2.1 Excitatory Driven Network Phenotypes. Glutamate is the major chemical neurotransmitter in the human brain acting via AMPA type glutamate receptors. As such glutamate receptor antagonists will reduce the ability of neurons to excite one another. In an active interconnected network this antagonism led to a de-synchronization of firing patterns and a cessation of network activity. Neurons remain capable of firing action potentials, although the transmission of signals to post-synaptic partners will be attenuated. As this attenuated communication moves through the network the result will be a reduced incidence of network events, where large numbers of neurons fire together. However, individual neurons may spontaneously fire action potentials leading to a desynchronized activity pattern.

In addition to AMPA receptors, glutamate also acts via NMDA type receptors, which are generally co-localized at individual synapses. Despite their common ligand these receptor subtypes alter neural activity in distinct ways. NMDA receptors are often considered 'coincidence detectors', where they remain in a non-conducting state (because of blockade by

Mg ions) until a large barrage of synaptic input. Because of this voltage dependent property, agents altering NMDA receptor properties may alter the properties of network bursting events, while the incidence of network events is unchanged. When the network was disinhibited by GABA blockade with PTX, NMDA receptor antagonism (APV) brought the network toward baseline bursting, but not complete desynchronization as expected from APV alone. This is likely a result of the increased AMPA receptor activity and influence throughout the network. The addition of CNQX to the PTX and APV treated culture, abolished network bursting. Thus, in the presence of inhibition, NMDA and AOV receptors synergized to drive the network bursting behavior. However, in the absence of inhibition, AMPA receptors mainly drive the synchronous activity, with NMDA receptors contributing to network event frequency.

3.3.3.2.2 Depolarization Block. Paradoxically, the depolarization of neurons may occlude cellular and network action potential firing. Although moderate depolarization brings a neuron closer to action potential threshold, increasing the rate of firing, a chronic depolarization near or beyond action potential threshold has the opposite effect. During sustained depolarization voltage dependent sodium channels (VGSC) cycle into a nonconductive inactivated state. As the number of sodium channels in the inactivated state increases a neuron will lose the ability to fire. We observed depolarization block due to both intrinsic modification of sodium channel dynamics during the drug exposure phase of many pyrethroids, such as Deltamethrin and Cypermethrin, and also due to hyperexcitation, likely through fast synaptic transmission, with compounds such as monosodium glutamate and lindane.

3.3.3.2.3 Sensitivity of MEA Screening Assay to Neurotransmitter and Ion Channel Targets. Overall, the assay was sensitive to compounds within every major class of neurotransmitter and ion channel target. We analyzed whether compounds affected basal firing rates and number of active electrodes. We also investigated network properties such as network burst frequency and percentage. Network burst percentage indicates the degree of burst synchrony within the culture. A hit was defined as a significant effect in any of these 4 measures during the acute or washout phase.

One class of compounds which did not perform as expected was the GABA receptor antagonists. Lindane, which acts at the Picrotoxin binding site to block both synaptic and extrasynaptic tonic GABA signally, decreased firing rate and did not reach significance in its burst frequency increase. This was in contrast to the significant effect on network burst frequency measured during assay development. Additionally, Dieldrin, another GABA-A antagonist, caused significant increase to network burst frequency, but only at the 2 hour post-washout timepoint, and not during compound exposure. Dieldrin has complex effects in the VTA, including increasing dopamine and glutamate release. Dopamine as a neuromodulator can act as an inhibitory signal at D2 autoreceptors [17] and glutamate can decrease firing in the VTA through metabotropic glutamate receptor signaling [18]. Therefore, various mechanisms of disinhibition, particularly when non-specific, do not result in overall measurable changes to network output.

Voltage gated calcium channel (VGCC) regulators also did not impact the network as predicted, aside from aluminum lactate and mercury chloride. In particular, Cadmium showed strong and persistent effects on decreasing network bursting in the test set. The concentrations screened in our validation assay were determined by examining the cellular phenotypes dataset to predict maximum dose tolerated before cytotoxicity. As our goal was to determine specific

effects on neuronal networks due to functional changes rather than cell death, cadmium chloride was screened on the MEA at a lower dose. Also, Lead is known to block T-type calcium channels in the hippocampus [19], whereas dopamine neuron bursting relies on L-type calcium channels, so the negative result could indicate network influence of these two calcium channel types or neuron type specificity [20]. We therefore conclude that the VGCC modifiers are effective at doses either that lead to cytotoxicity or above the range tested.

By comparing the 4 primary measures (wMFR, number active electrodes, Network burst frequency and percentage) between acute and washout amongst the various compound classes identified by target, phenotypes emerge such as the persistent effect of VGSC modifiers on network activity. Many of these compounds caused depolarization block throughout the network during treatment, and did not recover during the immediate washout period, similar to the effect observed on rodent neurons. In addition, these results suggest the human neurons cultured in our assay express appropriate levels of functional membrane voltage gated ion channels to influence action potential dynamics.

In conclusion, we have developed and validated a platform for measuring changes to human neuronal networks from toxin exposure. Our MEA based assay detects compound effect not only on basal neurotransmission, but also allows examination of burst properties underlying complex mechanisms of intrinsic and extrinsic regulation. The assay was robust to classify 59/81 compounds as hits, by significantly altering one of four primary network activity outputs. These compounds represent a variety of chemical classes and targets known and unknown. Thus, the MEA platform functions as a screen for network level phenotypes.

We have created an informatics tool for the generation of toxicity signatures between neurite outgrowth, mitochondrial toxicity, and MEA assay validation datasets. The database is included in the project deliverable package (Figure 56). The database features include CAS numbers, chemical structure clustering, SMILES, hit classification and Z-scores for all data points in the neurite outgrowth, mitochondrial toxicity, and fibroblast cytotoxicity assays, as well as mean percent change responses in the MEA neurophysiology assay. Chemical structure clustering was performed in Seurat (ChemAxon) using the conservative feature connectivity FCFP4_055 algorithm. The data is displayed in heatmap and fully sortable by any parameter or characterization.

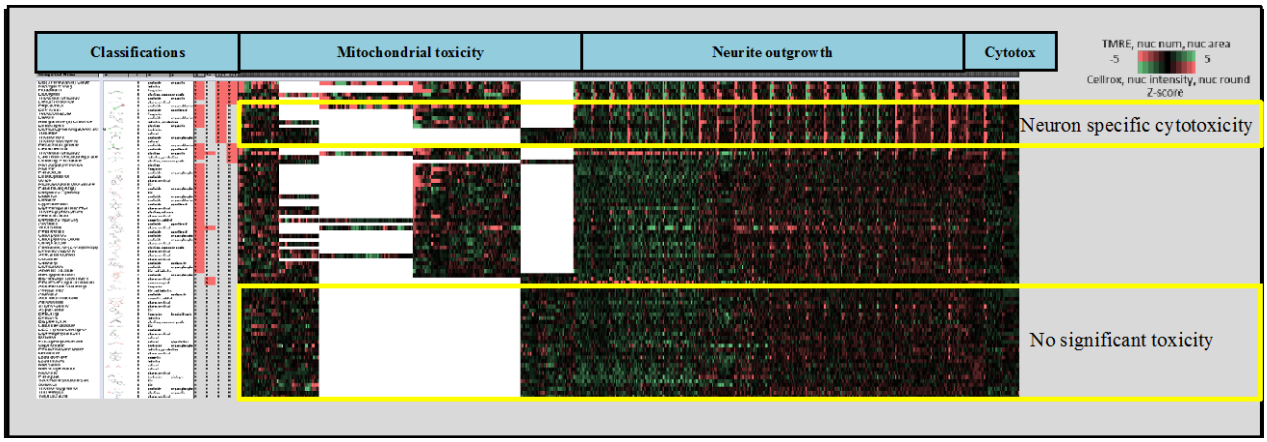

Figure 56. Neuron module database (subset displayed). *Data is sortable by assay response as well as compound classification.*

4.0 CONCLUSIONS

The current approach to quantitatively assessing the health risks of chemical exposure relies extensively on expensive, low-throughput animal studies that are unsuitable for assessing the potential toxicities of the 10,000's chemicals to which the population is exposed. Scientists at SBP leveraged recent breakthroughs in cell engineering, as well as high content imaging and physiological assays, to produce the Cellular Sentinels Toxicity Platform (CSTP). This highly relevant platform technology utilizes high throughput, physiologically relevant cell-based assays to elucidate the mechanistic basis of toxicity. Over the last three years, we have advanced and validated the platform producing a robust suite of highly relevant bioassays to systematically identify compounds with neurotoxic, cardiotoxic and hepatotoxic potential. During this time, we have met virtually all of the criteria set-forth in our original proposal. Those that were not met were replaced by more robust or more tractable technologies or cells as described above. The CSTP can be deployed at scale to screen large compound collections and identify those that represent a toxic hazard to humans. Active compounds can then be prioritized over inactive compounds and subsequently advanced for more detailed studies of toxicity. Conversely, should an individual or group of individuals encounter a new compound whose potential toxicity is unknown, the CSTP can be used to rapidly assess the effect of the compound on neurons, cardiomyocytes and hepatocytes, or other cell types as future modules are developed. These efforts will inform public health officials and toxicologists about the molecular basis of the toxicity, facilitating the development of maximal exposure levels, engineering controls and safety procedures. In short, the CSTP is ready for deployment as a research tool for use by USAF, other branches of the armed forces, and public health officials.

Looking forward there are several areas for further development and advancement of the platform that can improve its overall utility and positive predictive value. As indicated above, hiPSC-derived models will continue to be developed and commercialized. More cell types that more accurately represent human biology are expected to be produced and validated. These can be rapidly applied to the CSTP in its current form simply by replacing the cells currently used. New assay technologies will further the development of additional assays of cellular function beyond neuronal firing and cardiac myocyte contraction. As those develop, software to collect and analyze the data will develop in parallel. Likewise, efforts to develop and integrated body-on-a-chip system will bring new engineering solutions to bear which could theoretically be applied to the CSTP. Perhaps the most exciting advancement will be the combination of the CSTP platform with specific patient-derived hiPSCs and comprehensive genomic analyses. When combined, these three technologies will allow for the generation of a toxicogenomic database that can be used to correlate genetic risk with toxic response and chemical structure. Such tools will require the further development of the CSTP modules to more fully represent key cell types; the development of quantitative structure activity relationships between compound and toxic effect *in vitro* and *in vivo*; and the establishment of a database representing the human genome and the software tools needed to integrate these data sets. All of this will come to fruition in the near future, and the CSTP as currently configured represents a critical piece of that future toxicogenomic approach to assessing risk and limiting exposure.

5.0 REFERENCES

1. Metsalu T, Vilo J. ClustVis: a web tool for visualizing clustering of multivariate data using Principal Component Analysis and heatmap, Nucl Acids Res. 2015; 43(W1):W566-W570.
2. Attene-Ramos MS, Huang R, Michael S, Witt KL, Richard A, Tice RR, et al. Profiling of the Tox21 Chemical Collection for mitochondrial function to identify compounds that acutely decrease mitochondrial membrane potential. Environ Health Perspect. 2015; 123(1):49-56.
3. Kirby RJ, Qi F, Phatak S, Smith, LH, Malany S. Assessment of drug-induced arrhythmic risk using limit cycle and autocorrelation analysis of human iPSC-cardiomyocyte contractility. Toxicol Appl Pharmacol. 2016; 305:250-258.
4. Radio NM, Mundy WR. Developmental neurotoxicity testing in vitro: models for assessing chemical effects on neurite outgrowth. Neurotoxicology 2008; 29(30):361-376.
5. Robinette BL, Harrill JA, Mundy WR, Shafer TJ. In vitro assessment of developmental neurotoxicity: use of microelectrode arrays to measure functional changes in neuronal network ontogeny. Front Neuroeng. 2011; 4:1.
6. Hoschouer EL, Yin FQ, Jakeman LB. L1 cell adhesion molecule is essential for the maintenance of hyperalgesia after spinal cord injury. Exp Neurol. 2009; 216:22-34.
7. Zikopoulos B, Barbas H. Altered neural connectivity in excitatory and inhibitory cortical circuits in autism. Front Hum Neurosci. 2013; 7:609.
8. Chase L, Strathman M, Grinager J, Llanas R, Einhor S, Carlson C, et al. Applications of human iPSC-derived neurons using high content image-based assays. Society for Neuroscience Annual Meeting; 2012.
9. Hashimoto S, Hagino A. Staurosporine-induced neurite outgrowth in PC12h cells. Exp Cell Res. 1989; 184(2):351-359.
10. Rasouly D, Rahamim E, Lester D, Matsuda Y, Lazarovici P. Staurosporine-induced neurite outgrowth in PC12 cells is independent of protein kinase C inhibition. Mol Pharmacol. 1992; 42(1):35-43.
11. Powell SK, Kleinman HK. Neuronal laminins and their cellular receptors. Int J Biochem Cell Biol. 1997; 29(3):401-414.
12. Zhang JH, Chung TD, Oldenburg KR. A simple statistical parameter for use in evaluation and validation of high throughput screening assays. J Biomol Screen. 1999; 4(2):67-73.
13. Jin X, Costa, RM. Start/stop signals emerge in nigrostriatal circuits during sequence learning. Nature 2010; 466(7305):457-462.
14. Sulzer D, Cragg SJ, Rice ME. Striatal dopamine neurotransmission: regulation of release and uptake. Basal Ganglia 2016; 6(3):123-148.
15. Morozova EO, Myroshnychenko M, Zakharov D, di Volo M, Gutkin B, Lapish CC. Contribution of synchronized GABAergic neurons to dopaminergic neuron firing and bursting. J Neurophysiol. 2016; 116(4):1900-1923.
16. Illes S, Jakab M, Beyer F, Gelfert R, Couillard-Despres S, Schnitzler A. Intrinsically active and pacemaker neurons in pluripotent stem cell-derived neuronal populations. Stem Cell Reports 2014; 2(3):323-236.
17. Ford CP. The role of D2-autoreceptors in regulating dopamine neuron activity and transmission. Neuroscience 2014; 282:13-22.
18. Fiorillo CD, Williams JT. Glutamate mediates an inhibitory postsynaptic potential in dopamine neurons. Nature 1998; 394(6688):78-82.

19. Yan D, Xiao C, Ma FL, Wang L, Luo YY, Liu J, et al. Excitatory effects of low-level lead exposure on action potential firing of pyramidal neurons in CA1 region of rat hippocampal slices. J Neurosci Res. 2008; 86(10):3665-3673.
20. Durante P, Cardenas CG, Whittaker JA, Kitai ST, Scroggs RS. Low-threshold L-type calcium channels in rat dopamine neurons. J Neurophysiol 2004; 91(3):1450-1454

LIST OF SYMBOLS, ABBREVIATIONS AND ACRONYMS

B	beta
µl	microliter
µM	micromolar
4-AP	4-aminopyridine
ACEA	ACEA BioSciences, Inc.
AchE	acetylcholinesterase
AMPA	α-amino-3-hydroxy-5-methyl-4-isoxazolepropionic acid
AOV	analysis of variance
APV	amino-5-phosphonovaleric
ATP	adenosine triphosphate
AUC	area under the curve
BDNF	brain-derived neurotrophic factor
BIO	retraction control, a GSK3β inhibitor
cAMP	cyclic adenosine monophosphate
CARDIO	cardiomyocyte
CAS	Chemical Abstracts Service
CBIS	Chemical and Biological Information System
CDI	Cellular Dynamics International
CELLROX	fluorescent dye for measuring reactive oxygen species in live cells
CI	cell index
CLUSTVIS	web tool for visualizing clustering of multivariate data
CNQX	cyano nitroquinoxaline
CO	chlorpyrifos oxon
CSIRO	Commonwealth Scientific and Industrial Research Organization

CSTP	cellular sentinels toxicity platform
CV	coefficient of variance
CYP	cytochrome P450
DA	dopaminergic
DMEM	Dulbecco's modified eagle medium
DMSO	dimethyl sulfoxide
DPBS	Dulbecco's phosphate-buffered saline
DRC	dose response curve
EPA	United States Environmental Protection Agency
GABA	*gamma*-aminobutyric acid
GDNF	glial cell line-derived neurotrophic factor
GUI	graphical user interface
HC	high-content imaging
HEP	hepatocyte
HepG2	human liver cancer cell line
hERG	human ether-a-go-go-related gene
hiPSC	human-induced pluripotent stem cell
hiPSC-HEP	human-induced pluripotent stem cell-derived hepatocytes
HTS	high-throughput screen
HZ	hertz
IBI	interburst interval
IC_{50}	drug concentration causing 50% inhibition of the activity
IMI	Innovative Medicines Initiative
iPSC	induced pluripotent stem cells
iPSC-CM	induced pluripotent stem cell cardiomyocyte

JC-10	dye for determining mitochondrial membrane potential
LC-MS	liquid chromatography-mass spectrometry
MEA	multielectrode array
MFR	mean for firing rate
mM	millimolar
MMP	mitochondrial membrane potential
MTG	mitotracker green
NIH	National Institutes of Health
NMDA	*N*-methyl-D-aspartate
OCR	oxygen consumption rate
PBDE	polybrominated diphenyl ethers
PBS	phosphate-buffered saline
PC1	principal component 1
PC2	principal component 2
PCA	principal component analysis
pM	picomolar
PTX	pertussis toxin
PX	pixel
QSAR	quantitative structure activity relationship
QT	measure of time between the start of the Q wave and the end of the T wave in the heart's electrical cycle.
RAW	unprocessed
ROS	reactive oxygen species
RTCA	real-time cell analyzer
SBP	Sanford Burnham Prebys Medical Discovery Institute
SD	standard deviation

SMILES	simplified molecular-input line-entry system
SOW	statement of work
STDDEV	standard deviation
t	time
TDP	torsade de pointes
TMRE	tetramethylrhodamine, ethyl ester
TOX21	Toxicology in the 21st Century (National Toxicology Program)
TOXCAST	EPA's toxicity forecaster
TUJ1	neuron-specific beta-III tubulin antibody
USAF	United States Air Force
VGCC	voltage gated calcium channel
VGSC	voltage dependent sodium channels
VTA	ventral tegmental area
wMFR	weighted firing rate